

**Magmatic evolution and REE mineralization in the
early Cambrian Jbel Boho igneous complex
in the Bou Azzer inlier
(Anti-Atlas/Morocco)**

**Dissertation
zur Erlangung des Doktorgrades
der Mathematisch-Naturwissenschaftlichen Fakultät
der Christian-Albrechts-Universität
zu Kiel**

vorgelegt von

Rachid Benaouda



Kiel 2015

**Magmatic evolution and REE mineralization in the
early Cambrian Jbel Boho igneous complex
in the Bou Azzer inlier
(Anti-Atlas/Morocco)**

**Dissertation
zur Erlangung des Doktorgrades
der Mathematisch-Naturwissenschaftlichen Fakultät
der Christian-Albrechts-Universität
zu Kiel**

vorgelegt von

Rachid Benaouda



Kiel 2015

Vorwort

Die vorliegende Arbeit wurde zwar als monographische Dissertation verfasst, jedoch wurde für die einzelnen Kapitel ein unabhängiger Aufbau bewusst gewählt, da diese voneinander in internationalen Fachzeitschriften getrennt publiziert werden sollen. Daher befinden sich in jedem Kapitel eine eigenständige Einleitung, Diskussion und Literaturverzeichnis. Auch die Länge und etwaige Formatierungen sind in Hinblick auf die jeweiligen Vorgaben der Fachzeitschriften bewusst gewählt. Der Leser sei darauf hingewiesen, dass es durch den gewählten Aufbau zu Wiederholungen kommen kann und möge diesen Sachverhalt bei der Lektüre berücksichtigen.

Kiel 2015
Rachid Benaouda

Erster Gutachter: Prof. Dr. Colin Devey

Zweiter Gutachter: Dr. rer. nat. Jörg Geldmacher

Tag der mündlichen Prüfung: 08.10.2015

Zum Druck genehmigt:

Prof. Dr. Wolfgang J. Dushl

Table of contents

Vorwort.....	i
Table of contents.....	iii
List of figures.....	vii
List of tables.....	ix
Danksagung.....	xi
Abstract.....	xiv
Zusammenfassung.....	xviii
CHAPTER 1.....	1
General Introduction.....	1
1.1 Motivation and aim of the work.....	1
1.2 Overview of the main geological subdivision of Morocco.....	4
1.2.1 The Rif belt.....	4
1.2.2 The Meseta.....	5
1.2.3 The High and Middle Atlas.....	6
1.2.4 The Anti-Atlas and Sahara.....	6
1.3 Basic geology of REE.....	8
1.3.1 Geochemistry.....	8
1.3.2 REE deposits and principal source minerals.....	13
1.3.2.1 Igneous REE deposits.....	13
1.3.2.2 Placer REE deposits.....	14
1.3.2.3 Lateritic ion-adsorption deposits.....	14

1.3.2.4 Principal REE minerals	15
1.4 Rare earth Importance and global processing	16
1.5 Fieldwork and strategy in Jbel Boho.....	17
References:.....	21
CHAPTER 2.....	25
Magmatic evolution of the Jbel Boho alkaline complex in the Bou Azzer inlier (Anti-Atlas/Morocco) and its relation to REE mineralization.....	25
Abstract.....	25
2.1 Introduction	27
2.2 Geologic setting.....	30
2.3 Summary of field work	36
2.4 Petrography of the Jbel Boho rocks	39
2.4.1 The alkaline volcanics.....	39
2.4.2 Syenite.....	40
2.4.3 Late intrusives: microsyenitic and rhyolitic dykes.....	42
2.5 Analytical methods.....	43
2.6 Whole-rock compositions	44
2.6.1 Major elements.....	44
2.6.2 Trace and rare earth elements geochemistry.....	52
2.7 Mineral chemistry	57
2.7.1 Olivine in the olivine-syenite	58
2.7.2 Amphibole in quartz- and olivine-syenite.....	59

2.7.3	Clinopyroxene in olivine-syenite	61
2.7.4	Synchysite in a rhyolite dyke	62
2.8	Discussion	65
2.8.1	Sources and magma generations	65
2.8.2	Element fractionation	67
2.8.3	Syenite petrogenesis	69
2.8.4	REE enrichment	70
2.9	Conclusion.....	72
	References.....	75
	CHAPTER 3.....	83
	REE enrichment and synchysite mineralization in the late hydrothermal quartz carbonate veins in the Jbel Boho complex in the Bou Azzer inlier (Anti-Atlas/Morocco).	83
	Abstract.....	83
3.1	Introduction	86
3.2	Geological setting.....	87
3.3	Samples and methodology	91
3.4	Petrography and geochemistry of the late hydrothermal veins.	93
3.4.1	Petrography	93
3.4.1.1	The ore bearing veins	93
3.4.1.2	The ore barren veins	99
3.4.2	Geochemistry	101
3.5	Composition of the observed accessory rare earth minerals.	106

3.5.1	Synchysite-(Ce).....	106
3.5.2	Rhabdophane-(Ce)	108
3.6	REE distribution patterns	110
3.7	Fluid inclusions	111
3.7.1	Petrography	111
3.7.2	Microthermometry	114
3.8	Discussion	116
3.8.1	Speciation of REE in hydrothermal fluids	117
3.8.2	REE in the ore bearing veins.....	119
3.8.3	REE in the ore-barren veins	123
3.9	Conclusion.....	125
	References.....	128
	GENERAL CONCLUSION.....	136
	Erklärung.....	139
	Lebenslauf.....	140

List of figures

Figure 1.1 Geological map of the Moroccan Anti-Atlas.	2
Figure 1.2 Geographic locations of the principal mines of Morocco.	3
Figure 1.3 Structural map of the Moroccan Anti-Atlas	7
Figure 1.4 Relative abundance of REE.	9
Figure 1.5 Plot showing ionic radius vs atomic number for REE a.....	11
Figure 1.6 Cross section through the Jbel Boho complex.	18
Figure 2.1 Geological map of the Moroccan Anti-Atlas showing schematically the major geological domains of Morocco.	29
Figure 2.2 Simplified geologic map of the Bou Azzer and Jbel Boho.	33
Figure 2.3 Intercalation of Jbel Boho volcanics with the Adoudounian dolomites.....	35
Figure 2.4 Stratigraphic column of the Bou Azzer sequence at Jbel Boho.	36
Figure 2.5 (A) Geological map of J.Boho showing the sample locations..	37
Figure 2.6 Conglomerate deposit with material from surrounding rocks interbedded with the Jbel Boho volcanics.	38
Figure 2.7 Photomicrographs of the main Jbel Boho magmatic rocks.	41
Figure 2.8 TAS diagram showing the compositional fields of the alkaline rocks.....	50
Figure 2.9 Harker variation diagrams for the rocks of the J.Boho alkaline complex.....	51
Figure 2.10 The Zr/Ti vs Nb/Y classification diagram.....	53
Figure 2.11 Plot of selected HFSE versus SiO ₂	53
Figure 2.12 Plot of Nb/Ta and Zr/Hf ratios versus SiO ₂ and TiO ₂	54
Figure 2.13 Tectonic discrimination diagrams for the Jbel Boho basaltoids.....	55

Figure 2.14 The REE (left column) and other trace elements pattern.	56
Figure 2.15 Typical synchysite occurrences in the LREE-enriched rhyolitic dyke B35..	64
Figure 3.1 A) Simplified geological map of Anti Atlas showing the location of the Bou Azzer inlier.	88
Figure 3.2 A) Magnetic anomaly map (Managem internal document).	91
Figure 3.3 Geological map of Jbel Boho complex	92
Figure 3.4 Examples of hydrothermal ore barren veins.....	94
Figure 3.5 Examples of synchysite bearing veins.....	95
Figure 3.6 The picture displays structural characteristics of the fault hosting LREE.	96
Figure 3.7 Photomicrographs showing the occurrence of synchysite and carbonate in the ore bearing veins.....	98
Figure 3.8 Sample micrographs.	100
Figure 3.9 Chondrite normalized REE patterns.....	102
Figure 3.10 REE pattern of synchysite and rhabdophane.....	111
Figure 3.11 Photomicrographs (room temperature) of fluid inclusions	113
Figure 3.12 Histogram of homogenisation temperatures.....	115

List of tables

Table 1-1 Selected REE minerals economic or potentially economic importance classified by group, after Castor and Hedrick (2006). REO: rare earth oxides.	15
Table 2-1 Major (wt%) and trace element (ppm) contents of selected basic alkali volcanics of the Jbel Boho complex	45
Table 2-2 Major (wt%) and trace elements (ppm) contents of selected trachyandesites and trachytes	46
Table 2-3 Major (wt%) and trace elements (ppm) contents of selected trachytes and rhyolites.	47
Table 2-4 Major (wt%) and trace elements (ppm) contents of selected quartz syenite, olivine syenite and microsyenitic dykes	48
Table 2-5 Major (wt%) and trace elements (ppm) contents of selected microsyenitic and rhyolitic dykes	49
Table 2-6 Representative microprobe analyses of olivine in the Jbel Boho olivine syenite.	59
Table 2-7 Representative microprobe analysis of amphiboles of the two syenite types from Jbel Boho	60
Table 2-8 Representative microprobe analyses of clinopyroxene in the olivine syenite from Jbel Boho.	61
Table 2-9 Chemical analyses for synchysite from the REE enriched rhyolitic dyke (B35) of Jbel Boho complex. Ionic formulae calculated based on 7 oxygens following Guastoni et al. (2009)	63

Table 3-1 Major (wt%) and trace elements (ppm) contents of Jbel Boho hydrothermal veins (G1 group).....	103
Table 3-2 Major (wt%) and trace elements (ppm) contents of Jbel Boho hydrothermal veins (G2 group).....	104
Table 3-3 Major (wt%) and trace elements (ppm) contents of Jbel Boho hydrothermal veins (G3 group).....	105
Table 3-4 Chemical analysis of synchysite-(Ce) in the REE-rich quartz veins (B47 and B46-3). The values of BA35 (Chap 2).	107
Table 3-5 Chemical analysis of rhabdophane-(Ce) in the REE-rich quartz vein (B46-3)	109

Danksagung

Mein Dank gilt insbesondere meinem Betreuer Herrn Prof. Dr. Colin Devey für die kompetente und sympathische Betreuung. Er hat sehr großes Interesse an meiner Arbeit gezeigt und in entscheidenden Momenten durch fachliche Diskussionen eingegriffen um mir den Weg zu weisen und mich durch meine eigene Interpretation an meinem Ziel zu führen. Außerdem stand er mir trotz hoher Belastung durch seine eigene Forschungsarbeit regelmäßig und immer gut gelaunt zur Verfügung.

Mein Dank gilt auch Frau Prof. Dr. Astrid Holzheid, die mir die Möglichkeit gegeben hat, eine Promotion in Kiel aufzunehmen. Sie und Herrn Prof. Dr. Volker Schenk möchte ich auch für die Diskussion und die Beteiligung an einem Anteil meiner Geländearbeit danken.

Meine Arbeit wäre auch nicht zustande gekommen ohne die Hilfe von Herrn Dr. Aomar Ennaciri und Herren Dr. Badra Lakhlifi, die mir dieses Projekt am Anfang durch die Explorationsfirma Managem angeboten haben und mich durch Diskussionen und bei meiner Arbeit im Gelände unterstützt haben. Ebenso danke ich den Firma Managem für die logistische Hilfeleistung bei meinem Aufenthalt in Marrakech und Bou Azzer. Mein Dank geht auch an Prof Romain Bousquet für die umfangreiche Diskussion über die regionale Geologie vom Anti-Atlas.

Mein herzlicher Dank gilt auch Frau Dr. Petra Herms, deren Erfahrung mit Flüssigkeitseinschlüsse, mir bei der Untersuchung von Einschlüsse weiter gebracht hat. Der Dank gebührt natürlich auch Herrn Dr. Peter Rase für die geführten Gespräche und seine Hilfe beim Mikroskopieren.

Dr. Peter Appel danke ich für seine Bereitschaft meine Fragen zur EPMA Analytik immer zu beantworten und zu diskutieren. Genauso geht mein Dank an Frau Barbara Mader für ihre Unterstützung und Assistenz während der EPMA Arbeit. Herrn Andreas Fehler möchte ich auch für die Präparation unzähliger Dünnschliffe und Dickschliffe danken. Ich möchte mich auch bei Wilhelm Schink danken für die Daten, die er für mich zur Verfügung gestellt hat.

Ein besonderer Dank gilt auch Prof. Dr. Klaus Mezger, der immer und ohne zu zögern bereit war, meine Fragen zu beantworten und mit mir telefonisch zu diskutieren. Das gleiche gilt auch für Prof. Dr. Erik Sherer und Prof. Dr. Stephan Klemme für ihre wertvollen Diskussionen.

Außerdem möchte ich meinen Arbeitskollegen Dr. Christopher Giehl, Sebastian Möller, Dr. Oliver Beermann und Dr. Erik Düsterhöft für ihre Bereitschaft zu, diskutieren, zu helfen und ihr Wissen zu teilen, danken. Ein ganz besonderer Dank geht an Dr. Emmanuel Kazimoto, mit dem ich monatelang den Arbeitsraum geteilt habe und von ihm sehr viel gelernt habe. Er war immer bereit Stundenlang mit mir zu sitzen um mir Software beizubringen, was meine Arbeit viel einfacher gemacht hat.

Für meinen Aufenthalt in Bou Azzer, Bleida und Jbel Boho möchte ich sehr herzlich Herrn Dr. Mostapha El Ghorfi, Herrn Hssain Baoutoul und Herrn Mostpha Amarakı von Firma Managem danken. Ohne ihre Erfahrung und Einführung in Jbel Boho, wäre meine Geländearbeit bestimmt viel schwieriger gewesen.

Natürlich möchte ich unbedingt meine sehr lieben Eltern sehr herzlich und unendlich für alles danken, was sie mir gegeben haben und zwar auf alle Ebenen, moralisch und materialistisch. Ohne ihre Unterstützung und Liebe wäre diese Arbeit für mich nicht möglich. Leider zwang der Tod meinen Vater diese Welt vor Ende meiner Dissertation zu verlassen. Ich hätte sehr gerne die Freude und den Stolz in seinen Augen nach meiner PhD Verteidigung gesehen.

Als letztes möchte die Familie von Herrn Lahssen (Ba Hassoun) danken. Diese großzügige Familie hat mich die ganze Zeit wie ein eigenes Mitglied der Familie behandelt. Jeden Tag begleitete mich einer der Söhne oder Neffen mit einem Esel ins Gelände um die zahlreiche Proben tragen zu können. Dazu kam auch Verpflegung. Vielen Dank Ba Hassoun.

Zuletzt möchte ich allen denen danken, die mir bei meiner Arbeit hilfsbereit waren und die hier von mir nicht genannt worden sind.

Rachid Benaouda

Abstract

The Jbel Boho igneous complex in the Bou Azzer inlier (Anti-Atlas / Morocco) represents some of the country's best preserved igneous rocks from the Precambrian/Cambrian transition. The complex is located south of the Anti-Atlas major fault (AAMF) on the northern edge of the West African Craton (WAC). It was formed together with the lower Adoudounian dolomite in an extensional regime under shallow marine conditions after the emplacement of the Bou Azzer ophiolite. The igneous rocks of Jbel Boho emerged in three phases: an initial phase with alkaline volcanism followed by the intrusion of a syenitic pluton and later the emplacement of a dyke swarm. Geochemical and mineralogical data suggest that these rocks are the result of different petrogenetic processes and were formed from three different magma generations. The first magma generation produced the series of volcanic rocks, which evolved by fractional crystallization from primitive basanite/tephrite at the base of the sequence to trachytes and rhyolites showing enrichment of LREE over HREE towards the end of the eruptive phase. The second magma generation is represented by a syenitic pluton, which is composed of both olivine syenite (alkali feldspar, fayalitic olivine, Ca-pyroxene and hornblende) and quartz syenite (alkali feldspar, arfvedsonit and quartz). Both syenites have high alkali contents and REE patterns without negative Eu anomalies, similar to those of the basic volcanics. The syenites were probably produced by partial melting of underlying mafic cumulates at deep crustal levels. In addition, the occurrence of quartz and

positive Pb anomalies in the quartz-syenite suggests that their petrogenesis also involved crustal contamination.

The microsyenitic and rhyolitic magmas of the dyke swarm are more plagioclase-rich than either the syenite or the most evolved volcanics. This and their strongly differing high field-strength element (HFSE) contents suggest that they are derived from a third batch of magma. Negative correlations between Nb/Ta or Zr/Hf ratios and SiO₂ cannot be well explained by magmatic processes. This indicates that elemental fractionation may have been influenced by the addition of mineralized (and halogen-rich) fluids. This is attested to by the presence of fluorite, both in the groundmass of the trachytes and as inclusions in the Na-amphibole of rhyolite, and by the occurrence of the REE-F-Ca carbonate synchysite in some of the late rhyolitic dykes.

The geochemical signatures of Jbel Boho alkaline magmas suggest intraplate magmatism. Moreover, the basic volcanics and syenites have very high Nb/Ta and Zr/Hf ratios. This points to a mantle source that produces alkaline rocks, such as a hot spot or plume. This implies that the compressive regime, which led to the formation of the Bou Azzer ophiolite, had ended by the time of Jbel Boho magmatism.

The Jbel Boho alkaline complex shows some interesting aspects of hydrothermal REE mineralization in the late differentiation stage. REE mineralization is found in a rhyolitic dyke with Σ LREE of ~ 1750 ppm. Synchysite-(Ce), which was identified by EPMA analysis, is the only REE mineral in this dyke. The unusually

high LREE content associated with synchysite mineralization, chlorite and iron oxides probably do not reflect a magmatic signature, but instead most likely a crystallization from REE-rich hydrothermal fluid in the presence of F, Cl, Ca and CO₃. Such highly-fractionated intrusives in alkaline complexes are good prospects for REE mineralization.

REE mineralization also occurs in some late hydrothermal veins (the "G1" veins, with Σ REE up to 1505 ppm). These veins are typically composed of quartz, carbonate and jasper in variable amounts. The REE host minerals are mainly small synchysite-(Ce) minerals (up to 200 μ m in size), although very small amount of REE-P rhabdophan-(Ce) is also found together with synchysite. Other hydrothermal veins, termed G2 and G3 veins are ore-barren veins. They have very low REE contents, suggesting they were formed from REE- and ligand-depleted geothermal fluids, with either enrichment of LREE over HREE (G2) or with quite flat REE patterns (G3). The flat REE patterns of the G3 veins are associated with high carbonate and iron contents reflected by the presence of jasper and carbonate coated with Fe-oxides. Their REE patterns may be the result of sideritization preferably extracting HREE (owing to its similar ionic size to Fe²⁺) from the inherently LREE/HREE enriched mineralizing fluid.

Evidence for highly saline hydrothermal fluids comes from fluid inclusions in quartz from the ore bearing veins which show salinities which would lie between 32 and 37 wt% NaCl equivalent in a pure system. However, very low T_e ranging between -50 and -54°C argue for a more complex salinity of the fluid.

Representative homogenization temperatures that range from 150 to 250°C indicate the minimum temperature conditions for the vein formation.

Based on recent experimental data, the REE mineralization model proposed here is the transport of REE as chloride complexes in low pH and REE-rich hydrothermal fluids, with fluorine present as HF and high Ca^{2+} activity. The precipitation of synchysite-(Ce) happens as the result of the neutralization of the acidic fluids by its interaction with carbonate, which both buffers the fluids to high pH values and provides the CO_3^{3-} necessary for synchysite formation.

Synchysite is a very important REE mineral that can provide a new potential source of rare earth elements. It, in addition to minerals such as bastnaesite, are a good indicator for REE mineralization in late hydrothermal veins associated with highly differentiated alkaline rocks.

Zusammenfassung

Der magmatische Jbel Boho Komplex im Bou Azzer Distrikt (Anti-Atlas / Marokko) bietet die am besten erhaltenen magmatischen Gesteine aus der Zeit des Präkambrium/Kambrium Übergangs. Der Komplex befindet sich südlich der Anti-Atlas Hauptstörung (AAMF) am nördlichen Rand des westafrikanischen Kratons (WAC). Er wurde zusammen mit dem unteren Adoudounian Dolomit unter flachen marinen Bedingungen nach der Platznahme des Bou Azzer Ophioliths in einem extensionalen Regime gebildet.

Die magmatischen Gesteine von Jbel Boho entstanden in drei Phasen. Zunächst eine Phase mit alkalischem Vulkanismus, dann die Intrusion eines syenitischen Plutons und anschließend die Platznahme eines Gangschwarms. Geochemische und mineralogische Daten deuten darauf hin, dass diese Gesteine verschiedene petrogenetische Prozesse erfahren haben und durch drei unterschiedliche Magma-Generationen gebildet wurden.

Die erste Magma-Generation erzeugte eine Reihe von vulkanischen Gesteinen, die sich durch fraktionierte Kristallisation von primitiven Basaniten/Tephriten über Trachyte zu Rhyoliten entwickelte, wobei LREE gegenüber HREE angereichert wurden. Die zweite Magma-Generation wird durch einen syenitischen Pluton repräsentiert, welcher aus Olivin-Syenit und Quarz-Syenit zusammengesetzt ist. Der Mineralbestand beinhaltet fayalitischen Olivin, Ca-Pyroxen, Hornblende und Arfvedsonit. Beide Syenite haben hohe Alkaligehalte und REE Muster ohne negativen Eu-Anomalien ähnlich wie die basischen Vulkanite. Dies deutet darauf

hin, dass sie wahrscheinlich durch partielles Aufschmelzen von unterliegenden mafischen Kumulatgesteinen produziert wurden. Darüber hinaus deuten das Auftreten von Quarz und die positive Pb Anomalie in dem Quarz-Syenit auf krustale Kontamination hin. Der Gangschwarm, welcher aus mikrosyenitischen und rhyolitischen Gängen besteht führt mehr Plagioklas als der Syenit aus der zweiten Intrusionsphase und die höchstentwickelten Vulkanite. Dies und die stark unterschiedlichen HFSE (*high field strength elements*) Gehalte zeigen, dass sie von einer dritten Magmageneration stammen müssen.

Negative Korrelationen zwischen Nb/Ta und Zr/Hf Verhältnisse gegen SiO₂ lässt sich durch magmatische Prozesse nicht gut erklären. Das weist darauf hin, dass Elementfraktionierung möglicherweise durch Zufuhr von Halogen-reichen Fluiden beeinflusst wurde. Dies wird durch die Anwesenheit von Fluorit, sowohl in der Grundmasse der Trachyte als auch als Einschlüsse in den Na-Amphibolen der Rhyolite, sowie das Auftreten des REE-F-Ca Carbonats Synchysit in einigen der späten rhyolitischen Gängen belegt.

Die geochemischen Signaturen der Jbel Boho Alkali Magmen lassen auf Intraplattenmagmatismus schliessen. Außerdem haben Die basische Vulkanite und Syenite sehr hohe Nb/Ta und Zr/Hf Verhältnisse. Das deutet auf eine Mantelquelle hin, die Alkaligesteine produziert wie etwas Hot spot oder Plum. Dies impliziert das Ende des kompressiven Regimes, welches zur Bildung des Bou Azzer Ophioliths geführt hat.

Der Jbel Boho Alkali Komplex zeigt im späten Differenzierungsstadium einige interessante Aspekte der hydrothermalen REE-Mineralisation. Die Seltene Erden-Mineralisation befindet sich in einem rhyolitischen Gang mit einem Σ LREE Anteil von ~ 1750 ppm. Synchronit-(Ce) ist das einzige REE Mineral, das durch EPMA-Analysen identifiziert wurde. Synchronit ist als Träger von REE's ein sehr wichtiges Erzmineral. Diese ungewöhnlich hohen LREE Gehalte und Synchronit Mineralisation im Zusammenhang mit Chlorit und Eisenoxiden spiegeln wahrscheinlich keinen magmatischen Prozess, sondern eher eine hydrothermale Überprägung wider.

REE Mineralisationen treten auch in einigen späten hydrothermalen Adern (G1 Adern mit Σ REE bis zu 1505 ppm) auf. Sie bestehen in der Regel aus Quarz, Karbonat und Jasper in variablen Mengen. Die REE Mineralträger sind hauptsächlich kleine Synchronit-(Ce) Minerale (bis 200 μ m groß), aber sehr kleinen Mengen von REE-P Rhabdophan-(Ce) sind auch gelegentlich vorhanden. Die anderen hydrothermalen Adern (bezeichnet als G2 und G3 Adern) sind keine erzführenden Adern. Sie haben sehr niedrige REE Gehalte mit LREE Anreicherung über HREE (G2) oder mit flachen REE-Mustern (G3). Dies deutet darauf hin, dass die hydrothermalen Fluide bezüglich REE verarmt sind. Im Gegensatz zu den anderen Adern haben G3 Adern höhere Karbonat- und Eisen-Gehalte. Jaspis und Karbonat sind mit Eisenoxiden überzogen. Die LREE/HREE Fraktionierung wurden wahrscheinlich durch Sideritierung

Prozesse kontrolliert. Die HREE werden dann aufgrund ihrer ähnlichen Ionengrößen mit Fe^{2+} bevorzugt.

Hinweise für die Beteiligung hochsalinärer Lösungen wurden durch Fluideinschlussstudien an Quarzen der erzhaltigen Adern überprüft. Die Fluideinschlüsse zeigen hohen Salzgehalte zwischen 32 und 37 Gewichts-%, die NaCl äquivalent in reinen System entsprechen. Allerdings, sehr niedrig T_e im Bereich zwischen -50 und -54 °C argumentieren für mehr komplexe Salze. Repräsentative Homogenisierungstemperaturen von 150 bis 250°C entsprechen den Mindesttemperaturbedingungen für die Aderbildung.

Basierend auf experimentellen Daten wird vermutet, dass der Transport von REE durch REE-Chloridkomplexe mit niedrigem pH-Wert in Anwesenheit von Fluor als HF und hoher Ca^{2+} Aktivität erfolgt. Die Ausfällung von Synchysit geschieht durch die Neutralisation der sauren Fluide durch z.B. Karbonat, welches die pH-Werte der sauren Fluiden erhöht und CO_3^{2-} für die Synchysitbildung zur Verfügung stellt.

Die späten differenzierten Ganggesteine und hydrothermalen Adern, die mit hohem differenziertem Alkali Gesteine verbunden sind, können ein sehr gute Indikator für die REE-Mineralisation sein.

CHAPTER 1

General Introduction

1.1 Motivation and aim of the work

Although Morocco is rich in mineral resources (phosphate, cobalt, copper, gold, silver, iron, lead, zinc... etc), only 20% of the country had been geologically mapped and since 1921 exploration and mining permits have only been granted for 16% of the country ([Newman, 2012](#)). Following the rapid increase in world-wide demand for rare earth metals and the dominance of China as supplier of about 97% of the global rare earth production, many countries in the world, including Morocco, have started exploration studies in their territory in order to diversify supply.

In Morocco the Tamazert alkaline magmatic complex in the High-Atlas (about 300 km NE of Bou Azzer, see [Fig.1.1](#)) was until recently the only geologic province known for REE mineralization, notably with occurrence of synchysite, parisite and monazite ([Bouabdellah et al., 2010](#); [Woolley, 2001](#)). It consists principally of nepheline syenite, carbonatites cross-cut by several dykes (mainly lamprophyres).

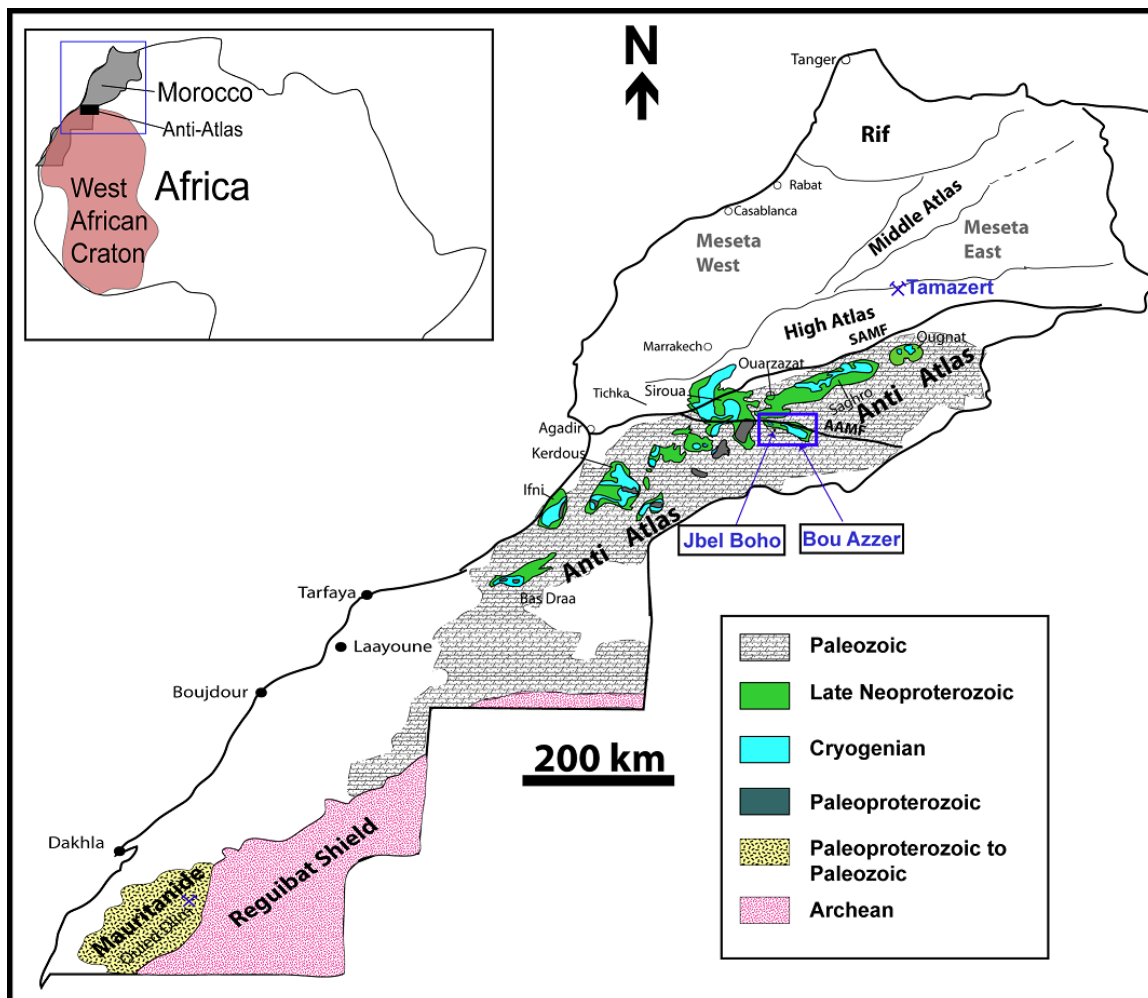


Figure 1.1 Geological map of the Moroccan Anti-Atlas showing schematically the major geological domains of Morocco (Rif, Meseta East and West, Middle and High Atlas as well as Anti-Atlas) with the approximate REE ore locations of the Tamazert alkaline complex in in the High Atlas. Map Modified after [Gasquet et al. \(2005\)](#) and [Mouttaqi et al. \(2011\)](#).

In the last years the Government's ONHYM (National Office for Hydrocarbon and Mines) published new exploration data with very promising Fe-Nb-REE concentrations in the region of Ouled Dlim south of Morocco (Moroccan Mauritanides) ([Fig. 1.2](#)). It consists of Fe-carbonatite including three intrusions

associated with Archean protoliths. The results show generally very high REE contents up to 3% (Mouttaqi et al., 2011; ONHYM, 2015, 2013; Qalbi et al., 2011; Zerdane et al., 2011).

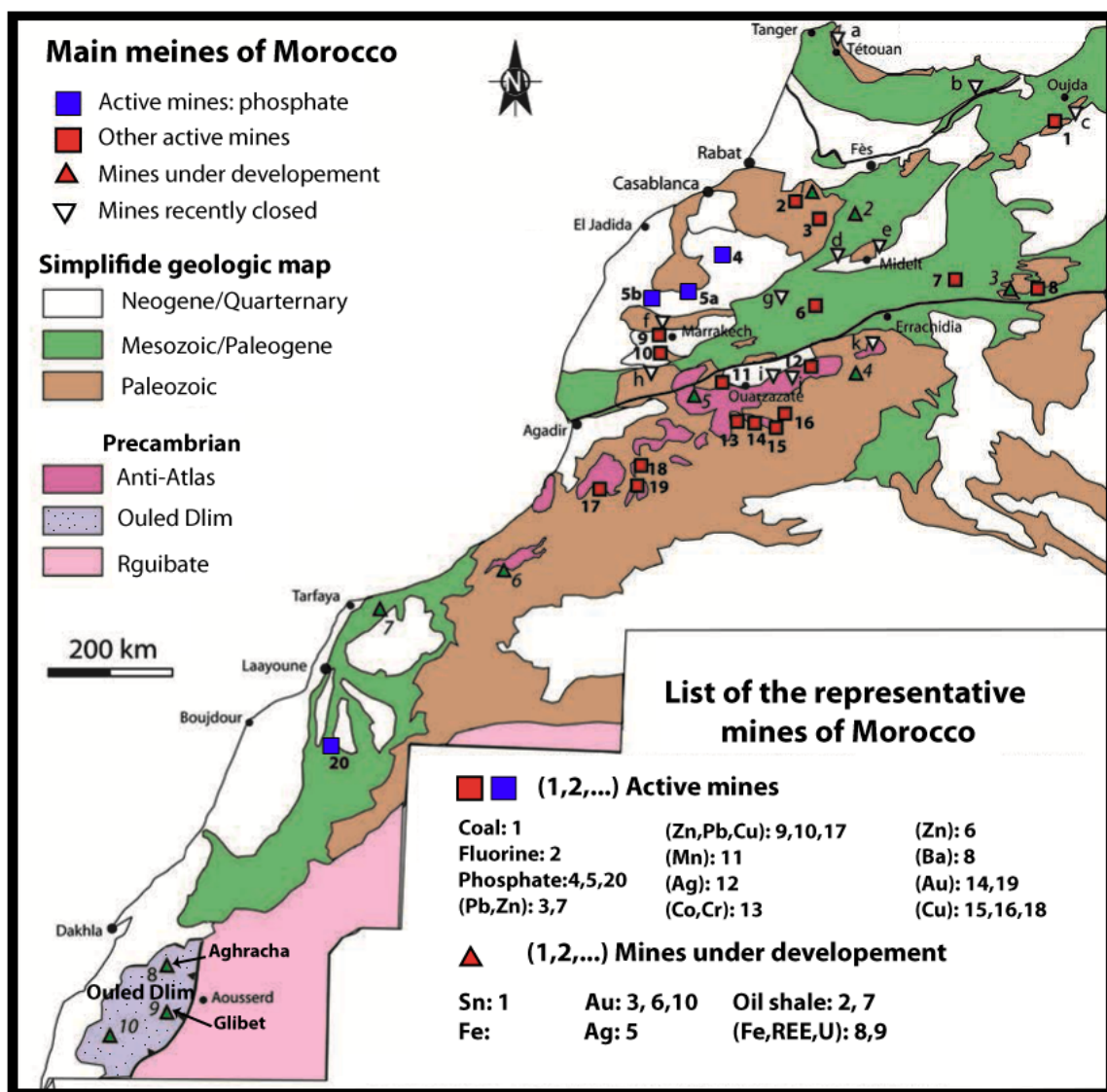


Figure 1.2 Geographic locations of the principal mines of Morocco, classified according to their present status. Modified after Mouttaqi et al., (2011).

The Jbel Boho alkaline igneous complex, which is the focus of this work occurs as a part of the Bou Azzer inlier in the Anti-Atlas (Fig. 1). Jbel Boho is a well

preserved example of intrusive and extrusive alkaline magmatism during the Precambrian-Cambrian transition. As might be expected, governments and geologists have high hopes for such magma types, which are the most important sources of rare earth elements (REE). The Jbel Boho complex has up to present received little geological study, especially with respect to its ore deposit potential. In the last decade the Moroccan mining company Managem established some test works in the Jbel Boho area (see Chapter 3). Soil and rock samples were collected and analyzed, yet the results have remained unpublished. According to these unpublished data some samples display encouraging enrichments in various commercially relevant elements including REE. This motivated the Managem company to support the actual study for more detailed work to check the occurrence and geological setting of rare earth mineralization in this area.

1.2 Overview of the main geological subdivision of Morocco

Morocco is subdivided into four major geological domains (Rif, Atlas, Meseta and Anti-Atlas, see [Fig. 1.1](#)).

1.2.1 The Rif belt

The Rif belt is part of the alpine belt formed in the Tertiary during the Africa-Eurasia collision. It extends along the North Moroccan coast with important bending of its boundary toward the southwest. The Rif belt is subdivided into three domains from north to the south: (i) *internal zone* consists of several units from high-grade metamorphic rocks (granulite) associated with diamond bearing

garnet of Beni-Bousera to lightly metamorphosed carbonate rocks of the Dorsal calcaire; (ii) *flyschs zone* composed of several flysch nappes that corresponds to detrital sediments of Cretaceous to Miocene ages; (iii) external zone correspond to Mesozoic and Cenozoic series filling the North African margin. these consist mainly of limestones, sandstones and shales. The Rif is characterised by its complex displaced units, some of which were thrust up to hundreds of kilometres ([Chalouan et al., 2008](#)).

1.2.2 The Meseta

The Meseta domain is subdivided into Meseta West and Meseta East which are separated by the Middle Atlas. The Meseta is characterized by tabular sediments (sandstone, marl, limestones..etc) onlapping Variscan paleozoic massif, which crop out as isolated small inliers within a sediment cover. This discontinuous occurrence of the Variscan basement is the result of the complex Atlas orogeny deformation. Consequently the occurrence of pre- and late orogenic magmatism and metamorphism is prevalent in this domain. In addition, Neoproterozoic outcrops represented by felsic volcano-clastic rocks have also been recognized in some locations in the Meseta domain ([Hoepffner et al., 2005](#); [Michard et al., 2008](#)).

1.2.3 The High and Middle Atlas

The Atlas belts are characterized, unlike the Rif, by an intracontinental autochthonous system, however both Rif and Atlas belts are the products of the alpine orogeny (de Lamotte et al., 2008). The High and Middle Atlas trend generally from NE-SW to ENE-WSW (Fig. 1.1). The high uplift of the continental basement in the Moroccan Atlas has resulted in extensive outcrops of several Paleozoic inliers within Mesozoic and Cenozoic cover. Proterozoic rocks are also best exposed in the Marrakech High Atlas and connected to the Anti-Atlas through the Siroua massif.

1.2.4 The Anti-Atlas and Sahara

The Anti-Atlas belt (called also the Pan-African belt) is a large exposure of NE-SW-oriented Precambrian inliers within a Paleozoic sediment cover. The paleogeodynamic setting of the belt is still discussed (for more detail see e.g. Gasquet et al. (2008, 2005); Blein et al. (2014) and literatures therein). The rocks of this belt formed during the Neoproterozoic along the northern border of the West African Craton (WAC) and include abundant granites and rhyolites. They are underlain by a paleoproterozoic basement including magmatic and metamorphic rocks, which crop out only south of the Anti-Atlas major fault (AAMF, Fig. 1.1) The Mesoproterozoic is not reported in the literature and is considered to be absent in the Anti-Atlas. The Paleoproterozoic is covered by Neoproterozoic units (magmatic, metamorphic and volcano sedimentary rocks) including an ophiolite, which is well exposed in the Bou Azzer inlier along the

AAMF. The late Neoproterozoic is marked by ca. 2000 m of volcanoclastic rocks, referred to as the “Ouarzazate supergroup” in the concept of Thomas et al. (2004). Figure 1.3 summarizes the locations of the different Paleoproterozoic to Neoproterozoic rocks of the Anti-Atlas and their radiometric ages.

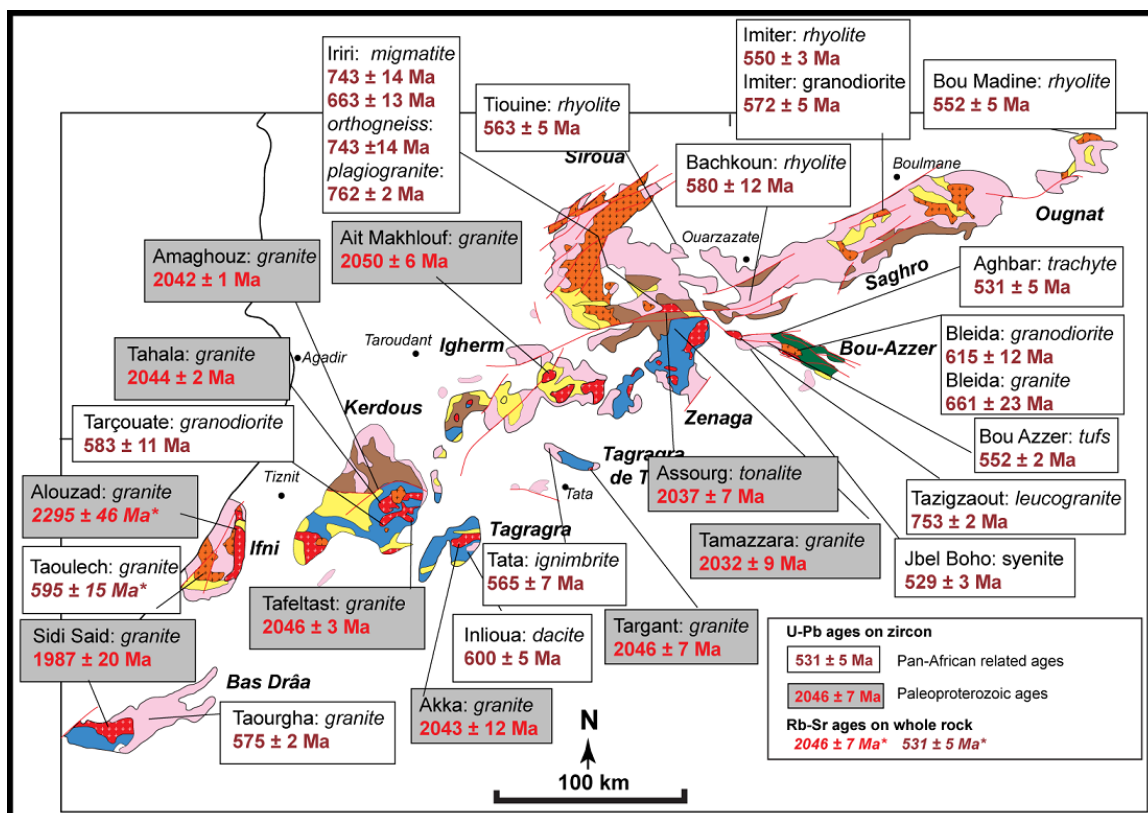


Figure 1.3 Structural map of the Moroccan Anti-Atlas displaying available radiometric ages of its outcropping Precambrian Rock (Bousquet, unpub., pers. com)

The transition Precambrian-Cambrian is characterized by widespread carbonate sedimentation which occurred contemporaneously with important volcanism in an extensional environment. The Jbel Boho alkaline magmatic complex, the topic of this study, is the best preserved magmatic centre formed during this transition.

South of the Anti-Atlas, a wide Saharan platform is located in southern Morocco. The oldest rocks in the Sahara are situated mostly in the southwest of the country to the southeast of the coastal town of Dakhla. They consist of the Archean Reguibate shield overlapped by Proterozoic and Paleozoic rocks from the Ouled Dlim massif, which contains the REE bearing carbonatite. This area is still however poorly understood due to a lack of sufficient chronological and structural data ([Michard et al., 2010](#); [Zerdane et al., 2011](#)).

1.3 Basic geology of REE

1.3.1 Geochemistry

REE are the 15 elements of the inner transition series of the group IIIa in the periodic table (Lanthanides) with increasing atomic numbers from Lanthanum (^{57}La) to Lutetium (^{71}Lu). Melting point and density also increase in this order, but the ionic radii slightly decrease from La (1.032 Å) to Lu (0.861 Å), the so called "lanthanide contraction".

The REE are not rare as the group's name suggests ([Fig. 1.4](#)). They were called rare earth elements because most of them were identified as oxide components within seemingly rare minerals during the 18th and 19th centuries. Cerium (Ce), the most common of all REE, is actually more common in the Earth's crust than copper or lead. All REE except promethium are more common than silver or mercury ([Castor and Hedrick, 2006](#)).

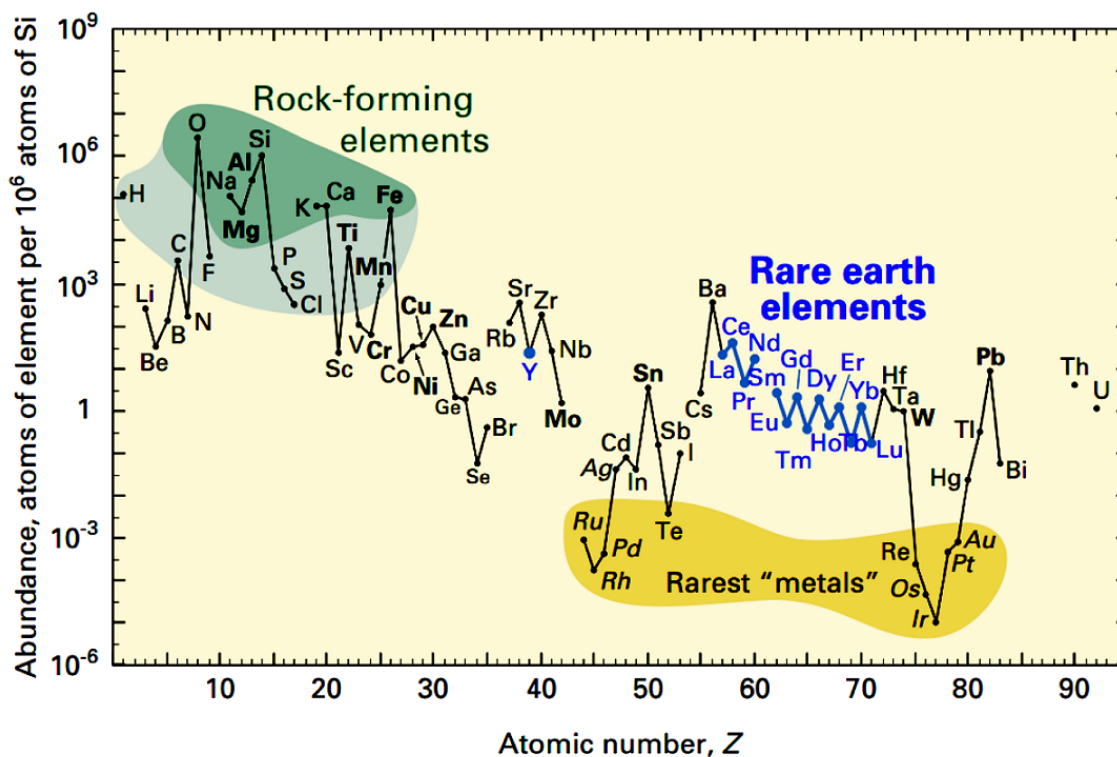


Figure 1.4 Relative abundance of REE with respect to other chemical elements in the earth's crust (Haxel et al., 2002).

Geoscientists often divided the REE into two groups: light REE (LREE: La to Nd) and heavy REE (HREE: Sm to Lu). REE are difficult to separate chemically, because they all possess similar outer electron shells (6s² 5p⁶), although they differ only in the electron configuration of the 4f and 5d sub-shells and so behave similarly in chemical reactions. In nature, they are generally characterized by 3+ oxidation states, although some REE occur also as bivalent or tetravalent ions when in reducing or oxidizing environments (e.g. Eu²⁺ and Ce⁴⁺). Although not lanthanides, the other members of the IIIB group scandium (²¹Sc) and yttrium (³⁹Y) are also included in the REE group owing to their very similar chemistry,

although due to its very small ionic radius Sc, whose ion is smaller than that of Lu, behaves much more like Fe^{2+} and Mg^{2+} (Fig. 1.5). The behaviour of yttrium is very similar to the HREE Dy-Ho. Consequently most geologists have excluded Sc from the REE group (Chakhmouradian and Wall, 2012; McLennan and Taylor, 2012).

In magmatic systems the REE are lithophile and tend to be partitioned into the melt. Therefore they are regarded as incompatible elements during magma differentiation. Despite their very similar chemical behaviour, a fractionation between LREE and HREE during magmatic processes (batch melting and fractional crystallization) is possible. This is driven principally by the differences in ionic radius at similar charge, although oxidation states and interactions with bonding ligands also play a role. When behaving as trace elements, the degree of incompatibility generally decreases with the ionic radius/charge ratio from La to Lu. Such behaviour is generally seen during melting of mantle lithologies, in which HREE are more compatible in the mantle minerals garnet and clinopyroxene. Thus melts derived from low degree partial melting of peridotite are highly enriched in LREE.

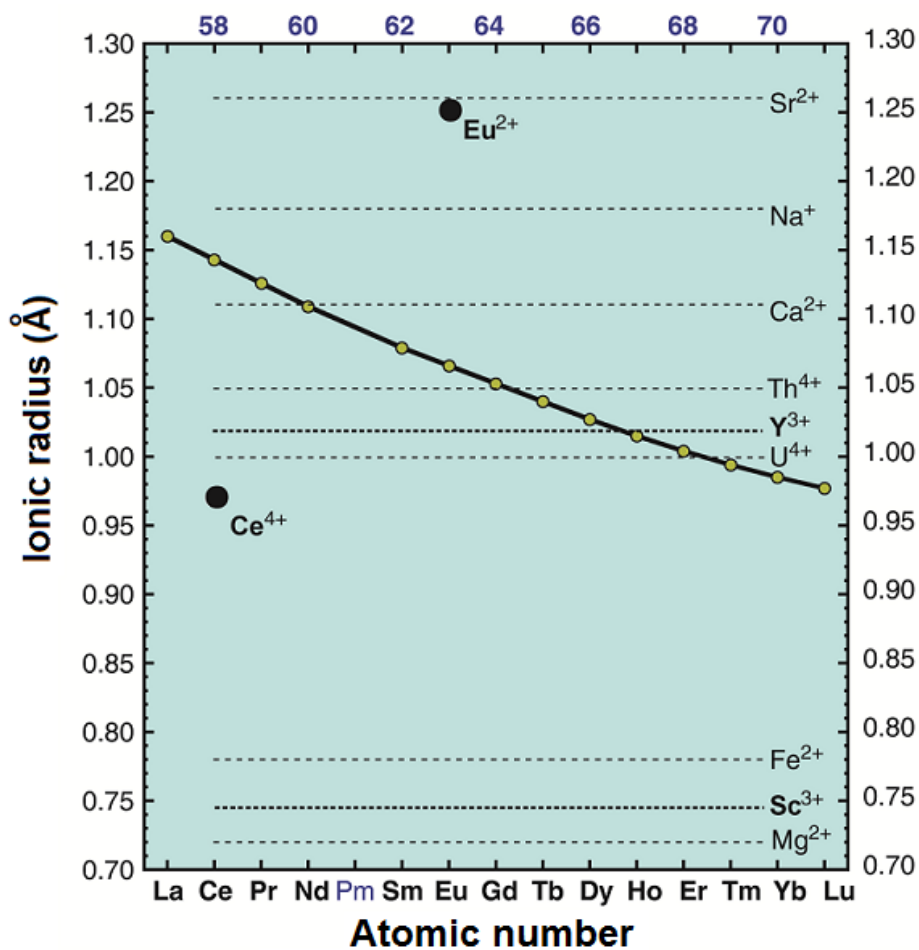


Figure 1.5 Plot showing ionic radius vs atomic number for REE and other selected cations. Ca^{2+} and Na^{2+} are much similar to LREE. Y^{3+} , Th^{4+} , U^{4+} and Ce^{4+} are similar to HREE. Sc^{3+} and is much similar to Fe^{2+} as well as Mg^{2+} . Eu^{2+} has the highest ionic radii that is more similar to Sr^{2+} . Plot modified after McLennan and Taylor (2012).

The REE also are essential elements in some minerals. There are only a few minerals that require HREE e.g. xenotime, whereas the most abundant rare earth minerals are those that incorporate the LREE e.g. monazite, bastnäsité, synchysite, parisite, loparite and rhabdophane.

The bivalent and tetravalent states of Eu^{2+} and Ce^{4+} are also very important in geochemistry. Owing to its substitution behaviour into the Ca site, Eu^{2+} is compatible in plagioclase. This process results in anomalous REE patterns due to the separation of Europium from the other 3+ REE if plagioclase fractionates or accumulates during magma differentiation. The same phenomena occur for Ce^{4+} under oxidizing surficial conditions, notably during continental weathering. The 4+ cerium forms a highly insoluble hydroxide that gets precipitated, separating cerium from the 3+ REE during weathering. As a result, a Ce anomaly occurs in weathering profiles ([Mclennan and Taylor, 2012](#)).

A large geochemical database has been accumulated on REE distribution in various rocks and minerals. In most igneous rocks, REE occur only as trace elements, which are mostly concentrated in accessory minerals (apatite, zircon, monazite, xenotime, alanite... etc.).

Alkaline igneous rocks, which are considered to be derived from very low degrees of partial melting of mantle peridotite, have generally high enrichment in volatile and incompatible elements including LREE. Such igneous rocks (which include carbonatites) show LREE and HFSE (high-field-strength elements) enrichments that can reach several hundred to several thousand of ppm in total. REE ore deposits are therefore expected to occur most likely in association with highly differentiated alkaline igneous rocks, especially in association with hydrothermal systems ([Linnen et al., 2014](#)).

1.3.2 REE deposits and principal source minerals

In addition to the alkaline igneous rocks (including carbonatite) and associated hydrothermal systems, REE deposits can occur as a) placer deposits and b) lateritic ion-adsorption deposits.

1.3.2.1 Igneous REE deposits

The alkaline igneous rocks with which magmatic REE deposits are principally associated are often also enriched in Zr, Nb and were often originally mined for these elements. Only with the advent of high-tech products did the REE they contain also become economically relevant. REE deposits in the USA Mountain Pass carbonatite and in China's Mauniuping carbonatite are the principal carbonatite deposits of the world ([Kanazawa and Kamitani, 2006](#); [Kynicky et al., 2012](#); [Mariano and Mariano, 2012](#)). Alkaline rocks are often associated with carbonatite. Economic concentrations of REE were found e.g. in the Khibiny and Lovozero alkaline complex (Russia), Ilímaussaq alkaline complex (Greenland) and Strange Lake (Canada) ([Chakhmouradian and Zaitsev, 2012](#)). In most instances mobilization and concentration of REE to economic concentrations in alkaline and peralkaline system is principally controlled by late hydrothermal fluids as in the world's largest Bayan Obo REE deposits ([Gysi and Williams-Jones, 2013](#); [Williams-Jones et al., 2012](#)).

1.3.2.2 Placer REE deposits

Sedimentary concentrations of REE minerals as placer deposits occur by the effect of gravity on moving sand grains. Heavy minerals like e.g. monazite, xenotime, zircon and ilmenite, which are resistant to mechanical weathering, will be physically separated from less-dense grains and concentrated in streams or beaches. Monazite-bearing placer deposits formed the majority of the early REE sources prior to the discovery of the Mountain Pass deposits. The best known REE placer deposits occur in paleobeach placers in Australia. Owing to their high thorium contents and associated radioactivity, monazite and xenotime are undesirable for REE production. Thus Australia currently exports little or no REE minerals from such sources ([Castor and Hedrick, 2006](#)).

1.3.2.3 Lateritic ion-adsorption deposits

In tropical environments, weathering of many rock-forming minerals causes in situ residual deposits to form by leaching of certain elements, generating the so-called laterite deposits. If the parent rock is enriched in REE like carbonatite or alkali igneous rocks, the released REE may be adsorbed and incorporated into new minerals and occur as a weathering crust on top of the source rock. The process leading to such deposits is poorly understood. The most important REE hosting minerals in such deposits with economic significance are clay minerals like kaolinite, which likely incorporate HREE ([Sanematsu et al., 2013, 2009](#)). Laterite deposits are therefore the main source of HREE. The world's most important source of HREE is located in south China (province of Jiangxi) and

consists of ion-adsorption clays, which formed by lateritic weathering of originally REE-rich carbonatite and granite (Kanazawa and Kamitani, 2006; Kynicky et al., 2012).

1.3.2.4 Principal REE minerals

Hundreds of minerals such as silicates, carbonate, oxides... etc with pronounced quantities of REE have already been discovered (Miyawaki and Nakai, 1993). However only a small number of them is commercially important or may yield a marketable product in the future (see Table 1; (Castor and Hedrick, 2006)).

Table 1-1 Selected REE minerals economic or potentially economic importance classified by group, after Castor and Hedrick (2006). REO: rare earth oxides.

Groupe	Name	Formula	Approximate REO %
Silicates			
	Allanite	$(Ca,REE)_2(Al,Fe)_3(SiO_4)_3(OH)$	30
	Gadolinite	$REEFeBe_2Si_2O_{10}$	52
	Kainosite	$Ca_2(Y,REE)_2Si_4O_{12}CO_3 \cdot H_2O$	38
	Thalenite	$Y_3Si_3O_{10}(OH)$	63
Carbonates			
	Bastnaesite	$REECO_3F$	76
	Synchysite	$CaREE(CO_3)_2F$	51
	Parisite	$CaREE_2(CO_3)_3F_2$	64
	Anyclite	$SrREE(CO_3)_2(OH) \cdot H_2O$	46
Phosphates			
	Monazite	$(REE,Th)PO_4$	71
	xenotime	YPO_4	61
	Britholite	$(REE,Ca)_5(SiO_4,PO_4)_3(OH,F)$	62
	Churchite	$YPO_4 \cdot 2H_2O$	44
	Florencite	$REEAl_3(PO_4)_2(OH)_6$	32
Oxides			
	Loparite	$(REE,Na,Ca)(Ti,Nb)O_3$	36
	Fergusonite	$REE(Nb,Ti)O_4$	47
	Euxenite	$(REE,Ca,U,Th)(Nb,Ta,Ti)_2O_6$	40
	Aeschynite	$(REE,Ca,Fe,Th)(Ti,Nb)_2(O,OH)_6$	36
	Cerianite	$(Ce,Th)O_2$	81

The majority of REE resources are related to bastnäsite, monazite, xenotime and ion-adsorption clays. The bulk of global LREE (mainly Ce, La and Nd) comes from bastnäsite and monazite, whereas xenotime and ion-adsorption clays are the primary sources of HREE (mainly Y). Bastnäsite is principally contained in carbonatite and related deposits and monazite as well as xenotime are commonly found in igneous rocks and placer deposits. In ion-adsorption deposits the REE are adsorbed onto clay mineral surface like kaolinite.

1.4 Rare earth Importance and global processing

The rare earth elements (REE) are critical resources for high-technology and become today essential for many applications in modern industry. The principal six use categories of REE are: 1) *permanent magnets* used e.g. in hybrid motors and disc drives , 2) *fluid-cracking catalysts* used e.g. in petroleum refining industry 3) *polishing materials* and 4) *glass* used e.g. in cameras lens, monitors and smartphone, 5) metal alloys used e.g. in wind turbines and NiMH batteries, 6) *phosphors* used e.g. in colour televisions and all types of light bulbs ([Castor and Hedrick, 2006](#); [Walters and Lusty, 2010](#)) . REE are also very important in military applications including defence guided missile systems, airframes and aerospace engines, radar systems, sonar and electronic countermeasures ([Grasso, 2011](#)) .

The U.S Geological Survey (USGS) estimates the rare earth world production in 2014 of 110,000 t rare earth oxides (with 95,000 t REO from China alone) and the global reserves of 130,000,000 REO ([USGS, 2015](#)). Beside China, other

countries that notably produced REE in 2014 were: USA, Russia, Australia, India, Thailand, Malaysia and Vietnam.

China is the only country in the world that can produce and offer all specifications of rare earths, because it produces both the light and heavy REE. It is the only country that has the complete production chain for the REE industry, ranging from mineral processing to final product manufacture. Consequently it continues to monopolize the global supply of rare earths. In the last years China decided to issue no new mining licenses and reduced the official export quotas of REE. This policy coupled with a growing global demand for REE led to a sharp increase in REE prices, which caused the so-called REE Crisis. Consequently the search for new alternative sources of REE has become very serious.

1.5 Fieldwork and strategy in Jbel Boho

The Jbel Boho igneous complex was first described by [Choubert \(1952\)](#) as an igneous complex composed of a syenitic core surrounded by widespread volcanic lava flows, which he described as basalts, andesites and trachytes, that reach dozens of kilometres from the complex center and intercalate with the lower parts of the sequence of carbonate rocks which were being deposited at the same time. These observations were later confirmed by [Leblanc \(1981, 1971\)](#) and therefore the Jbel Boho magmatism was initially classified as calcalkaline. More descriptions of the Jbel Boho complex and its coeval sedimentary rocks were recently reported by [Alvaro et al., \(2006\)](#) who demonstrated the alkaline nature of the magmatism using geochemical data.

The lavas and intercalated sediments at Jbel Boho dip moderately to the south, meaning that a north-south transect covers the stratigraphic sequence (Fig 1.6). The basaltic rocks are intercalated with the lower dolomites north of the complex. Further south (i.e. up-sequence) the lavas become progressively more differentiated (trachyandesite/trachyte and rhyolite) although locally basalts also occur in this sequence. The syenitic pluton, which intrudes the volcanics, was the next magmatic event to affect the area. The dyke swarm, which cuts both the volcanics and the syenite, represents the late magmatic activity of Jbel Boho. Evidence for hydrothermal activities associated with the Jbel Boho igneous rocks is expressed by the occurrence of many late hydrothermal quartz carbonate veins with different thicknesses and directions, which within all rock types of the complex.

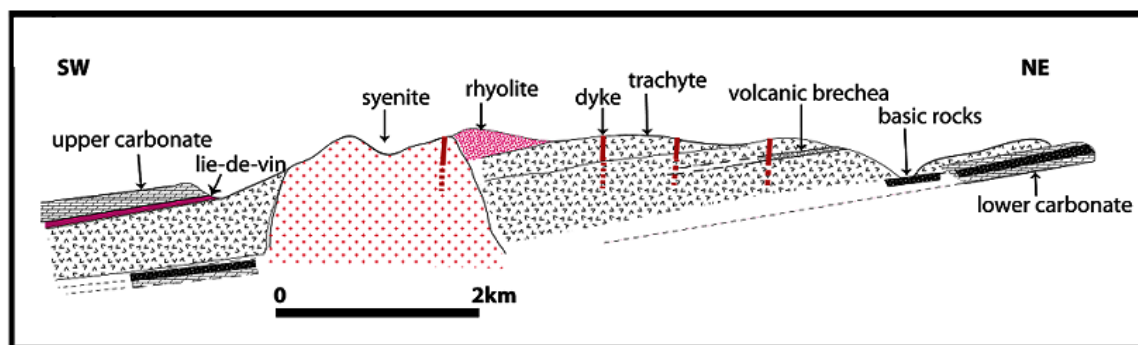


Figure 1.6 Cross section through the Jbel Boho complex showing NE-SW trend of its related rocks.

The aim of this work is to understand the magmatic evolution and the associated REE mineralization. Following this general introduction (**Chapter1**) the study goes into more detail in the two next chapters.

Chapter 2 focused on the magmatic rocks and the geological processes. Based on the field observations, a systematic sampling from the north to the south of the complex was carried out in order to cover the whole suite of rocks that crop out in Jbel Boho. Detailed mineralogical and geochemical analyses were conducted to best classify and identify the different Jbel Boho igneous rocks as well as to understand their petrological and genetic relationships and the processes leading to high REE enrichment and mineralization.

In **chapter 3**, the hydrothermal quartz carbonate veins were investigated further by exploring their mineralogy and geochemistry in order to understand the nature of the hydrothermal fluids and the conditions of REE ore deposits formation. For this we performed fluid inclusion and mineral chemical studies on the ore-bearing veins and propose a model for its formation as well as metal complexing in aqueous solutions by which means REE ores are formed.

The major outcomes of this study are a confirmation of the alkaline nature of the Jbel Boho complex, although some late intrusive dykes with rhyolite composition are subalkaline. Geochemical indicators are in agreement with tectonic reconstructions in suggesting an intraplate setting for the formation of the complex. Three periods of magma generation led successively to the emplacement of the volcanics, the syenite pluton and the dykes. The whole

complex shows high LREE enrichment over the HREE with REE mineralization mainly in the form of the REE-F-Ca carbonate mineral synchysite-(Ce).

References:

- Álvaro, J.J., Ezzouhairi, H., Vennin, E., Ribeiro, M.L., Clausen, S., Charif, A., Ayad, N.A., Moreira, M.E., 2006. The Early-Cambrian Boho volcano of the El Graara massif, Morocco: Petrology, geodynamic setting and coeval sedimentation. *Journal of African Earth Sciences* 44, 396–410.
- Blein, O., Baudin, T., Chèvremont, P., Soulaïmani, A., Admou, H., Gasquet, P., Cocherie, A., Egal, E., Youbi, N., Razin, P., Bouabdelli, M., Gombert, P., 2014. Geochronological constraints on the polycyclic magmatism in the Bou Azzer-El Graara inlier (Central Anti-Atlas Morocco). *Journal of African Earth Sciences* 99, 287–306. doi:10.1016/j.jafrearsci.2014.04.021
- Bouabdellah, M., Hoernle, K., Kchit, A., Duggen, S., Hauff, F., Klugel, A., Lowry, D., Beaudoin, G., 2010. Petrogenesis of the Eocene Tamazert Continental Carbonatites (Central High Atlas, Morocco): Implications for a Common Source for the Tamazert and Canary and Cape Verde Island Carbonatites. *Journal of Petrology* 51, 1655–1686.
- Castor, S.B., Hedrick, J.B., 2006. Rare Earth Elements, in: *Industrial Minerals Volume*. Society for Mining, Metallurgy, and Exploration, Littleton, Colorado, pp. 769–792.
- Chakhmouradian, A.R., Wall, F., 2012. Rare Earth Elements: Minerals, Mines, Magnets (and More). *Elements* 8, 333–340.
- Chakhmouradian, A.R., Zaitsev, A.N., 2012. Rare Earth Mineralization in Igneous Rocks: Sources and Processes. *Elements* 8, 347–353.
- Chalouan, A., Michard, A., El Kadiri, K., Negro, F., de Lamotte, D.F., Soto, J.I., Saddiqi, O., 2008. The Rif Belt, in: *Continental Evolution: The Geology of Morocco*. Springer-Verlag, Berlin Heidelberg, pp. 203–302.
- Choubert, G., 1952. Geologie du Maroc: Histoire géologique du domaine de l'Anti-Atlas, in: *XIX^e Congrès Géologique International, Monographies Régionales 3*. Rabat, pp. 75–195.
- De Lamotte, D.F., Zizi, M., Missenard, Y., Hafid, M., Azzouzi, M., Maury, R.C., Charrière, A., Taki, Z., Benammi, M., Michard, A., 2008. *The Atlas System, Continental Evolution: The Geology of Morocco*. Springer-Verlag, Berlin Heidelberg.

- Gasquet, D., Ennih, N., Liégeois, J.-P., Soulimani, A., Michard, A., 2008. The Pan-African Belt, in: Michard, A., Saddiqi, O., Chalouan, A., de Lamotte, D.F. (Eds.), *Continental Evolution: The Geology of Morocco*. Springer, Berlin Heidelberg, pp. 33–64.
- Gasquet, D., Levresse, G., Cheilletz, A., Azizi-Samir, M.R., Mouttaqi, A., 2005. Contribution to a geodynamic reconstruction of the Anti-Atlas (Morocco) during Pan-African times with the emphasis on inversion tectonics and metallogenic activity at the Precambrian–Cambrian transition. *Precambrian Research* 140, 157–182.
- Grasso, V.B., 2011. Rare earth elements in national defense: background, oversight issues, and options for Congress, Congressional Research Service, CRS Report for Congress.
- Gysi, A.P., Williams-Jones, A.E., 2013. Hydrothermal mobilization of pegmatite-hosted REE and Zr at Strange Lake, Canada: A reaction path model. *Geochimica et Cosmochimica Acta* 122, 324–352.
- Hoepffner, C., Soulimani, A., Piqué, A., 2005. The Moroccan Hercynides. *Journal of African Earth Sciences* 43, 144–165.
doi:10.1016/j.jafrearsci.2005.09.002
- Kanazawa, Y., Kamitani, M., 2006. Rare earth minerals and resources in the world. *Journal of Alloys and Compounds* 408-412, 1339–1343.
doi:10.1016/j.jallcom.2005.04.033
- Kynicky, J., Smith, M.P., Xu, C., 2012. Diversity of Rare Earth Deposits: The Key Example of China. *Elements* 8, 361–367.
- Leblanc, M., 1971. Faible teneurs de Niobium dans un filon lamprophyrique du volcan Infracambrien, calco-alcalin, du Jbel Boho (Anti-Atlas central). *Service d'Etudes des Gites Minéraux (S.E.G.M) N° 913*, 5.
- Leblanc, M., 1981. The late Proterozoic ophiolites of Bou Azzer (Morocco): evidence for Pan-African plate tectonics. *Developments in Precambrian Geology* 4, 435–451.
- Linnen, R.L., Samson, I.M., Williams-Jones, A.E., Chakhmouradian, A.R., 2014. Geochemistry of the Rare-Earth Element , Nb , Ta , Hf , and Zr Deposits, in: Holland, H.D., Turekian, K.K. (Eds.), *Treatise on Geochemistry: Second Edition*. Elsevier Ltd., Oxford, pp. 543–568. doi:10.1016/B978-0-08-095975-7.01124-4

- Mariano, A.N., Mariano, A., 2012. Rare Earth Mining and Exploration in North America. *Elements* 8, 369–376.
- Mclennan, S.M., Taylor, S.R., 2012. Geology , Geochemistry , and Natural Abundances of the Rare Earth Elements, in: Atwood, D.A. (Ed.), *The Rare Earth Elements: Fundamentals and Applications*. John Wiley & Sons, pp. 1–19.
- Michard, A., Hoepffner, C., Soulaïmani, A., Baidder, L., 2008. The variscan belt, in: *Continental Evolution: The Geology of Morocco*. pp. 65–132.
doi:10.1007/978-3-540-77076-3_3
- Michard, A., Soulaïmani, A., Hoepffner, C., Ouanaimi, H., Baidder, L., Rjimati, E.C., Saddiqi, O., 2010. The South-Western Branch of the Variscan Belt: Evidence from Morocco. *Tectonophysics* 492, 1–24.
doi:10.1016/j.tecto.2010.05.021
- Miyawaki, R., Nakai, I., 1993. Crystal structures of rare earth minerals, in: Gschneidner, K.A., Eyring, L. (Eds.), *Handbook on the Physics and Chemistry of Rare Earths*. Elsevier Science Publishers B.V., pp. 249–518.
- Mouttaqi, A., Rjimati, E.C., Michard, A., 2011. Moroccan Mines : An Introduction. *Notes et Mémoires du Service géologique du Maroc*. N°564 9, 13–22.
- Newman, H.R., 2012. The mineral industries of Morocco and Western Sahara, in: *US Geological Survey Minerals Yearbook - 2012*. pp. 1–9.
- ONHYM, 2013. Annual Report 2013. Office National des Hydrocarbures et des mines (ONHYM), Morocco.
- ONHYM, 2015. Les Terres Rares Au Maroc. Office National des Hydrocarbures et des mines (ONHYM), Morocco.
- Qalbi, A., Mouttaqi, A., Rjimati, E.C., Zemmouri, A., Michard, A., Saddiqi, O., 2011. The Nb-Ta-U-REE Prospects of the Glibat Lafhouda Carbonatites (Awserd Province). *Notes et Mémoires du Service géologique du Maroc*. N°564 9, 183–187.
- Sanematsu, K., Kon, Y., Imai, A., Watanabe, K., Watanabe, Y., 2013. Geochemical and mineralogical characteristics of ion-adsorption type REE mineralization in Phuket, Thailand. *Mineralium Deposita* 48, 437–451.
doi:10.1007/s00126-011-0380-5

- Sanematsu, K., Murakami, H., Watanabe, Y., Duangsurigna, S., Vilayhack, S., 2009. Enrichment of rare earth elements (REE) in granitic rocks and their weathered crusts in central and southern Laos. *Bulletin of the Geological Survey of Japan* 60, 527–558.
- Thomas, R.J., Fekkak, A., Ennih, N., Errami, E., Loughlin, S.C., Gresse, P.G., Chevallier, L.P., Liégeois, J.-P., 2004. A new lithostratigraphic framework for the Anti-Atlas Orogen, Morocco. *Journal of African Earth Sciences* 39, 217–226.
- USGS, 2015. Mineral Commodity Summaries - Rare earths.
- Walters, A., Lusty, P., 2010. Rare earth elements. British Geological Survey. Nottingham, Uk 1–45.
- Williams-Jones, A.E., Migdisov, A.A., Samson, I.M., 2012. Hydrothermal Mobilisation of the Rare Earth Elements - a Tale of “Ceria” and “Yttria.” *Elements* 8, 355–360.
- Woolley, A.R., 2001. Alkaline rocks and carbonatites of the world: Africa. Geological Society of London, pp. 187–192.
- Zerdane, A., Rjimati, E.C., Zemmouri, A., Mouttaqi, A., Michard, A., 2011. Aghracha Iron Mine and Uranium-REE prospect (Awserd Province). *Notes et Mémoires du Service géologique du Maroc*. N°564 9, 177–182.

CHAPTER 2

Magmatic evolution of the Jbel Boho alkaline complex in the Bou Azzer inlier (Anti-Atlas/Morocco) and its relation to REE mineralization

Abstract

The Jbel Boho complex (Anti-Atlas/Morocco) is an alkaline magmatic complex that was formed during the Precambrian-Cambrian transition, contemporaneous with the lower Adoudounian (Infracambrian) dolomite sequence. The complex consists of a volcanic sequence comprising basanites, trachyandesites, trachytes and rhyolites that is intruded by a syenitic pluton. Both the volcanics and the pluton are cut by later microsyenitic and rhyolitic dykes.

Although all Jbel Boho magmas were probably ultimately derived from the same, intraplate or plume-like source, our new geochemical evidence supports the concept of a minimum of three principal magma generations having formed the complex. Whereas all volcanics (first generation) are LREE enriched and appear to be formed by fractional crystallization of a mantle-derived magma, resulting in strong negative Eu anomalies in the more evolved rocks associated with low Zr/Hf and Nb/Ta values, the younger syenitic pluton displays almost no negative Eu anomaly and very high Zr/Hf and Nb/Ta. The syenite is considered to be

formed by a second generation of melt and likely formed through partial melting of underplated mafic rocks. The syenitic pluton consists of two types of syenitic rocks; olivine syenite and quartz syenite. The presence of quartz and a strong positive Pb anomaly in the quartz syenite contrasts strongly with the negative Pb anomaly in the olivine syenite and suggests the latter results from crustal contamination of the former. The late dyke swarm (third generation of melt) comprises microsyenitic and subalkaline rhyolitic compositions. The strong decrease of the alkali elements, Zr/Hf and Nb/Ta and the high SiO₂ contents in the rhyolitic dykes might be the result of mineral fractionation and addition of mineralizing fluids, allowing inter-element fractionation of even highly incompatible HFSE at high fluorine concentrations. The occurrence of fluorite in some volcanics and Ca-REE-F carbonate mineral synchysite in the dykes with very high LREE contents (Ce ~700 ppm found in one rhyolitic dyke) suggest the fluorine-rich nature of this system and the role played by addition of mineralizing fluids.

The alkaline, within-plate nature of Jbel Boho contrasts strongly with the subduction/obduction setting of the Bou Azzer ophiolite and calc-alkaline Ouarzazate Group which preceded it, implying a major change in the regional tectonics at this time.

2.1 Introduction

Rare earth element (REE) deposits are often associated with alkaline magmatic rocks. Deposits of economic importance are, for example, the syenite-hosted loparite $((\text{Ca},\text{La},\text{Na},\text{Ca},\text{Sr})(\text{Ti},\text{Nb})\text{O}_3)$ deposit in the Khibiny and Lovozero complex in the Kola peninsula, Russia, (~ 30,000 tonnes of ore with 34 wt% rare earth oxides (REO)), the syenite-hosted eudialyte $(\text{Na}_{15}(\text{Ca})_6(\text{Fe},\text{Mn},)_3\text{Zr}_3(\text{Si},\text{Nb})(\text{Si}_{25}\text{O}_{73}) (\text{O},\text{OH},\text{H}_2\text{O})_3(\text{Cl},\text{OH})_2)$ deposit in the Ilimaussaq alkaline complex in Greenland (~ 2 million tonnes with 1.5 wt% REO), and the Thor Lake syenite- and alkaline granite-hosted REE deposit in south-western Canada that contain about 65.6 million tonnes of ore with 2.53 wt% REO derived from monazite, allanite and REE-F-carbonate minerals (Orris and Grauch, 2002; Salvi and Williams-Jones, 2005). Economically relevant concentrations of REE in alkaline rocks most likely originate from fractional crystallization of primary mantle melts that led to the formation of evolved rocks with high REE contents (Chakhmouradian and Zaitsev, 2012). Understanding the magmatic evolution of alkaline magmatic complexes may therefore provide basic information to allow better identification, during prospection, of those rocks of a complex that may contain elevated REE concentrations.

Alkaline rocks are relatively rare on Earth (ca 1vol% of all igneous rocks) and, although the majority of them occur in extensional geodynamic settings (e.g. in the East African rift system in Kenya; Baker (1987)), they can also form in other geodynamic settings, namely in compressive regimes like the Tamazert alkaline

complex in the central high Atlas of Morocco ([Bouabdellah et al., 2010](#)) or even in the oceanic crust as exposed on Maio of the Cape Verde Islands ([Le Bas, 1987](#)).

Several alkaline provinces occur in Morocco: Oujda, Taourit, Rekkam, Azrou and Oulmes in the Middle Atlas and the Tamazert complex in the High Atlas, whereas the Saghro and Siroua complex are situated in the Anti Atlas. Until recently only the Tamazert alkaline complex in the central High Atlas ([Fig. 2.1](#)) was known for REE mineralization e.g., monazite, parasite and synchysite ([Woolley, 2001](#)). In the last years the Government's ONHYM (National Office for Hydrocarbon and Mines) published new exploration data with very promising Fe-Nb-REE concentration in the region of Ouled Dlim south of Morocco (Moroccan Mauritanides) ([Fig. 2.1](#)). It consists of Fe-carbonatite including three intrusions associated with Archean protoliths. The results show generally very high REE contents up to 3% ([Mouttaqi et al., 2011](#); [ONHYM, 2015, 2013](#); [Qalbi et al., 2011](#); [Zerdane et al., 2011](#)). In addition, this study reports the occurrence of REE mineralization in the late rhyolitic dykes in the Jbel Boho alkaline complex. [Leblanc \(1971\)](#) assumed a possible REE enrichment in the later alkaline intrusive dykes of Jbel Boho without testing this hypothesis by geochemical studies.

The Jbel Boho in the Bou Azzer inlier (Anti-Atlas) ([Fig. 2.1, 2.2](#)) is an alkaline complex that was first described by [Choubert \(1952\)](#) and later by [Leblanc \(1981a, 1971\)](#). Both authors focused on petrographic and structural descriptions,

whereas [Álvarez et al. \(2006\)](#) concentrated mainly on the coeval sedimentation and, to a lesser extent, on the magmatic evolution of the complex.

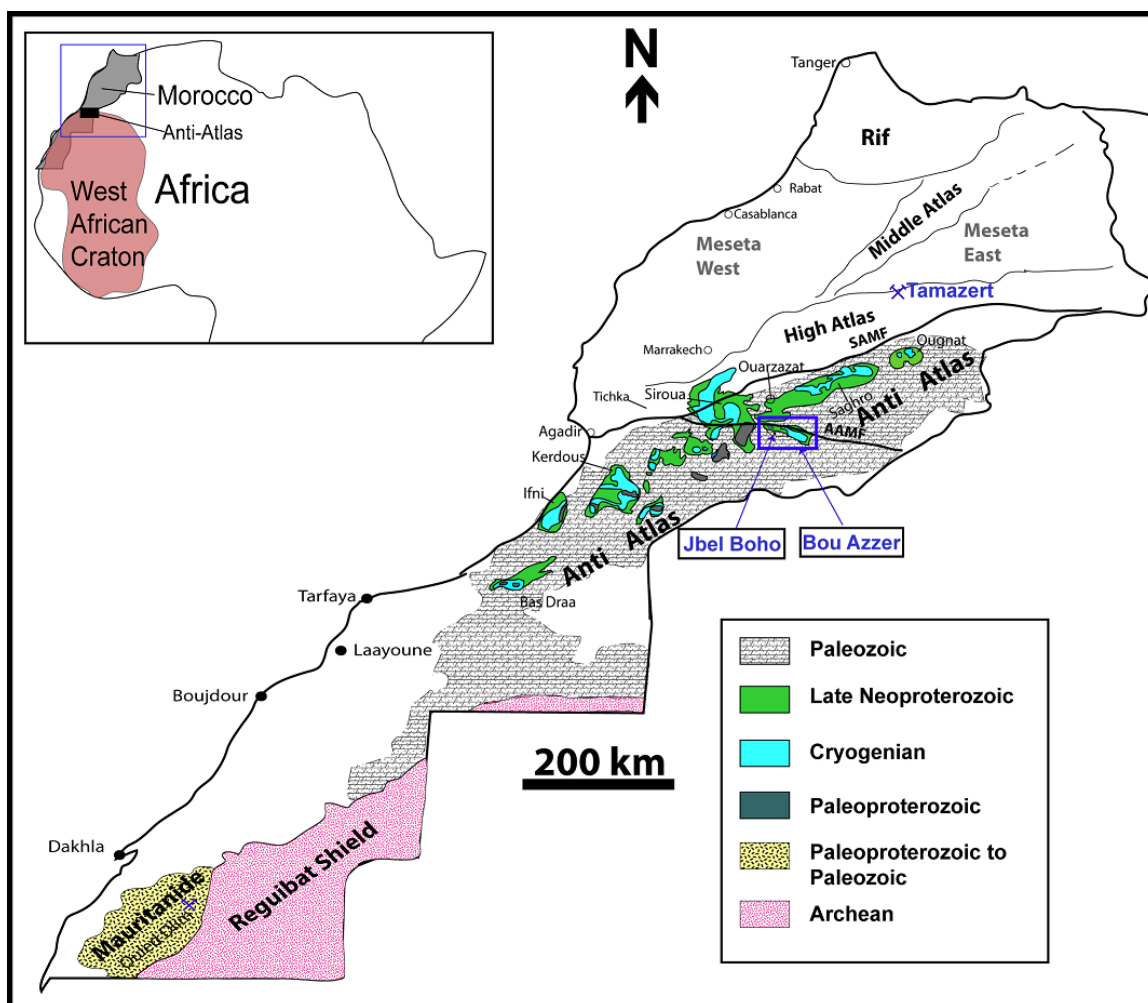


Figure 2.1 Geological map of the Moroccan Anti-Atlas showing schematically the major geological domains of Morocco (Rif, Meseta East and West, as well as Middle and High Atlas) with the Jbel Boho complex within the Bou Azzer inlier in the Anti-Atlas. The approximate location of the Tamazert alkaline complex in the High Atlas, the location of the REE carbonatite complex of Ouled Dlim in the Mauritanide and the names of cities and other locations are added for orientation. Map modified after [Gasquet et al., \(2005\)](#) and [Mouttaqi et al., \(2011\)](#)

The aim of the present study is to decipher in more detail the magmatic evolution of the Jbel Boho complex from primary to evolved rocks and the relationship of this evolution to the REE mineralization. We describe for the first time the occurrence of two types of syenites (olivine and quartz syenite) and of subalkaline rhyolitic dykes in the Jbel Boho complex as well as the occurrence of the Ca-REE-F-carbonate mineral synchysite in one subalkaline rhyolitic dyke.

Evolutionary trends related to three generations of melts of the Jbel Boho magmatic rocks are deduced from geochemical data: 1) An earlier magma generation resulted in the formation of basanite, trachyandesite, trachyte and rhyolite; 2) a second magma generation formed the syenite pluton and 3) the late dyke swarm (microsyenitic and rhyolitic dykes) with high concentrations of LREE in one rhyolitic dyke.

In addition we describe the mineralogy of the different rocks, the mineral assemblage of the syenitic pluton and the chemistry of the REE hosting mineral synchysite-(Ce) in the LREE-enriched dyke.

2.2 Geologic setting

The Moroccan Anti-Atlas is located south of the High Atlas and is separated from it by the South Atlas Major Fault (SAMF; [Fig. 2.1](#)). It is a large area of Precambrian rock-units that consist of several Proterozoic erosional windows that display the NE-SW oriented Pan-African structures along the northern boundary of the Paleoproterozoic West African Craton (WAC) ([Choubert, 1952](#); [Leblanc, 1981a, 1981b](#)). The Bou Azzer inlier is situated in the Central Anti-Atlas along the

NE-SW oriented Anti Atlas Major Fault (AAMF, [Fig. 2.1](#)). It is well-known for its Precambrian ophiolite with economically important cobalt mines ([Leblanc, 1981a, 1981b, 1972](#)). Since the discovery of this ophiolite complex, various Pan-African geodynamic settings have been proposed for its emplacement: Subduction zone setting with the subduction of the oceanic lithosphere towards the south ([Gasquet et al., 2005; Leblanc and Lancelot, 1980; Leblanc and Moussine-Pouchkine, 1994](#)), or towards the north ([Bousquet et al., 2008; El Hadi et al., 2010; Naidoo et al., 1991; Saquaque et al., 1989; Soulaïmani et al., 2006](#)). Geophysical magnetic studies support the hypothesis of the north dipping subduction zone ([Soulaïmani et al., 2006](#)). The actual location of the Bou Azzer ophiolite and the outcrops of the Eburnean basement restricted to the south of the AAMF led some authors to consider this fracture as the suture along the northern boundary of the WAC ([Bouougri, 2003; Bousquet et al., 2008; El Hadi et al., 2010; Hefferan et al., 2000; Leblanc, 1981b; Saquaque et al., 1989; Soulaïmani et al., 2003](#)), but other authors suggest that the so-called AAMF represent in fact an intracratonic aulacogen and the Bou Azzer ophiolite could be an allochthonous unit deriving from the north of the SAMF that would represent the northern boundary of the WAC ([Ennih and Liégeois, 2008, 2003, 2001; Gasquet et al., 2008](#)). However the above-mentioned geophysical magnetic study supports the interpretation that the AAMF represents a suture along the northern boundary of the WAC.

Models of the ophiolite emplacement by obduction with formation of a mélange between the ophiolite and the underlying continental margin (Bousquet et al., 2008; Hefferan et al., 2002; Saquaque et al., 1989) or by exhumation after subduction and collision that were associated with formation of syn-orogenic deposits (El Hadi et al., 2010) are still discussed. Both models are equally supported in the literature cited above and still exist as two different possibilities for the ophiolite emplacement.

Figure 2.2 shows a detailed geological map of the Bou Azzer inlier. This map displays the Neoproterozoic ages of the Tamaliout ophiolitic gabbro as well as the granitoids of Oumlil and Tazigzaout. Prior to 2006 the granitoids of Tazigzaout and Oumlil in Bou Azzer were considered to belong to the Paleoproterozoic basement. New geochronological data (U-Pb zircon dating) indicate Neoproterozoic ages for “augen granite gneiss” at Tazigzaout (750-700 Ma, D’Lemos et al., (2006)) and for the Oumlil granite (741 ± 9 Ma) as well as for the ophiolitic Tamaliout metagabbro (697 ± 8 Ma, El Hadi et al., (2010)) and for an ophiolitic plagiogranite (658 ± 8 Ma, Blein et al., (2014)). The Bou Azzer inlier therefore consists of several Neoproterozoic units that evolved during the emplacement of the ophiolite. The geochronological data are summarized in the simplified geologic map of Bou Azzer (Fig. 2.2). This map displays the Neoproterozoic ages of the Tamaliout ophiolitic metagabbro as well as the granitoids of Oumlil and Tazigzaout. Also shown are the U-Pb zircon ages from the much younger Jbel Boho syenite and the Aghbar trachytic sills, and a

porphyric basalt in the Bou Azzer mine area related to the base of the Adoudounian. All of which have similar Cambrian ages (syenite: 534 ± 10 Ma, [Ducrot and Lancelot \(1977\)](#); Aghbar trachyte: 531 ± 5 Ma [Gasquet \(2005\)](#) and Bou Azzer basalt: 541 ± 6 Ma [Blein et al., \(2014\)](#))

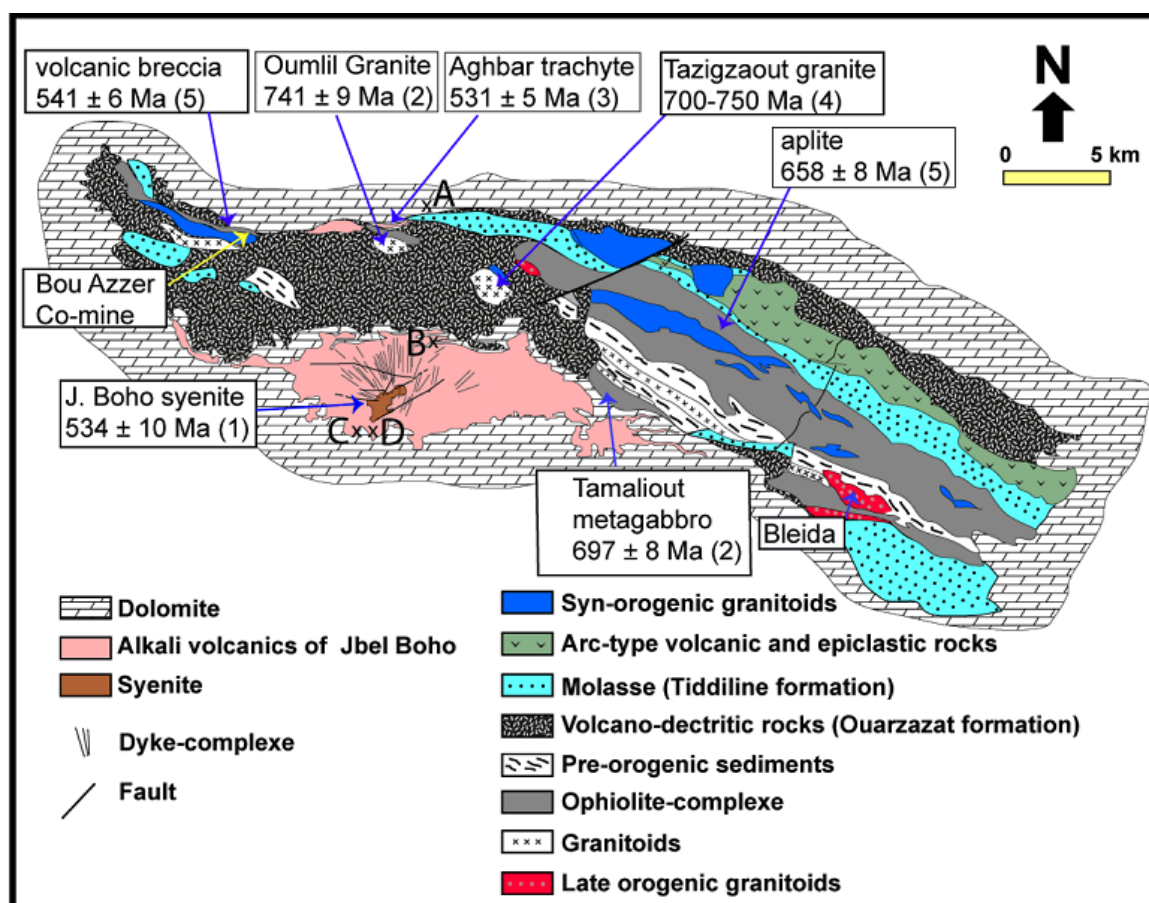


Figure 2.2 Simplified geologic map of the Bou Azzer and Jbel Boho with isotopic ages. Map modified after ([Leblanc, 1981](#)). Isotopic data from U-Pb zircon: (1) ([Ducrot and Lancelot, 1977](#)), (2) ([El Hadi et al., 2010](#)), (3) ([Gasquet et al., 2005](#)), (4) ([D'Lemos et al., 2006](#)), (5) ([Blein et al., 2014](#)). For A, B, C, D designations see Figure 3.

After the compressive phase of the Pan-African orogeny and the Bou Azzer ophiolite emplacement, the geodynamic situation changed to an extensional tectonic regime (Ezzouhairi et al., 2008; Gasquet et al., 2005; Thomas et al., 2004). In this new tectonic setting, calc-alkaline magmatism started. The related volcano-clastic rocks are part of the Ouarzazate Supergroup (580-550 Ma, up to ~2 km thick), which has been described in more detail by e.g. Gasquet et al. (2008, 2005) and Thomas et al., (2004, 2002). Following this magmatic stage, Adoudounian carbonates and red sandstone of the Lie-de-vin series were deposited on an epicontinental platform, which is attributed to a marine transgression on the northern edge of the WAC (Algouti et al., 2001; Piqué et al., 1999). The Jbel Boho alkaline complex was emplaced during this time under subaerial to shallow-water conditions as indicated by intercalation of Jbel Boho volcanic rocks with the lower Adoudounian dolomites. The Lie-de-vin series and the upper Adoudounian dolomites overlie the Jbel Boho volcanics (Álvaro et al., 2006; Choubert, 1952; Leblanc, 1981a).

The relationship of the Adoudounian dolomite and the Lie-de-vin series with the Jbel Boho volcanics is well exposed in the field. Figures 2.3 A-D show the intercalations of the lower dolomites with the volcanics (Fig. 2.3 A, B), the overlying upper dolomites (Fig. 2.3C) and the intercalation of the upper dolomites with the Lie-de-vin series (Fig. 2.4D). Figure 2.4 summarizes the stratigraphical sequence of the outcropping Bou Azzer units including the Jbel Boho complex.

As the main emphasis of the present study was on the magmatic evolution of the Jbel Boho alkaline complex, the regional geology of Bou Azzer is not described in detail. More information regarding the regional geology can be found e.g. in Blein et al. (2014), D’Lemos et al. (2006), El Hadi et al. (2010), Gasquet et al. (2008, 2005) and Villeneuve et al. (2010).

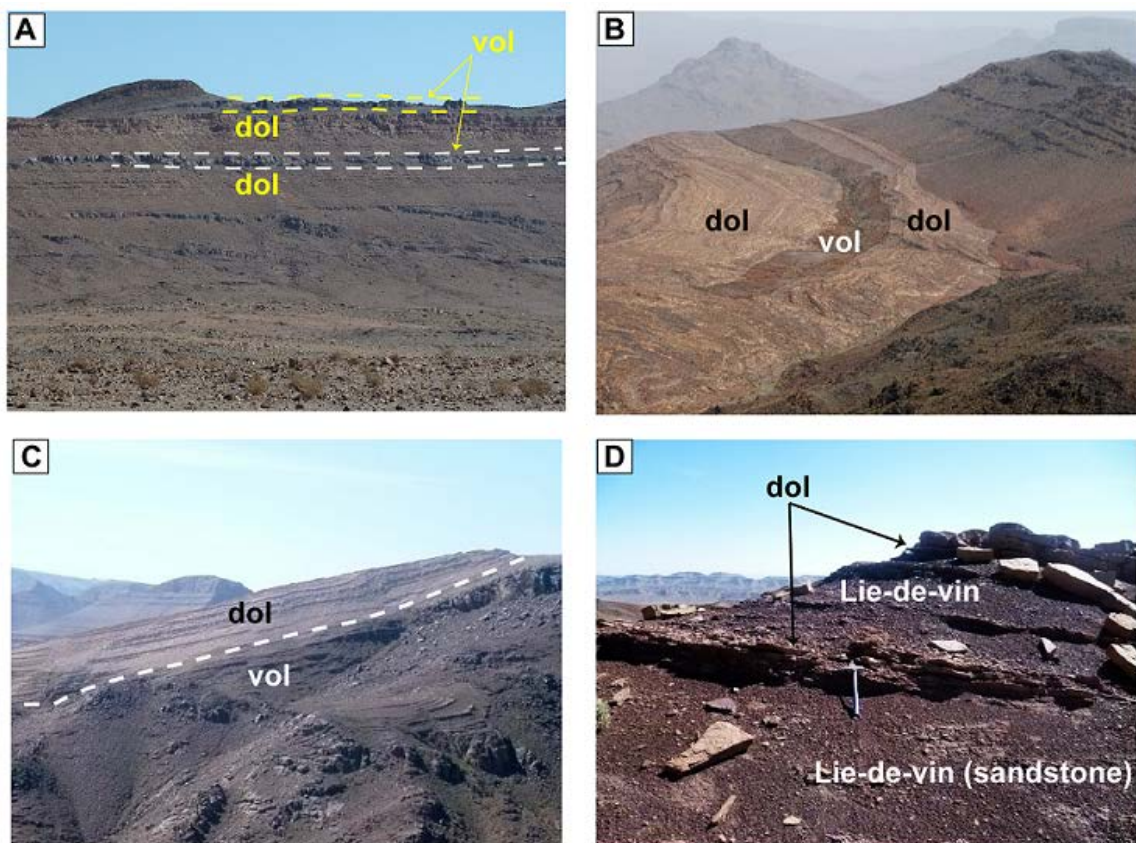


Figure 2.3 Intercalation of Jbel Boho volcanics with the Adoudounian dolomites north of Jbel Boho near Aghbar. A - view toward North; B – view toward east between the Ouarzazat formation and the Jbel Boho volcanics; C - view toward west with the upper dolomite covering volcanic rocks south of Jbel Boho, D - view toward east revealing the upper dolomite and the Lie-de-vin serie South of Jbel Boho. vol : volcanics, dol: dolomite.

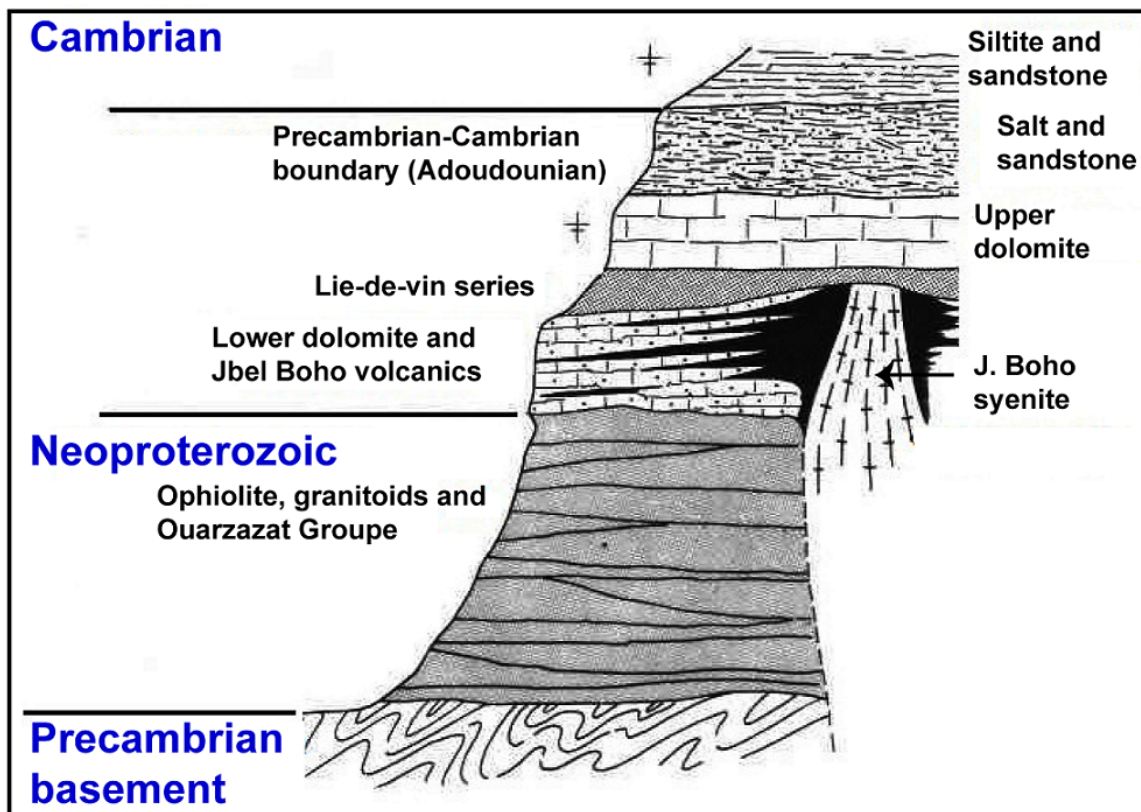


Figure 2.4 Stratigraphic column of the Bou Azzer sequence at Jbel Boho. Modified after [Ducrot and Lancelot \(1977\)](#).

2.3 Summary of field work

The Jbel Boho alkaline complex consists of three main igneous units: 1) a sequence of lava flows which become progressively more silica-rich up-sequence, 2) a polyphase syenite intrusion cutting the lavas and 3) a late suite of microsyenitic and rhyolitic dykes cutting the older sequence.

[Figure 2.5A](#) shows the geological map of Jbel Boho after [Leblanc \(1981a\)](#) including all sample locations. [Figure 2.5B](#) is a cross-section from the NE to SW through the Jbel Boho between the Adoudounian lower dolomites (north of the

complex) and the Adoudounian upper dolomite and Lie-de-vin series (south of the complex).

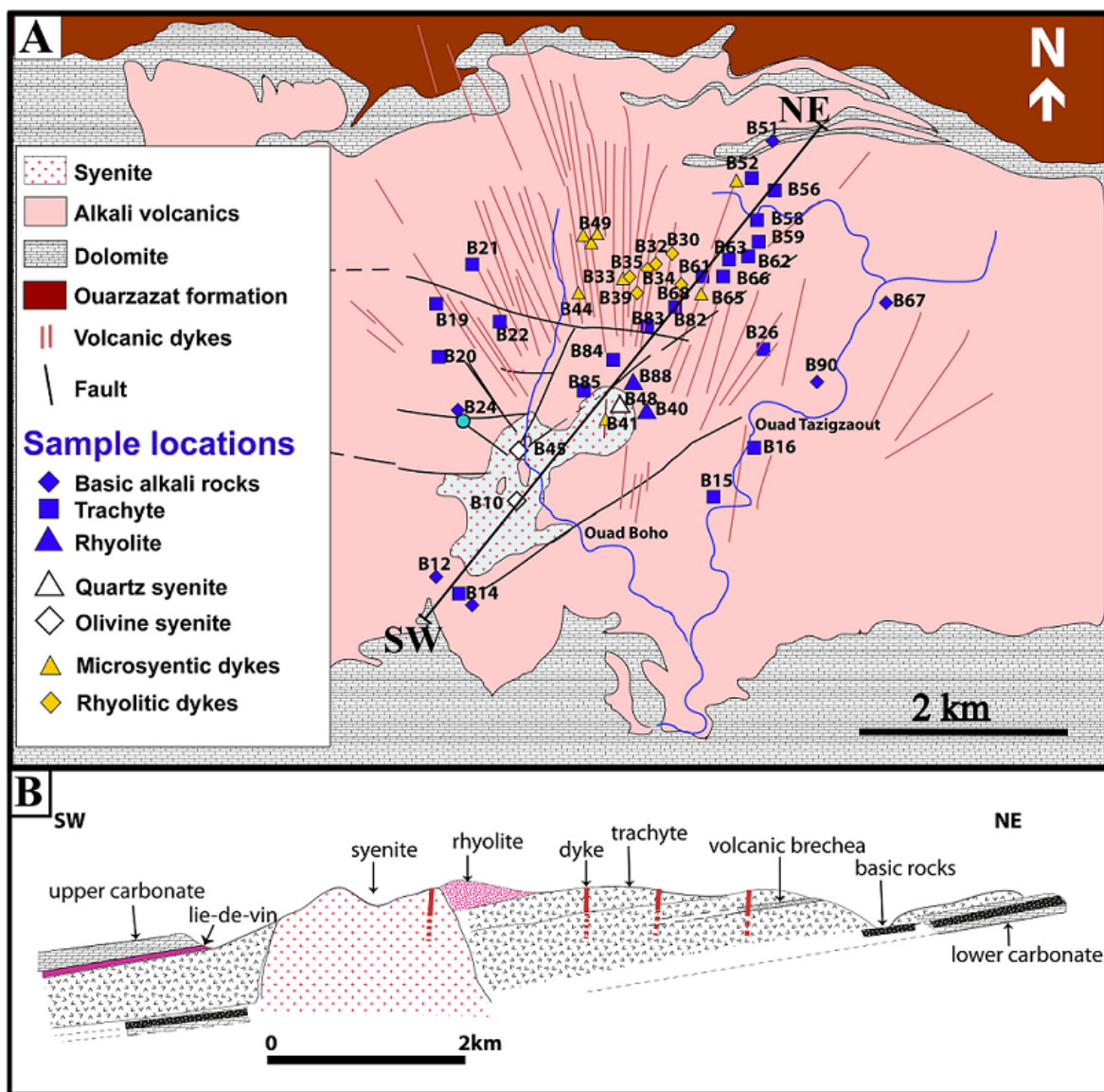


Figure 2.5 (A) Geological map of J.Boho showing the sample locations. (B) Geological NE-SW cross-section through the Jbel Boho complex showing an inclination of 30° towards south of the lava flows (trachyte, trachyandesite and trachydacite) and the volcanic breccia. Map modified after [Leblanc \(1981\)](#).

Figure 2.6A shows the field relations between the Jbel Boho volcanics and conglomerate. The inclination of the lava flows and the intercalated volcanic breccias and conglomerates is about 25° towards the south. The syenite pluton shows syenitic apophyses (with widths of up to 5 cm) within the adjacent volcanic rocks at the northern limit of the pluton (Figures 2.6B and 2.6C).

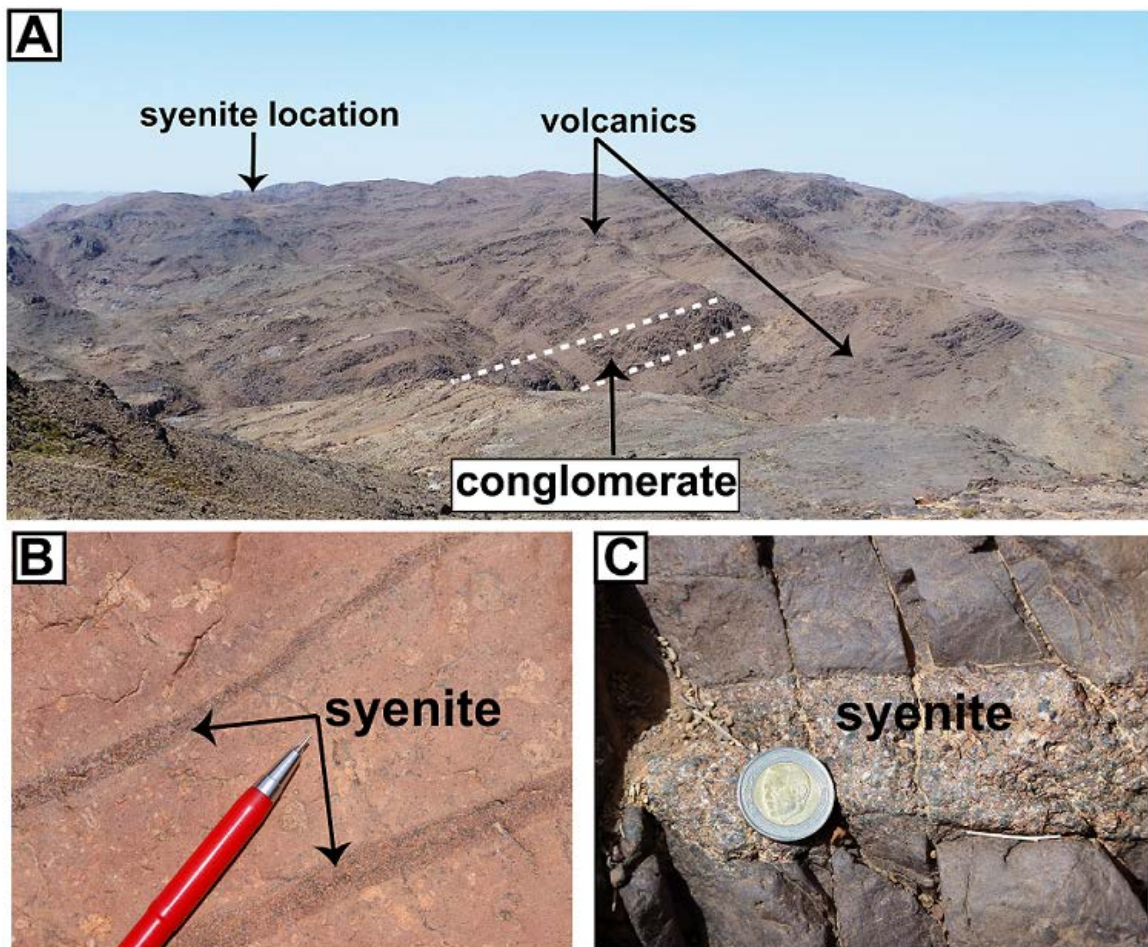


Figure 2.6 Conglomerate deposit with material from surrounding rocks interbedded with the Jbel Boho volcanics, with an inclination about 30° towards south, (view to the SE). B and C, Small syenitic apophyses within the adjoining volcanics at the northern border of the pluton.

The dyke swarm which cross-cut both lavas and pluton have a preferred orientation ranging from N20E to N20W. We performed systematic sampling through the stratigraphic succession of the Jbel Boho alkaline complex in order to cover all outcropping magmatic rock types for chemical analysis.

2.4 Petrography of the Jbel Boho rocks

2.4.1 *The alkaline volcanics*

The alkaline volcanic rocks sampled along the NE-SW profile ([Figure 2.5A](#)) range from basanit/tephrites, trachyandesites, trachytes and trachydacites to some alkali rhyolites. The dominant rocks of the complex are trachytes and trachydacites. The most basic members are mainly located in the lower part of the section. They are well exposed in the North (intercalated with the lower dolomites) and in the east along Ouad Tazigzaout ([Fig. 2.5A](#)). Locally, some basic rocks are also found south and northwest of the syenite, although they appear to be stratigraphically higher.

The basanites contain microphenocrysts of olivine and plagioclase in a microlitic matrix ([Fig. 2.7A](#)). The tephrites and phonotephrites contain larger phenocrysts predominantly of plagioclase ([Fig. 2.7B](#)), with olivine being less abundant or absent.

Most of the extrusive trachytes and trachydacites are very fine-grained and show a porphyritic texture in which large (up to 2cm) tabular phenocrysts of alkali feldspar are embedded in a very fine-grained feldspar-rich matrix. Small amounts

of plagioclase (magmatic), chlorite and fluorite (probably secondary) are also present (Fig. 2.7C). Some trachytes and trachyandesites show very fine-grained textures without phenocrysts, reflecting a change in the ascent and crystallization conditions of the magma.

Rhyolites occurring adjacent to the northern margin of the quartz syenite pluton can easily be distinguished in the field from other rock types by their reddish colour. The rhyolite has a texture similar to the trachyte, but contains fine-grained quartz crystals, Na-amphibole with fluorite inclusions and occasionally aegirine (Fig. 2.7D).

2.4.2 Syenite

The syenite of the Jbel Boho complex consists of two rock types: a coarse-grained reddish brown altered porphyritic quartz syenite and a coarse- to medium-grained pinkish altered olivine syenite, which forms the main volume of the pluton.

The quartz syenite (B48, Fig. 2.7E) contains tabular phenocrysts of alkali feldspar (> 70 vol%), dark green to blue-green Na-amphibole (arfvedsonite) and some quartz grains (0.5 to 2 mm in size). The quartz grains are generally interstitial between amphibole and alkali feldspar. Some Na-pyroxene (aegirine) and Ca-amphibole (hornblende) are also occasionally present. The most common accessory mineral is apatite. As a result of common alteration of aegirine and amphibole, iron oxides have been deposited in microcracks and veins in alkali feldspar.

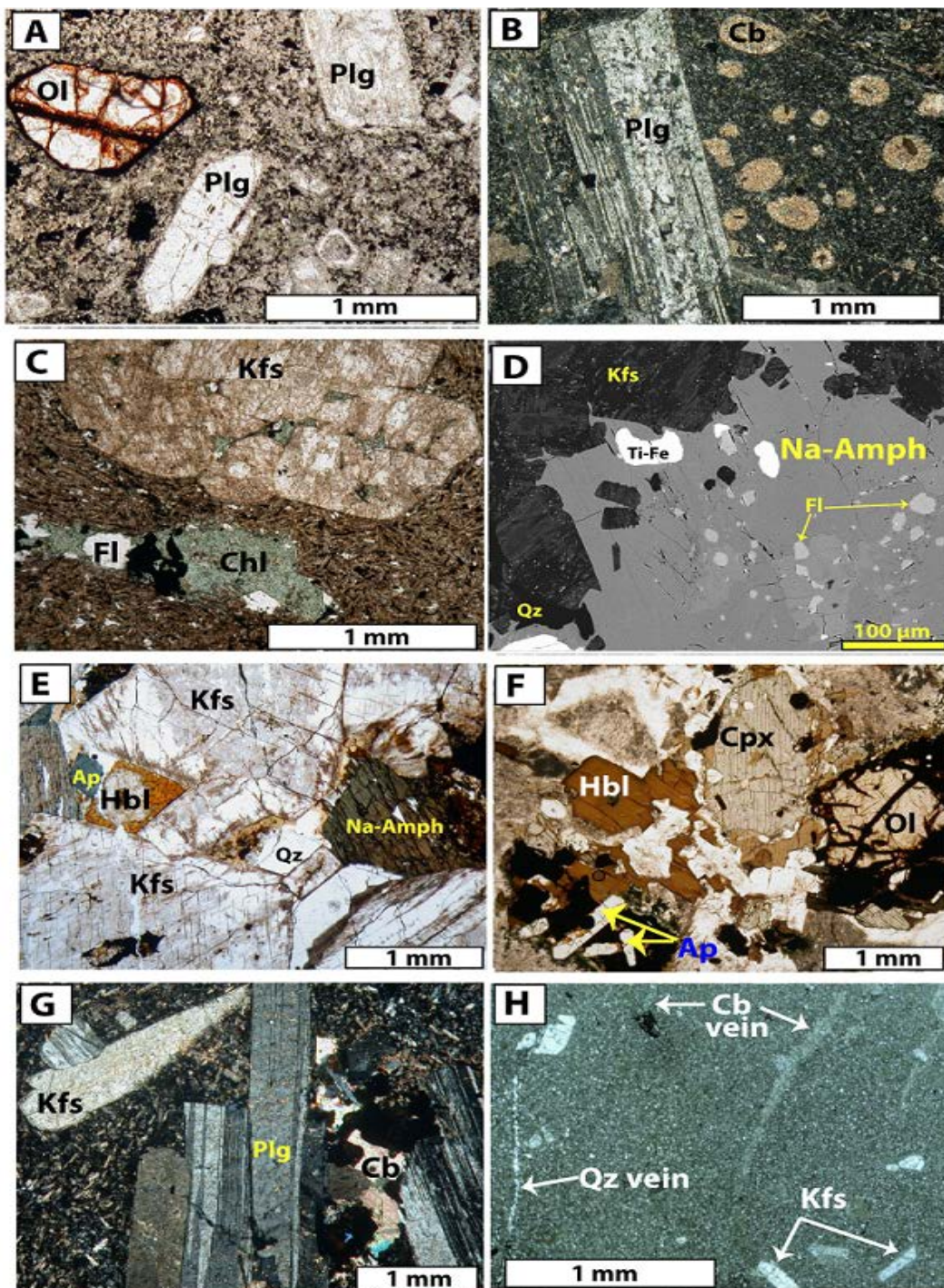


Figure 2.7 Photomicrographs of the main Jbel Boho magmatic rocks. (A) basanite B51-8, (B) phonotephrite B90, (C) trachyte B84, (D) rhyolite B88, (E) quartz syenite B48-3, (F) olivine syenite B10 (G) microsyenitic dyke B52 and (H) rhyolitic dyke B35. Mineral abbreviations from [Whitney and Evans \(2010\)](#)

The olivine syenite outcrops in the southern part of the pluton and is easy to identify thanks to its pink colour and coarse-grained texture. Fresh olivine occurs only in some locations, where a grey fresh syenite crops out within the altered pink syenite. The olivine syenite consists of alkali feldspar phenocrysts, pale green clinopyroxene (diopside), brown hornblende and sub- to anhedral fayalitic olivine. In the two thin sections studied (B10, B45) olivine and clinopyroxene are usually rimmed by biotite and brown amphibole (Figure 2.7F). The main accessory mineral is apatite. The opaque phases in both syenite types consist of Fe-Ti oxides. The grain sizes of clinopyroxene are up to 5 mm in length and of olivine and hornblende in the range of 1 to 2 mm. Dark small xenoliths (~10 cm) are also found in the olivine syenite. They consist of a similar mineral paragenesis as the syenite, but with more plagioclases and without hornblende.

2.4.3 Late intrusives: microsyenitic and rhyolitic dykes

Younger igneous rocks of Jbel Boho are represented by swarms of several vertical to sub-vertical dykes transecting all pre-existing igneous rocks. The dykes are parallel to sub-parallel and occur mainly on the northern flank of Jbel Boho (Fig. 2.5A). The dyke thicknesses range from 1m to 5m. The textures are porphyritic with feldspar phenocrysts. Their compositions generally range from trachyte to trachydacite (often named microsyenitic dykes in the literature) and subalkaline rhyolite. The different types of dykes are very difficult to distinguish in the field, as they all are pink in color and fine-grained with feldspar phenocrysts.

The microsyenetic dykes trend in N20E to N20W directions and are composed mainly of plagioclase and alkali feldspar phenocrysts (up to 2 cm in size) as well as chlorite and opaque phases (Fig. 2.7G). Some dykes show feldspar phenocrysts as large as 2 cm in the centre and only up to 0.3 cm at the margin of the dyke.

The subalkaline rhyolitic dykes (represented by samples B30, B32, B34, B35, B39 and B68), which are located near the northern border of the quartz syenite (Figure 2.5A) are described here for the first time. These silica-rich dykes trend mainly in a N-S direction and are composed of small amounts of alkali feldspar, chlorite, calcite and opaque altered minerals which occur in a quartz-rich matrix. Tiny quartz and carbonate veins are present in many of the late intrusives (e.g. Fig. 2.7H).

Leblanc (1971) reported the occurrence a late E-W lamprophyric dyke south of the syenite pluton cutting both the volcanic and the sediment cover. According to this author this dyke contains traces of niobium concentrated in biotites. Such dykes have not been sampled in the frame of the present study.

2.5 Analytical methods

A total of 53 samples were analysed for major and trace element concentrations, presented in Tables 2.1 to 2.5. The whole rock analyses were performed at the ACME Analytical Laboratories Ltd., Vancouver (Canada). Major element were analysed using X-ray fluorescence (XRF) on fused beads, which were prepared

with LiBO_2 flux. Loss on ignition was determined by ignition of sample splits at 1000°C to measure the weight loss. The analyses of the trace element concentrations were performed using inductively coupled plasma-mass spectrometer (ICP-MS) with 0.2 g of each sample fused with $\text{LiBO}_2/\text{Li}_4\text{B}_4\text{O}_7$ and 5% HNO_3 . The detection limits for major elements range between 0.001 and 0.1 wt% and for trace elements between 0.01 and 1 ppm. Minerals were analysed using the JEOL JXA 8900R electron microprobe of the Institute of Geosciences, University of Kiel, Germany. The microprobe measurement conditions were 15 kV accelerating voltage and 15 nA beam current.

2.6 Whole-rock compositions

2.6.1 Major elements

The Jbel Boho volcanics can be classified on the basis of their total alkali and silica contents ([Fig. 2.8](#)) into basanite/ tephrite/ phonotephrite/ basaltic trachyandesite (basic alkaline rocks), trachyandesite, trachyte, trachydacite and alkali rhyolite. The subdivision between the alkaline and the subalkaline fields (dashed line) is also on this figure ([Miyashiro, 1978](#)). From the basic to the most acidic volcanics the total alkalis gradually rise and then fall with increasing SiO_2 contents.

Table 2-1 Major (wt%) and trace element (ppm) contents of selected basic alkali volcanics of the Jbel Boho complex (* data from W. Schink, Pers.com)

Samples	Basic alkali volcanics								
	B24-1	B12-2	B51-7*	B51-8	B55-1*	B90	B67	B14-3	B14-1
SiO ₂	46	46.5	47.33	47.6	48.68	50.2	50.8	52.7	53.9
TiO ₂	1.32	1.83	2.06	2.03	2.78	1.73	1.92	1.24	1.29
Al ₂ O ₃	16.91	16.2	15.72	15.8	14.63	17	16.41	15.8	14.66
Fe ₂ O ₃	15.11	10.94	13.54	11.09	14.01	9	9.15	7.18	11.16
MnO	0.32	0.21	0.05	0.06	0.09	0.21	0.11	0.31	0.2
MgO	1.65	3.68	2.89	3.23	2.72	1.62	2	1.69	1.82
CaO	4.25	4.16	5.1	6.62	4.43	5.33	5.32	4.28	2.76
Na ₂ O	5.24	4.63	3.45	3.77	5.11	5.41	5.1	3.44	2.55
K ₂ O	2.02	3.66	2.99	2.88	2.97	4.26	3.02	5.49	4.87
P ₂ O ₅	0.41	0.29	1.01	1.02	0.65	0.61	0.6	0.36	0.47
LOI	5.82	7.08	5.65	6.65	2.91	5.3	5.75	6.88	4.88
Total	99.05	99.18	99.79	100.75	98.98	100.67	100.18	99.37	98.56
Ba	108	314	322	87	367	296	226	257	325
Rb	34.6	89.2	71.9	66.3	38.7	108	120.5	138	131
Sr	47.9	232.4	80.1	95.6	226	120.8	115.7	38.5	43.2
Zr	591.6	307.2	365.1	357.2	248.4	422.5	654.1	668.8	397
Nb	81.9	48	56.3	57.5	46.1	51.8	98.6	93.8	57.5
Ta	5.3	3.2	3.4	3.6	3	3	5.9	5.9	3.8
Hf	14	7.2	7.7	8.8	5.1	8.8	14.4	15.5	9
Pb	1.1	0.7	3.4	4.7	3	1.1	2.5	0.7	1.5
Th	11	5.2	4	3.9	4.1	5.8	12.7	12.9	10.4
Cs	0.2	1.4	1.7	2.7	0.2	3.1	1.1	1.9	1.2
U	2.4	3.8	1.2	1.2	2.2	2	5.4	3.6	3.5
Co	1	8.4	21.7	24.2	17.3	10.4	5.3	1.7	3.7
Zn	11	9	24	25	32	17	10	5	8
La	61.1	42.3	50.2	41.7	25	43.4	76.3	79.4	53.5
Ce	122.7	85	106.4	98.6	61.7	85.6	157.3	165.6	109.4
Pr	13.73	10.17	13.27	12.35	9.52	10.91	18.33	18.86	12.49
Nd	52.9	36	56.4	54.7	46.5	45.4	70.5	74.7	48.6
Sm	10.33	7.69	10.69	11.1	10.12	8.84	13.67	13.85	9.1
Eu	1.9	1.69	3.27	3.52	3.34	2.31	2.1	2.32	2.56
Gd	9.38	6.93	9.64	10.34	8.79	7.93	12.09	12.7	8.66
Tb	1.58	0.97	1.47	1.56	1.24	1.25	2.03	1.97	1.31
Dy	9.72	5.29	7.84	8.68	6.16	7.1	11.33	11.67	7.02
Y	48.7	28.2	39.8	42.8	27.7	33.4	56.7	57.2	39.8
Ho	1.97	1.07	1.66	1.63	1.15	1.27	2.08	2.26	1.47
Er	5.56	2.84	4.42	4.29	2.99	3.66	5.67	6.02	3.84
Tm	0.81	0.44	0.61	0.62	0.45	0.51	0.85	0.88	0.59
Yb	4.99	2.7	4.09	3.81	2.69	3.54	5.51	5.65	3.93
Lu	0.77	0.41	0.6	0.57	0.4	0.54	0.81	0.87	0.57
As	1.7	1.5	5.5	11.5	4.3	3.4	3.3	<0,5	1
Ga	40.8	23.1	20.8	19.8	15.3	20	30.7	27.1	23.2
Mo	1	0.2	1.7	3.7	<0,1	0.2	3.1	5.3	2.6
Cu	0.6	0.6	0.5	0.6	1.6	4.3	1.1	0.7	3.1

Table 2-2 Major (wt%) and trace elements (ppm) contents of selected trachyandesites and trachytes

Samples	Trachyandesite to trachyte										
	B14-2	B20	B19	B26-1	B52	B63	B16	B62	B15	B82	B22-1
SiO ₂	54.6	58.4	58.9	59.3	59.62	61.9	61.9	62.05	62.8	62.7	63.8
TiO ₂	1.41	0.89	0.89	1.01	0.94	0.46	0.53	0.4	0.35	0.57	0.4
Al ₂ O ₃	16.68	16.03	16.59	15.63	16.04	15.42	16.59	15.06	14.89	15.03	15.89
Fe ₂ O ₃	7.1	6.6	6.85	7.67	6.88	8.27	5.16	6.26	6.15	5.3	6.68
MnO	0.16	0.09	0.13	0.14	0.07	0.06	0.06	0.24	0.11	0.06	0.11
MgO	1.51	1.04	0.94	0.85	1.39	0.47	0.74	0.55	0.58	0.9	0.03
CaO	3.29	2.79	2.09	1.66	2.24	1.15	1.29	1.09	2.45	2.44	0.31
Na ₂ O	4.91	5.96	6.15	5.31	6.03	5.97	5.66	4.63	6.09	2.24	6.24
K ₂ O	4.45	4.38	4.65	5.77	3.83	5.08	5.42	6.64	2.77	8.1	4.69
P ₂ O ₅	0.55	0.23	0.22	0.27	0.27	0.05	0.14	0.05	0.03	0.09	0.04
LOI	4.67	2.98	1.94	1.69	2.47	1.89	1.69	0.95	3.09	3.15	0.99
Total	99.33	99.39	99.35	99.3	99.78	100.7	99.18	97.92	99.31	100.6	99.18
Ba	217	547	692	519	375	144	619	191	110	704	226
Rb	91	92	90.3	80.6	43.5	75.4	107.2	126.5	58	181.9	76.8
Sr	99.3	107.7	136.4	44.7	104.6	35.5	153.1	52.6	33.7	34.9	28.5
Zr	426.3	543.6	548.5	294.3	322.2	455.8	572.3	527.8	589.8	458.9	832.9
Nb	61.9	98.6	89.9	46.7	63.6	78.8	80.3	96.2	97.6	90.3	153.9
Ta	4	7.3	6.3	3.3	3.9	5.4	5	6.5	6.7	6	10.3
Hf	10.4	13.3	14	7.4	8.5	11.1	14.6	12.5	15.4	11.1	19
Pb	1.4	2.5	3.6	11.8	3.8	2.9	2.5	6.8	2.7	2	6
Th	10.5	15.3	13.1	5.2	6	12.1	14.4	14.6	11	12.8	21.1
Cs	0.7	0.5	0.5	1.3	0.3	0.4	0.6	0.4	0.5	0.8	0.4
U	3.3	4.7	3.9	1.3	2.5	5.6	4	3.1	1.7	2.2	4.6
Co	3.2	4.5	6.2	1.9	8.2	0.4	2.7	0.6	<0,2	0.6	1.1
Zn	11	20	81	74	19	29	21	33	23	8	8
La	27.6	68.6	76.5	41.9	26.6	67.8	73.7	70.3	87.2	61.7	139.4
Ce	59.8	136.5	149.6	89.6	55.5	132.3	145.4	139.5	177	114.5	262.1
Pr	7.17	15.54	17.06	10.52	7.56	15.95	16.19	17.56	19.95	13.97	30.32
Nd	27.7	59.6	63	41	34.3	63.6	60	67.5	79	53.2	117.6
Sm	6.14	11.18	11.67	7.7	7.24	11.04	11.21	12.62	14.12	10.7	21.45
Eu	1.34	2.12	2.47	3.31	1.91	1.45	2.46	1.19	0.95	1.71	2.26
Gd	6.72	10.59	10.87	7.29	6.29	9.81	9.69	11.19	12.95	10.1	17.75
Tb	1.19	1.65	1.61	1.1	1.06	1.67	1.52	1.83	2.08	1.7	2.63
Dy	7.46	10.14	9.38	5.59	6.38	9.67	9.6	9.96	12.7	9.55	16.48
Y	42.1	53.2	52.1	30.2	28.8	50.3	47.7	53.4	73.4	52.5	82.9
Ho	1.55	2.06	1.95	1.17	1.21	1.97	1.93	2.02	2.88	1.95	3.21
Er	4	5.87	5.68	3.15	3.4	5.5	5.54	5.49	8.31	5.86	8.7
Tm	0.63	0.9	0.83	0.44	0.52	0.82	0.8	0.77	1.24	0.85	1.23
Yb	3.94	5.77	5.45	2.76	3.34	5.04	5.12	5.72	6.98	5.83	8.04
Lu	0.58	0.82	0.81	0.43	0.52	0.8	0.75	0.83	1.04	0.79	1.17
As	4.5	1	3.4	1.9	<0,5	1.6	0.8	3.6	4.8	1.1	4.2
Ga	22.7	24.6	25.4	24.5	24.6	30.8	24.1	30.2	34.2	25.8	29.8
Mo	1.2	2.3	1.8	2.7	0.8	1.9	1.6	1.2	1.5	0.4	0.5
Cu	3.3	3.4	29.6	1.8	0.9	4.3	10.5	4.5	4.8	15.6	1.8

Table 2-3 Major (wt%) and trace elements (ppm) contents of selected trachytes and rhyolites.

Samples	Trachyte to rhyolite											
	B31	B56-2	B85-2	B84	B58	B56-1	B66	B83	B59	B24-2	B88-2	B40-3
SiO ₂	64.1	64.53	65.9	64.8	65.11	66.18	66.1	66.6	67	68.7	70.8	71.2
TiO ₂	0.42	0.44	0.36	0.54	0.42	0.45	0.42	0.45	0.37	0.41	0.3	0.28
Al ₂ O ₃	15.58	14.45	14.63	15.46	13.9	14.76	14	13.03	13.2	12.53	12.19	12.11
Fe ₂ O ₃	7.34	4.89	7.53	6.38	5.88	6.23	5.46	5.83	6.06	5.23	4.98	4.78
MnO	0.1	0.04	0.08	0.03	0.05	0.04	0.06	0.06	0.06	0.03	0.11	0.1
MgO	0.17	0.6	0.1	0.71	0.69	0.26	0.39	0.83	0.66	0.44	0.06	0.05
CaO	0.72	1.71	0.19	0.74	1.84	0.33	1.05	2.33	1.93	0.55	0.63	0.63
Na ₂ O	6.32	3.64	4.75	4.6	4.55	6.01	1.99	2.84	3.65	1.48	4.67	3.68
K ₂ O	4.75	6.63	5.72	5.31	4.56	3.91	8.85	5.15	4.57	7	5.29	5.9
P ₂ O ₅	0.05	0.04	0.03	0.08	0.03	0.04	0.03	0.03	0.03	0.04	0.02	<0,01
LOI	0.85	2.21	0.96	1.82	2.3	0.91	1.96	3.61	2.82	2.15	0.61	0.67
Total	100.4	99.18	100.3	100.5	99.33	99.12	100.3	100.8	100.4	98.56	99.66	99.4
Ba	166	579	380	272	333	247	598	227	263	273	77	76
Rb	77.1	125.3	102.8	103.4	86.3	66.9	148.1	110.3	100.3	111.9	216.8	189.1
Sr	44.7	62.9	18.5	25.4	52.2	40.5	27.7	26.5	57.7	23.7	16.6	32.2
Zr	405.7	550.2	649.4	526.3	746.2	535.2	698.3	816.4	696.5	1586	1046	860.4
Nb	89.5	95.5	105.3	90.3	122.5	93.8	117.8	131.6	113.1	230	140.8	123
Ta	6.1	6.7	7.6	6.3	8	7	8	9.7	7.6	17.4	12	13.4
Hf	10.9	13.8	16.9	12.9	17.8	14.9	16.7	20.8	16.6	40.5	26.8	29.2
Pb	5.8	6	4.5	1.3	12	5.1	16.7	3.2	5.5	2.2	11.7	6.3
Th	9	13.9	16.3	12.1	15.7	15.9	14	21.8	17.6	49	35.1	28.1
Cs	0.5	0.8	0.6	0.7	0.4	0.5	0.9	0.7	1.1	0.6	0.8	1.6
U	0.7	3.3	6.6	3.8	1.6	5.3	3.4	4.5	10.5	14.7	7.6	4.8
Co	0.2	2.2	11.2	3.4	7	1	1	0.9	1.7	2.6	0.5	0.3
Zn	24	7	4	8	13	5	11	11	13	6	57	112
La	74.1	92.1	118.2	67.1	95.9	127.9	221.1	98.1	103	178.6	138.2	150.8
Ce	155.7	178.8	218.8	134.7	189.8	200.6	448.1	194.3	195	328.4	258.6	301.9
Pr	17.61	20.9	24.95	15.21	22.77	26.73	49.83	22.45	24.72	33.9	30.64	33.13
Nd	73.7	75.7	94.9	62	82	95.9	189.6	85.6	97.7	111.3	117.4	121.9
Sm	12.63	12.77	16.29	11.56	15.96	16.55	35.28	16.08	18.6	19	20.88	22.86
Eu	1.27	1.34	1.44	1.58	1.3	2.02	3.21	1.72	1.67	2.43	1.18	1.12
Gd	10.82	9.97	13.83	10.18	13.89	13.82	29.72	15.09	16.07	18.53	19.18	21.3
Tb	1.76	1.55	1.89	1.52	2.25	2.1	3.61	2.87	2.54	3.99	3.36	3.33
Dy	10.1	9.01	11.23	8.2	13.54	11.01	16.24	16.26	13.58	28.72	21.38	20.07
Y	48.8	55.5	60.1	46.9	75.7	59.1	76.7	83.1	65.4	157.8	116.3	110.7
Ho	2.02	1.99	2.29	1.76	3	2.2	2.76	3.22	2.48	6.19	4.34	4.03
Er	5.45	6.09	6.76	5.33	8.06	6.23	7.96	8.73	6.88	17.35	12.81	11.36
Tm	0.8	0.9	1.06	0.85	1.14	0.91	1.24	1.29	1	2.44	1.87	1.78
Yb	5.29	5.66	6.91	5.92	7.25	6.02	8.24	7.97	6.65	14.68	10.88	10.81
Lu	0.79	0.83	1	0.82	1.03	0.81	1.08	1.17	0.95	2.05	1.48	1.53
As	5	0.8	1.3	1.8	1.1	1.2	1.6	2.8	0.8	4.4	4.9	0.9
Ga	32.2	29.4	24.7	30.6	32.8	31.6	22.7	36.6	29.8	19.1	33	32.1
Mo	0.8	1.9	0.6	1.4	1	0.7	0.6	5.2	1.7	5.2	1.2	8.9
Cu	0.6	0.8	286.1	148.6	13.5	0.6	90.2	3.8	1.1	2.8	2.4	4.9

Table 2-4 Major (wt%) and trace elements (ppm) contents of selected quartz syenite, olivine syenite and microsyenitic dykes

Samples	Qz-syenite				Ol-syenite		Microsyenitic dykes			
	B48-2	B48-3	B48-4	B48-5	B10	B45	B33	B41	B44-1	B44-2
SiO ₂	62	61.9	62.6	62.3	53	55.6	65.7	64.8	61.7	65.1
TiO ₂	0.68	0.7	0.62	0.61	1.54	0.83	0.6	0.42	0.67	0.61
Al ₂ O ₃	15.49	15.42	16.09	15.98	18.36	20.15	13.94	13.58	14.97	13.08
Fe ₂ O ₃	6.95	6.95	5.77	5.41	7.63	4.44	4.31	2.57	2.34	2.08
MnO	0.24	0.27	0.28	0.09	0.18	0.11	0.06	0.08	0.1	0.11
MgO	0.52	0.51	0.46	0.95	1.64	0.85	1.54	0.35	0.33	0.15
CaO	1.37	1.42	1.12	1.7	4.31	4.13	2.11	4.53	5.09	5.13
Na ₂ O	5.95	5.84	5.56	5.57	6.62	7.36	4.39	5.08	5.08	4.31
K ₂ O	5.55	5.79	5.83	5.52	4.2	3.63	4.01	4.45	5.31	5.21
P ₂ O ₅	0.16	0.15	0.19	0.15	0.42	0.24	0.1	0.05	0.12	0.05
LOI	1.17	1.26	1.9	2.4	1.13	1.49	2.99	4.12	4.71	4.75
Total	100.1	100.2	100.4	100.7	99.03	98.83	99.75	100	100.4	100.6
Ba	772	877	980	939	325	463	219	301	322	284
Rb	91.5	94.2	92.3	80.9	78.6	62.6	75.6	68.7	93	83.4
Sr	142.7	153.6	161	142.2	463.5	688.6	34	39.8	54.7	48
Zr	446.6	468.6	304.7	464.5	730.2	484	731.2	669.1	1307	2063
Nb	78.6	81.7	58.1	76.5	109.5	75.8	112.3	111.3	208.5	316.6
Ta	5.7	5.5	3.9	5.3	6.8	4.7	8.3	8.2	14.5	21.5
Hf	11.3	10.5	7.2	11.1	14.8	9.9	19.2	16.6	30.9	48
Pb	33.6	45.8	12.6	5.6	4.8	2.9	1.3	1.8	2.8	2.9
Th	9.9	11	6.4	10.7	13.4	9	21.8	16.8	30.7	50.4
Cs	1.7	3	2.4	1.3	2.2	1.4	0.5	0.3	0.5	0.5
U	2.9	3	2.3	2.8	4.1	2.8	6.3	4.1	8.4	13.6
Co	2.1	1.6	1.9	2.3	11.6	5.5	6.8	1.7	1	0.6
Zn	143	147	582	43	20	19	11	5	8	10
La	61.8	60.1	50.6	58.9	66.6	50.6	129.7	66.8	116.5	140.8
Ce	127.9	122.1	106.1	117.8	134.2	93.8	256.6	141.7	234	286.3
Pr	15.23	14.51	12.46	13.96	14.78	10.28	28.87	16.35	26.39	31.95
Nd	61.1	56.1	50.5	58.1	51.8	35.5	109.7	63.5	94.2	121.7
Sm	11.28	10.73	9.29	10.27	10.27	6.54	19.83	13.12	17.5	23.14
Eu	2.83	2.84	2.82	2.81	2.46	2.88	2.07	2.18	2.09	2.7
Gd	9.21	9.4	8.22	8.99	9.06	6.16	15.49	11.89	14.47	20.54
Tb	1.59	1.55	1.29	1.53	1.42	1	2.32	2.11	2.62	4.03
Dy	8.97	8.89	7.4	8.75	8.37	5.53	13.18	12.55	16.43	27.13
Y	47.1	48.4	35.9	46	46	30.6	73.5	65.1	90.7	148.3
Ho	1.78	1.71	1.44	1.68	1.63	1.13	2.45	2.45	3.41	5.57
Er	5.01	4.98	3.86	4.75	4.71	3.16	7.73	7.07	10.18	16.16
Tm	0.75	0.75	0.6	0.73	0.73	0.47	1.08	1.03	1.57	2.43
Yb	5.04	4.9	3.77	4.97	4.67	3.15	6.84	6.86	10.13	16.23
Lu	0.73	0.72	0.58	0.66	0.65	0.47	0.98	0.97	1.49	2.35
As	4.3	4.3	2.8	2.9	2.4	1.3	0.5	0.6	0.8	1.5
Ga	29.7	29.2	29.7	29.2	30	27.3	26.3	22.3	31.3	23.2
Mo	2.6	2.7	2.5	3.5	5.7	4.2	1.5	4.2	3	2.1
Cu	1.9	2.4	2.2	13.4	10.4	5.2	4.3	3.2	0.9	2.9

Table 2-5 Major (wt%) and trace elements (ppm) contents of selected microsyenitic and rhyolitic dykes

Samples	Microsyenitic dykes					Rhyolitic dykes					
	B52-4	B65-1	B49-1	B-49-2	B49-3	B30	B32	B34	B35	B39	B68
SiO ₂	59.39	66.1	60.4	61.2	65.6	73.7	70.3	75.8	78.3	72.6	71
TiO ₂	1.14	0.34	0.77	0.82	0.55	0.28	0.46	0.3	0.28	0.33	0.36
Al ₂ O ₃	17.51	16.14	13.24	13.97	13.84	11.31	12.98	10.02	9.77	10.27	12.95
Fe ₂ O ₃	4.37	4.78	7.3	5.76	4.85	2.26	3.65	2.48	2.84	2	3.94
MnO	0.06	0.01	0.15	0.12	0.07	0.04	0.04	0.05	0.02	0.05	0.02
MgO	1.14	0.72	0.97	1.22	1.38	1.29	1.2	1.03	1.22	0.33	1.31
CaO	2.93	0.19	4.07	4.67	1.82	1.94	1.2	2.04	0.72	3.48	0.53
Na ₂ O	6.72	3.88	4.95	5.38	4.27	2.4	3.21	1.84	4.19	2.42	2.35
K ₂ O	4.31	6.86	2.76	2.38	4.77	3.32	4.97	3.8	1.21	4.73	5.46
P ₂ O ₅	0.37	0.04	0.1	0.09	0.06	0.01	0.05	<0,01	<0,01	<0,01	0.02
LOI	2.17	1.68	4.71	4.89	3.26	3.47	2.41	2.96	1.7	3.82	2.37
Total	100.1	100.7	99.42	100.5	100.5	100	100.5	100.3	100.3	100	100.3
Ba	1162	382	105	133	194	172	299	145	56	236	235
Rb	48.2	146.6	77.7	40.4	77.6	108	103.2	109.9	25.5	83	124.8
Sr	135	41.1	32.5	36.6	19.3	98	28.9	21.3	22.1	26.4	18.3
Zr	533	996.4	1492	1432	778.5	1103	963.8	1362	1387	1372	1565
Nb	77.3	139.7	262.5	261.7	131.7	147.2	152.7	201.2	191.9	207	235.2
Ta	5.4	8.4	17.6	18.5	8.4	12	11.9	15.4	15	15.3	17
Hf	10.7	24.4	35.7	35.6	18.2	26.8	25.6	34.4	32.9	34.4	36.6
Pb	2.2	3.3	3.6	2.7	4.9	2	1.8	1.6	1.9	2.9	1.4
Th	13.9	22.7	39.4	41.1	17.2	33	29	36.9	40.9	43.5	35.3
Cs	0.4	1.8	0.6	0.2	0.4	1.9	0.9	1.3	0.4	0.8	1
U	21.8	5.3	12.1	13.1	5.7	12.5	8.3	11.8	10.1	9	9.6
Co	6.3	0.8	2	1.9	13.5	5.6	4.3	4.9	6.4	2.6	1.8
Zn	26	7	21	21	6	8	10	7	7	4	8
La	115.1	58.3	167.1	84.2	56.3	83.3	111.2	149.9	378.4	81.7	89.7
Ce	219.1	113.8	322.8	190.7	117.4	169.4	214	283.6	718.9	161.6	171.8
Pr	25.14	14.07	35.67	21.02	13.67	19.45	24.67	31.81	84.45	18.54	20.33
Nd	97.1	59	130.7	78.9	54.1	73.8	90.3	113.3	335.6	68.8	79.1
Sm	11.24	12.97	21.93	17.01	10.39	13.76	16.49	20.58	52.8	14.84	15.59
Eu	2.24	1.54	1.77	2.12	1.64	2.29	1.46	1.32	7.45	1.97	1.66
Gd	7.53	15.56	17.61	17.56	9.73	13.4	13.93	16.82	35.73	15.21	16.81
Tb	1.14	3.3	3.16	3.2	1.83	2.99	2.41	3.01	4.07	3.08	3.88
Dy	6.97	19.25	19.67	20.3	12.15	19.37	14.74	19.19	21.38	20.31	26.61
Y	35.5	93.2	105.9	109.7	67.7	99.1	90.3	123.3	124.6	121.3	133.4
Ho	1.44	3.65	3.97	4.08	2.69	3.93	3.12	4.22	4.31	4.39	5.32
Er	4.07	9.69	11.98	11.9	8	10.93	9.43	12.27	12.98	13.4	15.27
Tm	0.68	1.37	1.81	1.84	1.17	1.58	1.48	1.98	2.02	1.97	2.18
Yb	4.49	8.44	11.74	12.51	7.34	10.32	8.78	12.35	12.52	12.24	13.24
Lu	0.65	1.26	1.65	1.68	1.09	1.35	1.27	1.7	1.73	1.64	1.85
As	1.6	0.8	3.8	1.5	5.6	7.1	1.5	<0,5	3.1	3.4	2
Ga	22.2	33.5	35.3	29.3	25	24.9	26.7	33.4	12.1	19.6	41.8
Mo	0.7	0.4	11	8.4	4.8	3	0.8	0.4	<0,1	0.3	<0,1
Cu	1.1	0.9	17.9	63.5	4	0.6	9.7	0.5	1.3	1.1	15.5

The plutonic rocks (olivine bearing syenite and quartz bearing syenite) are also shown in the diagram for comparison. We note that the syenites have higher alkali contents than the volcanic rocks which they intrude. Both syenite types show relatively constant alkali contents over a range in SiO_2 . In contrast, the dykes show a clear decrease in alkalis with increasing SiO_2 and have trachytic to subalkaline rhyolitic compositions.

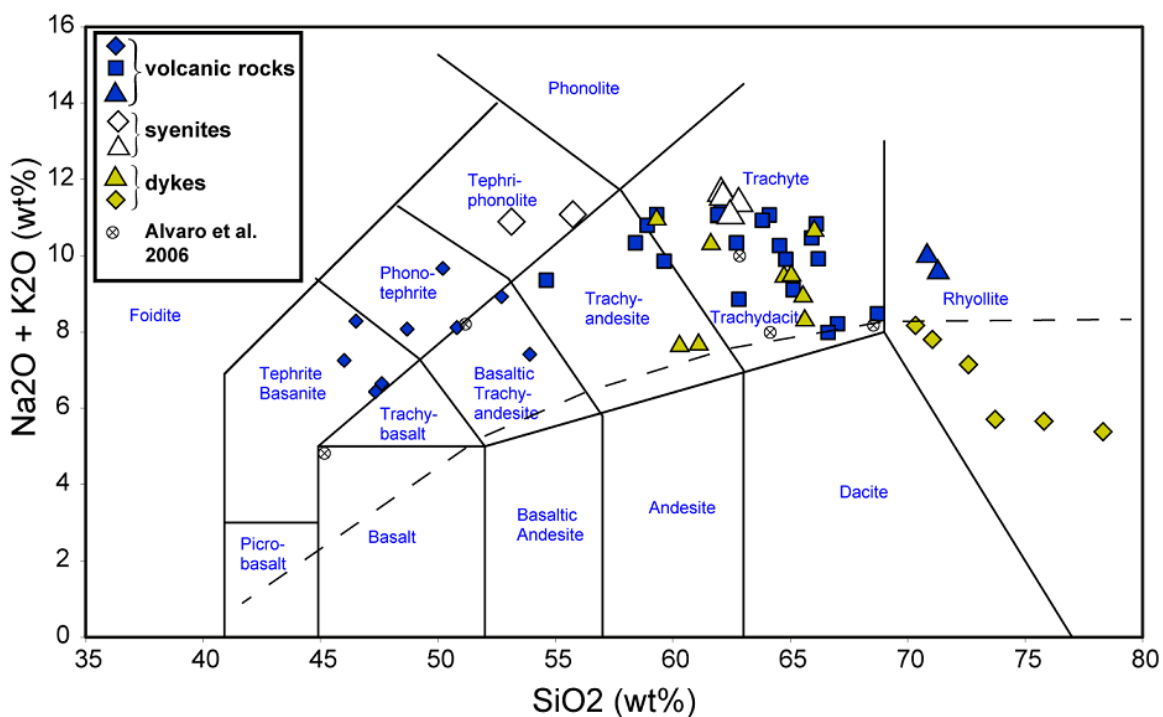


Figure 2.8 TAS diagram showing the compositional fields of the alkaline rocks of the Jbel Boho complex. Some rhyolitic dykes have high SiO_2 and low alkali contents. The data of [Alvaro et al. \(2006\)](#) are added for comparison. The alkaline subalkaline dashed line is from [Miyashiro \(1978\)](#).

Major element contents are plotted versus SiO_2 contents in Harker diagrams ([Fig. 2.9](#)). For the volcanic rock series, MgO, FeO, TiO_2 , P_2O_5 and CaO contents

decrease with increasing silica. The syenites and dykes generally follow these trends, although MgO in the dykes is not correlated with SiO₂ and some dykes have higher CaO at a given SiO₂ than the other rock types. The K₂O contents correlate with silica for all samples except the rhyolitic dykes, which show a negative correlation. The volcanics show no pronounced change in Al₂O₃ with increasing silica up to ca. 62wt.% SiO₂, after which Al₂O₃ then strongly decreases. This decrease is mimicked by the dykes.

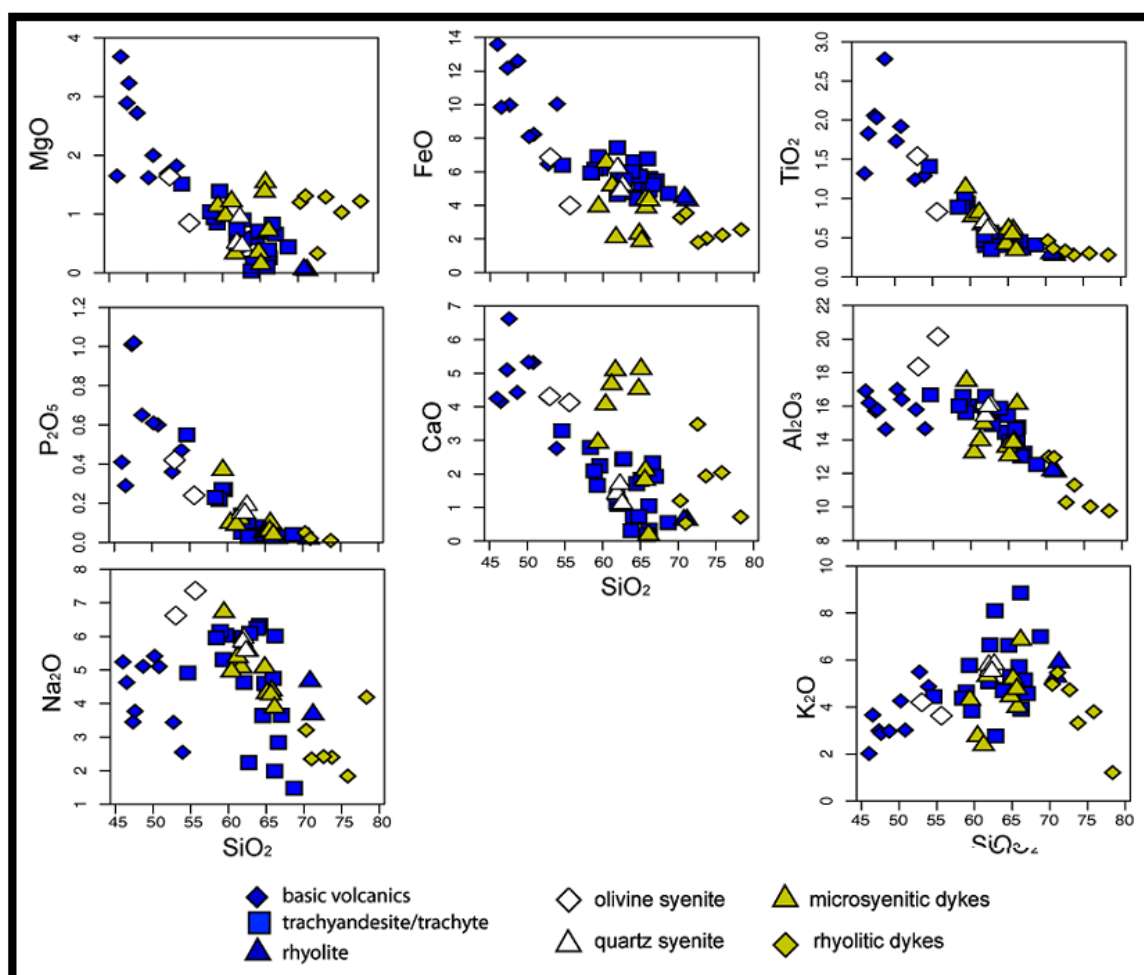


Figure 2.9 Harker variation diagrams for the rocks of the J.Boho alkaline complex. The magmatic evolution of the complex is reflected by the increase of SiO₂.

The olivine syenites do not lie on this trend. Na₂O displays no systematic variations with SiO₂ in the volcanics, but shows a strong negative relationship in the syenites and dykes. The quartz syenite and the microsyenitic dykes have, with the exception of high CaO contents in the latter, very similar major element compositions.

2.6.2 Trace and rare earth elements geochemistry

The Jbel Boho samples and their genetic relationships to one another can also be examined using trace element. To minimize the effects of post-crystallization element mobility on these studies, we have concentrated on the high-field-strength elements (HFSE) as they are not readily removed in solution as hydrated cations. Consistent with the TAS plot, the magmatic rocks show an alkaline affinity on the Zr/Ti vs Nb/Y diagram of Pearce (1996) (Fig. 2.10).

The HFSE (Nb, Zr, Ta, Hf) show very similar distribution in the Jbel Boho igneous rocks. They display little increase with increasing SiO₂ between 45-65 wt% SiO₂, after which the HFSE contents increase steadily. An exception to this statement is some of the microsyenite dykes, which show significantly higher HFSE concentrations (Fig. 2.11).

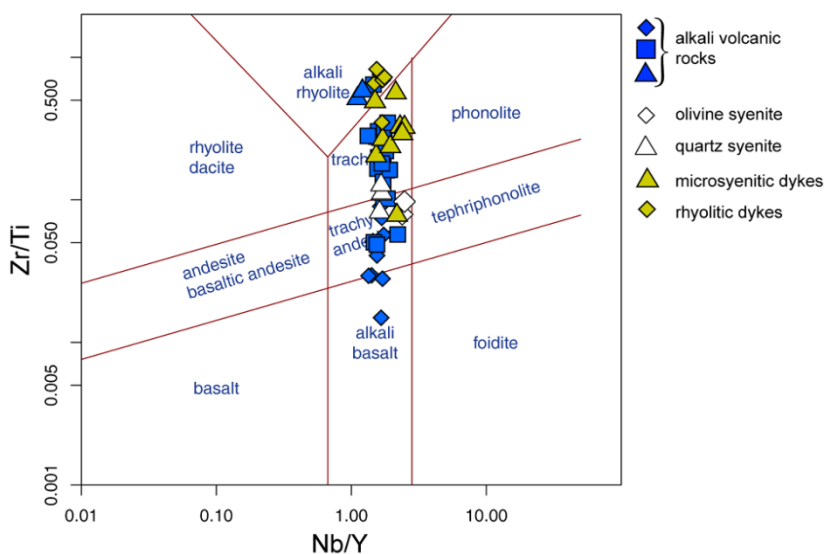


Figure 2.10 The Zr/Ti vs Nb/Y classification diagram after Pearce (1996) show alkaline magmatic affinity for the Jbel Boho magmatic rocks.

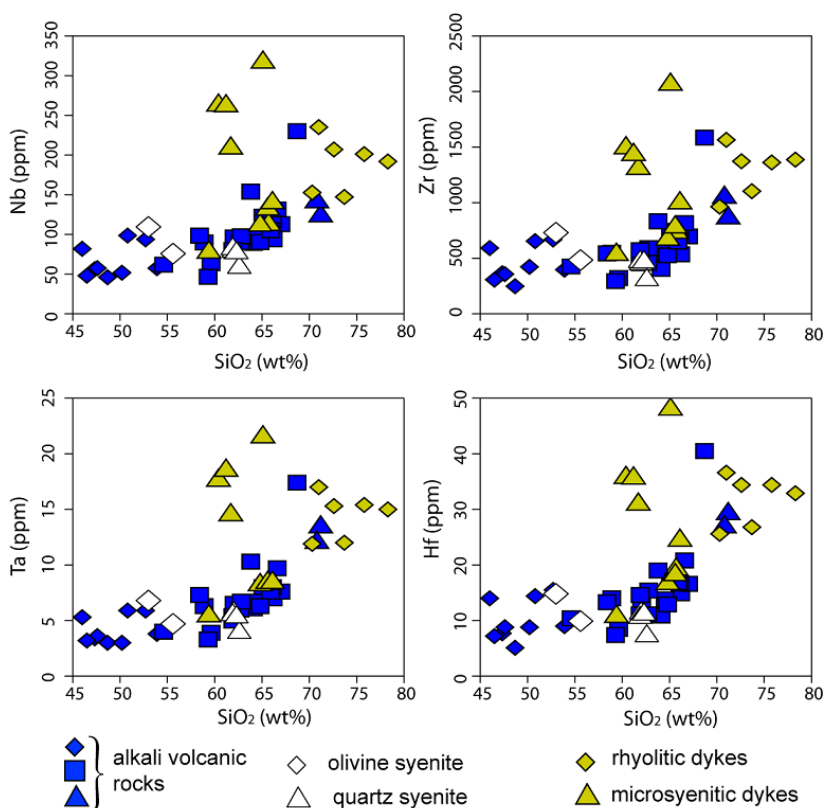


Figure 2.11 Plot of selected HFSE versus SiO₂. Note that the volcanics generally follow a trend of increasing HFSE with increasing silica above around 60% SiO₂ while the late dykes are less systematic in their variations.

In [Figure 2.12](#), the Nb/Ta and Zr/Hf ratios generally decrease with increasing SiO₂ in all rock types with the exception of the rhyolitic dykes, which show relatively constant Zr/Hf of 40. Nb/Ta ratios show an even clearer negative trend which in this case is also followed by the rhyolitic dykes. Relative to TiO₂, the two HFSE ratios show weak positive trends. According to the chondritic values of Zr/Hf (34.3) and Nb/Ta (19.9) measured by ([Münker et al., 2003](#)), the Jbel Boho magmatic rocks are generally over the chondritic value of Zr/Hf and under that of Nb/Ta.

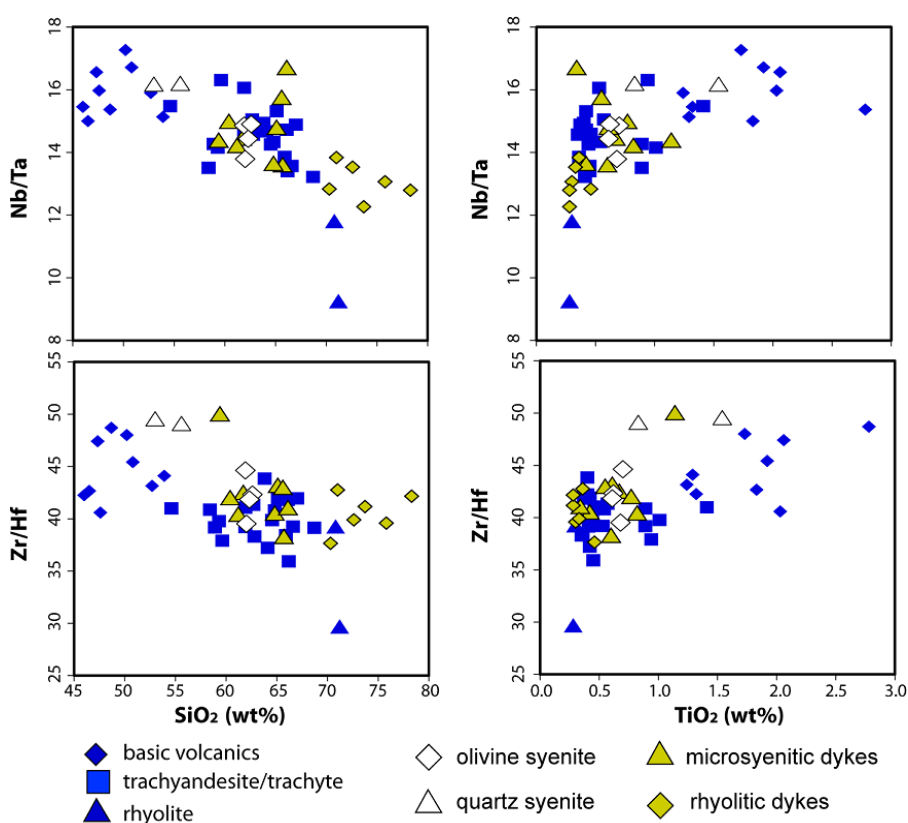


Figure 2.12 Plot of Nb/Ta and Zr/Hf ratios versus SiO₂ and TiO₂ to evaluate the relationships between the different magmatic rock types of Jbel Boho. Note that the progression from basic to silica-rich lithologies seen in the volcanics corresponds to a stratigraphic sequence.

On the tectonic discrimination diagram Ti-Zr after [Pearce \(1982\)](#) and the 2Nb-Zr/4-Y diagram after [Meshede \(1986\)](#) the Jbel Boho rocks lie in the field for rocks from an intraplate tectonic setting ([Fig. 2.13](#)).

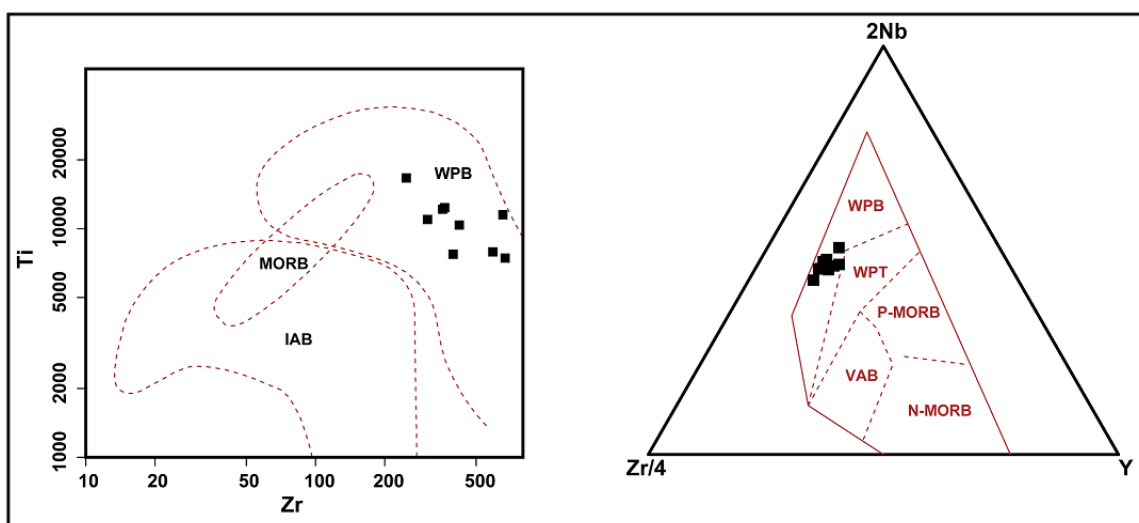


Figure 2.13 Tectonic discrimination diagrams for the Jbel Boho basaltoids, showing their intraplate magmatic affinity. Ti-Zr plot after [Pearce \(1982\)](#) and Zr/4-2Nb-Y plot after [Meschede \(1986\)](#). WPB (within plate basalt), WPT (within plate tholeiite), IAB (island arc basalt), VAB (volcanic arc basalt), MORB (mid ocean ridge basalt), N-MORB (normal MORB), P-MORB (plume MORB)

The similarity in trace element signatures of all Jbel Boho rocks is evident from the normalized REE and trace element plots shown in [Fig. 2.14](#). A strong enrichment of the LREE relative to the HREE and similar types of REE patterns with a ratio of LREE/HREE > 1 is evident in all samples. The diagrams are presented in stratigraphical order of the Jbel Boho magmatic rocks to facilitate the understanding of the geochemical evolution of the entire complex.

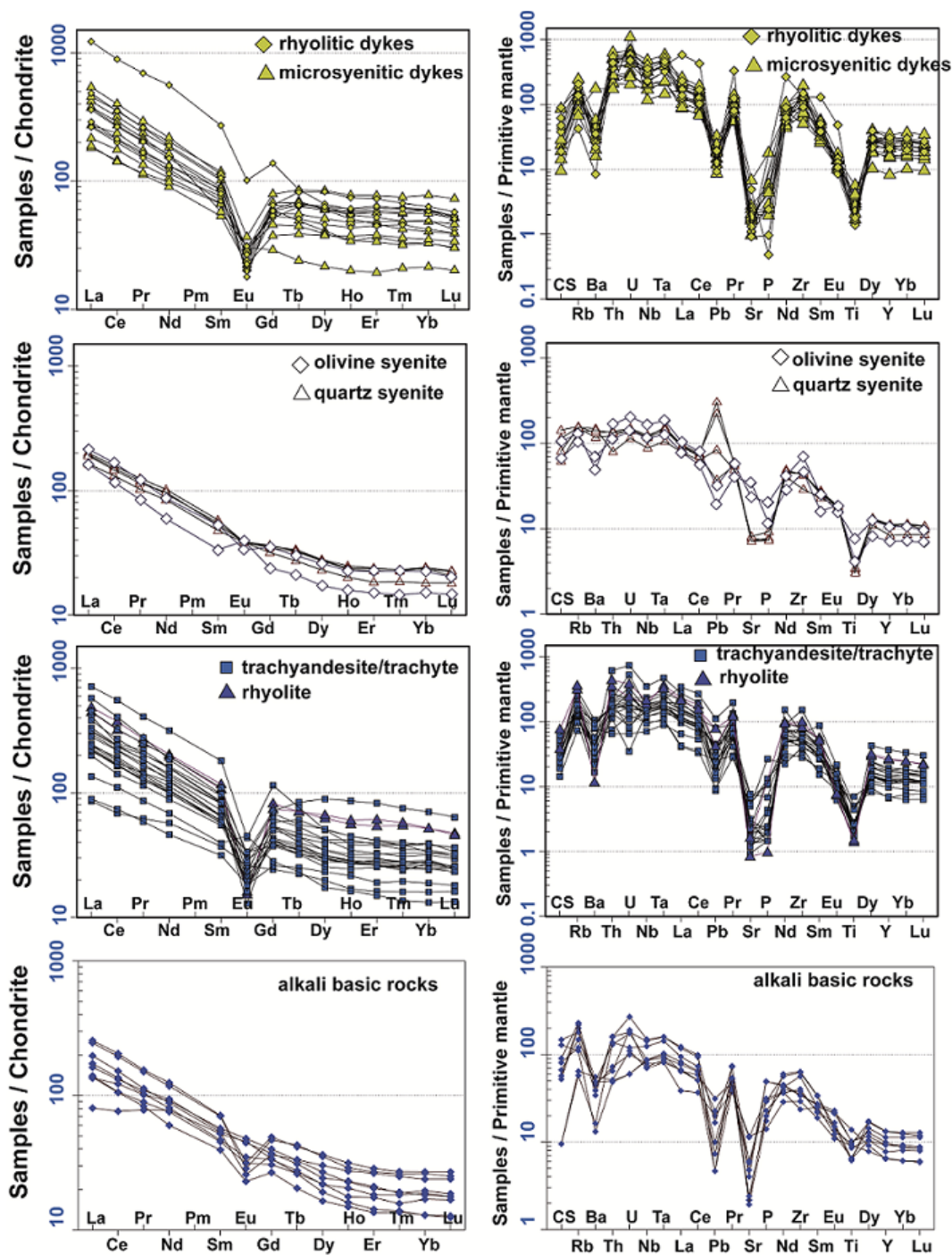


Figure 2.14 The REE (left column) and other trace elements pattern (right column) of the Jbel Boho igneous complex normalized to chondrite (Boynton 1984) and primitive mantle (McDonough and Sun 1995). The diagrams represent, from bottom to top, the relative chronology (from young to old) of the Jbel Boho rocks

The basic volcanic rocks show no or only slightly negative Eu anomalies with Eu/Eu^* from 0.5 to 1. The trachyandesites, trachytes and rhyolites display strong negative Eu anomalies, with Eu/Eu^* from 0.2 to 0.7, with the exception of sample B26-1 that has Eu/Eu^* about 1.3. All syenite samples but one (B45 with Eu/Eu^* about 1.3) show only very weak negative Eu anomalies (Eu/Eu^* between 0.75 and 0.95). The microsyenitic and rhyolitic dykes display pronounced negative Eu anomalies (Eu/Eu^* between 0.2 and 0.5). One rhyolite dyke (B35, see Figure 5) shows very high LREE contents, with e.g., Ce up to 720 ppm. This LREE enrichment is associated with the presence of the secondary LREE-Ca-F-carbonate mineral synchysite that is fine-grained and occurs only in the matrix.

The primitive mantle normalized trace element diagrams (right hand side of Figure 12) show similar sub-parallel patterns with negative Ti, P, Sr, Pb and Ba anomalies for all rocks except for the syenites, in which the negative anomalies of these elements are less pronounced. In contrast to all other Jbel Boho igneous rocks, the quartz syenite show only small negative or even distinctly positive Pb anomalies.

2.7 Mineral chemistry

Unlike the other differentiated alkaline volcanics of Jbel Boho, which show strong negative Eu anomalies, the quartz syenite shows no Eu anomaly and the olivine syenite shows a slight negative to positive Eu anomaly (Fig. 14E). Among the late intrusives one rhyolitic dyke (B35) displays much higher LREE contents than all other analyzed rocks of Jbel Boho (Fig. 2.14H).

In order to better understand how the syenites in particular fit into the magmatic evolution of the Jbel Boho complex and also to identify the minerals that are responsible for the high enrichments of LREE in dyke B35, microprobe analyses of the main minerals in the syenites and of the accessory REE mineral synchysite in the dyke B35 were performed. The mineral compositions of olivine, amphibole, clinopyroxene and synchysite are given in [Tables 2.6 – 2.9](#).

2.7.1 Olivine in the olivine-syenite

Olivine of the olivine syenite in Jbel Boho is generally subhedral, between 0.1 and 1 mm in size and is surrounded by broad rims of biotite and hornblende. Microprobe analyses show a fayalitic olivine type without regular zoning from the core to the rim, although at the border higher Fe contents were sometimes detected, resulting likely from alteration and oxidation. The fayalite contents in individual olivines vary slightly by up to ~ 3 mol % from Fa_{56} to Fa_{59} ([Table 2.6](#); 1-5) and reach Fa_{61} at the border. In some olivines (e.g., [Table 6](#); 7-10) the fayalite contents are somewhat higher in the range of Fa_{61} to Fa_{62} with higher fayalite content at the border (Fa_{65}). Small contents of manganese ($MnO \sim 2wt\%$) are present leading to calculated tephroite contents. Olivine was not observed in the quartz syenite.

Table 2-6 Representative microprobe analyses of olivine in the Jbel Boho olivine syenite.

Olivine analysis of the olivine syenite											
	1	2	3	4	5	6	7	8	9	10	11
SiO ₂	34.38	34.31	34.18	34.12	34.10	34.04	34.20	33.81	33.96	33.36	33.90
FeO	45.31	45.59	45.88	47.09	47.12	48.11	48.08	48.98	48.74	49.13	50.18
MnO	1.90	1.84	1.90	2.03	1.97	2.05	2.11	2.02	2.18	2.08	2.17
MgO	19.10	18.37	18.11	17.13	17.11	16.28	15.97	15.80	15.37	15.55	13.81
Total	100.69	100.11	100.07	100.37	100.30	100.48	100.36	100.61	100.25	100.12	100.06
Number of ions based on 4 O											
Si	1.01	1.01	1.01	1.01	1.01	1.01	1.02	1.01	1.02	1.01	1.03
Fe ²⁺	1.11	1.12	1.13	1.17	1.17	1.20	1.20	1.22	1.22	1.24	1.27
Mn	0.05	0.05	0.05	0.05	0.05	0.05	0.05	0.05	0.06	0.05	0.06
Mg	0.83	0.81	0.80	0.76	0.76	0.72	0.71	0.70	0.69	0.70	0.62
Endmember proportions											
Fo	41.89	40.83	40.31	38.33	38.31	36.64	36.18	35.57	34.97	35.11	31.98
Fa	55.74	56.84	57.28	59.09	59.18	60.74	61.10	61.85	62.21	62.22	65.17
Tp	2.37	2.32	2.40	2.58	2.51	2.62	2.72	2.58	2.82	2.67	2.85

2.7.2 Amphibole in quartz- and olivine-syenite

Two types of amphibole can optically be distinguished in the syenite: greenish to pale brownish Na-amphibole in the quartz syenite and brownish Ca-amphibole in the olivine bearing syenite.

The Na-amphiboles in the quartz syenite show two distinct compositions. The pale brownish amphibole (table 2.7; 1-4) has higher Ca (0.7 to 0.9), Ti (0.1 to 0.4) and Mg (0.4 to 0.8) than the greenish amphibole (table 2.7. 5-9) with Ca (0.2 to 0.5), Ti (up to 0.1) and Mg (~ 0.1). in Table 2.7).

The Ca-amphibole (brown hornblende) in the olivine syenite is more abundant in the rock than olivine and both minerals have similar grain sizes (up to 1mm). In contrast to the amphiboles of the quartz syenite, these amphiboles have much

higher Al₂O₃, MgO and TiO₂ and Mg/(Mg + Fe²⁺) contents and less SiO₂ and FeO contents (Table 2.7).

According to the classification scheme of the amphiboles of Hawthorne and Oberti (2007), the Na-amphiboles in the quartz syenite can be termed ferrichterite (pale brownish amphiboles) and arfvedsonite (greenish amphiboles). The Ca-amphibole in the olivine syenite can be termed titanian ferropargasite.

Table 2-7 Representative microprobe analysis of amphiboles of the two syenite types from Jbel Boho

	Amphiboles from quartz syenite								Amphiboles from olivine syenite				
	1	2	3	4	5	7	8	9	10	11	12	13	15
SiO₂	49.05	48.74	47.95	49.05	50.37	49.28	50.14	49.33	42.28	41.84	41.86	41.51	41.68
TiO₂	1.08	2.43	3.07	1.99	0.35	0.32	0.23	0.48	2.85	2.90	2.99	3.12	3.14
Al₂O₃	0.77	1.19	1.12	0.87	0.34	0.40	0.41	0.43	9.70	9.67	9.83	10.04	10.03
FeO	32.14	29.01	30.75	31.46	34.84	34.77	34.22	34.84	16.61	17.95	17.19	17.49	16.78
MnO	1.21	0.91	1.08	1.07	1.48	1.36	1.41	1.37	0.43	0.43	0.45	0.46	0.52
MgO	1.57	3.35	1.47	1.76	0.30	0.45	0.59	0.40	10.28	9.37	9.90	9.58	9.85
CaO	4.06	5.01	4.61	4.36	1.09	2.32	2.69	2.32	11.03	11.04	10.83	11.03	11.13
Na₂O	6.59	6.11	6.25	6.28	7.92	7.15	7.01	7.32	3.02	3.00	3.11	2.94	2.97
K₂O	1.37	1.52	1.46	1.48	1.31	1.43	1.44	1.39	1.80	1.83	1.78	1.84	1.76
Total	97.83	98.27	97.76	98.33	98.00	97.47	98.14	97.87	98.03	98.05	97.95	98.01	97.86
Number of ions based on 23 O													
Si	7.87	7.70	7.70	7.82	8.00	7.92	8.00	7.91	6.42	6.40	6.38	6.34	6.35
Al	0.13	0.22	0.21	0.16	0.00	0.08	0.00	0.08	1.58	1.60	1.62	1.66	1.65
Total	8.0	7.9	7.9	8.0	8.0	8.0	8.0	8.0	8.00	8.00	8.00	8.00	8.00
Al	0.02	0.00	0.00	0.00	0.06	0.00	0.08	0.00	0.16	0.14	0.15	0.15	0.15
Ti	0.13	0.29	0.37	0.24	0.04	0.04	0.03	0.06	0.33	0.33	0.34	0.36	0.36
Fe	4.31	3.83	4.13	4.20	4.63	4.67	4.57	4.67	2.11	2.30	2.19	2.23	2.14
Mn	0.16	0.12	0.15	0.14	0.20	0.19	0.19	0.19	0.06	0.06	0.06	0.06	0.07
Mg	0.37	0.79	0.35	0.42	0.07	0.11	0.14	0.10	2.33	2.14	2.25	2.18	2.24
Total	5.00	5.03	5.00	5.00	5.00	5.00	5.00	5.01	4.97	4.96	4.99	4.98	4.96
Ca	0.70	0.85	0.79	0.75	0.19	0.40	0.46	0.40	1.79	1.81	1.77	1.80	1.82
Na	2.05	1.87	1.95	1.94	2.44	2.23	2.17	2.28	0.89	0.89	0.92	0.87	0.88
K	0.28	0.31	0.30	0.30	0.27	0.29	0.29	0.28	0.35	0.36	0.35	0.36	0.34
Total	3.03	3.03	3.04	2.99	2.89	2.92	2.92	2.96	3.03	3.06	3.03	3.03	3.04
Mg/(Mg+Fe²⁺)	0.08	0.17	0.08	0.09	0.02	0.03	0.03	0.02	0.52	0.48	0.51	0.49	0.51

2.7.3 Clinopyroxene in olivine-syenite

Clinopyroxene is the predominant mafic phase in the olivine syenites. Analyses of selected pyroxenes (Table 2.8) show them to be relatively homogeneous Ca-rich clinopyroxenes with wollastonite contents between Wo_{48} and Wo_{49} , enstatite from En_{33} to En_{38} and ferrosilite from Fs_{13} to Fs_{17} . The Al content is about 0.1. The composition of these clinopyroxenes tend therefore toward the endmember diopside with X_{Mg} ($Mg/(Mg+Fe^{2+})$) between 0.6 and 0.7. Small amounts of Ti, Na and Mn were also detected.

Table 2-8 Representative microprobe analyses of clinopyroxene in the olivine syenite from Jbel Boho

Pyroxene analysis from olivine syenite B10												
	1	2	3	4	5	6	7	8	9	10	11	12
SiO ₂	50.92	51.15	51.22	51.42	51.46	50.56	51.25	51.19	51.2	50.21	51.35	51.31
TiO ₂	0.938	0.894	0.894	0.95	0.798	1.354	1	0.825	0.848	1.654	1.163	1.068
Al ₂ O ₃	2.14	2.07	1.875	2.29	1.848	2.89	2.13	2.02	1.93	3.48	2.41	2.38
FeO	11.57	11.56	11.58	9.69	11.8	9.77	11.08	11.09	10.76	9.68	8.93	8.99
MnO	0.502	0.482	0.42	0.431	0.55	0.45	0.417	0.452	0.45	0.397	0.376	0.403
MgO	11.26	11.19	11.19	12.34	10.84	11.99	11.19	11.26	11.32	11.52	12.43	12.61
CaO	21.99	21.8	21.67	22.09	21.8	22.1	21.98	22.21	22.11	22.09	22.52	22.45
Na ₂ O	0.723	0.739	1.06	0.747	0.752	0.806	0.863	0.834	0.812	0.829	0.759	0.727
Total	100.04	99.89	99.91	99.96	99.85	99.92	99.91	99.88	99.43	99.86	99.94	99.94
Numer of ions based on 6 O												
Si	1.93	1.94	1.94	1.93	1.95	1.91	1.94	1.94	1.95	1.89	1.93	1.93
Ti	0.03	0.03	0.03	0.03	0.02	0.04	0.03	0.02	0.02	0.05	0.03	0.03
Al	0.10	0.09	0.08	0.10	0.08	0.13	0.10	0.09	0.09	0.15	0.11	0.11
Fe ²⁺	0.37	0.37	0.37	0.30	0.37	0.31	0.35	0.35	0.34	0.31	0.28	0.28
Mn	0.02	0.02	0.01	0.01	0.02	0.01	0.01	0.01	0.01	0.01	0.01	0.01
Mg	0.64	0.63	0.63	0.69	0.61	0.67	0.63	0.64	0.64	0.65	0.70	0.71
Ca	0.89	0.89	0.88	0.89	0.89	0.89	0.89	0.90	0.90	0.89	0.91	0.90
Na	0.05	0.05	0.08	0.05	0.06	0.06	0.06	0.06	0.06	0.06	0.06	0.05
Mg/(Mg+Fe ²⁺)	0.63	0.63	0.63	0.69	0.62	0.69	0.64	0.64	0.65	0.68	0.71	0.71
Endmeber prportions												
En	34.68	34.36	35.17	37.64	33.20	37.18	34.54	34.83	34.93	35.85	37.85	38.40
Fs	16.63	17.53	15.87	13.93	18.82	13.56	16.71	15.79	16.03	14.74	12.87	12.46
Wo	48.68	48.11	48.96	48.43	47.98	49.26	48.76	49.38	49.04	49.41	49.28	49.14

2.7.4 Synchysite in a rhyolite dyke

This REE mineral synchysite is found in dyke B35, which is intruded itself by tiny quartz and carbonate veins (Fig. 2.7H). The different occurrences of synchysite within the dyke are summarized in Figure 2.15. The synchysites occur euhedral to anhedral with grain sizes varying in the range from 10 to 300 μm . They are mainly associated with quartz and chlorite within the matrix (Fig. 2.15A, 2.15B and 2.15C) and occasionally occur within Fe-oxide bodies together with chlorite (Fig. 15D). Representative analyses are reported in Table. 2.9. A fixed amount of 26.5 wt% CO_2 is added to each individual microprobe analysis corresponding to the average CO_2 content of synchysite after Guastoni et al. (2009). The highest average rare earth element content in synchysite, expressed as oxide, is 20.35 wt% Ce_2O_3 . Lanthanum and neodymium are also enriched with averages of 12.53 wt% La_2O_3 and 10.6 wt% Nd_2O_3 . The resulting structural formula with 0.99 atoms REE, 1.09 Ca, 1.99 C and 0.86 F corresponds very closely to the composition of the REE-Ca-F carbonate mineral synchysite that belongs to the bastnäs site group minerals. According to Guastoni et al. (2009) the missing pfu 0.14 of fluorine are probably related to OH content.

Table 2-9 Chemical analyses for synchysite from the REE enriched rhyolitic dyke (B35) of Jbel Boho complex. Ionic formulae calculated based on 7 oxygens following [Guastoni et al., \(2009\)](#)

Synchysite analysis of the rhyolitic dyke B10													
	1	2	3	4	5	6	7	8	9	10	11	12	average
F	4.07	5.41	5.23	5.01	4.75	4.71	5.09	4.71	4.42	4.67	5.59	5.66	4.94
CaO	18.76	18.37	18.40	18.74	18.78	18.75	18.39	18.64	18.88	18.89	18.29	18.05	18.58
La ₂ O ₃	12.25	12.67	12.25	11.96	12.50	13.16	13.61	13.11	12.30	12.25	12.21	12.15	12.53
Ce ₂ O ₃	20.03	19.66	20.92	19.65	19.83	20.19	20.83	20.92	20.55	20.61	20.92	20.07	20.35
Pr ₂ O ₃	3.04	2.67	2.84	2.64	2.90	2.87	2.72	2.75	2.75	2.72	3.19	2.77	2.82
Nd ₂ O ₃	11.49	10.61	11.33	11.05	10.60	9.69	9.66	9.81	10.59	11.00	10.42	10.97	10.60
Sm ₂ O ₃	1.54	1.58	1.36	1.68	1.29	1.24	1.25	1.37	1.40	1.62	1.39	1.34	1.42
Eu ₂ O ₃	0.18	0.20	0.00	0.01	0.00	0.31	0.17	0.18	0.00	0.00	0.00	0.06	0.09
Gd ₂ O ₃	1.25	1.10	0.61	1.34	1.21	0.95	0.78	0.81	1.09	1.19	0.83	1.16	1.03
Dy ₂ O ₃	0.00	0.03	0.00	0.00	0.00	0.07	0.04	0.02	0.00	0.00	0.00	0.00	0.01
Y ₂ O ₃	0.52	0.35	0.15	0.49	0.50	0.71	0.55	0.37	0.19	0.29	0.23	0.35	0.39
Er ₂ O ₃	0.05	0.00	0.02	0.00	0.00	0.05	0.04	0.00	0.00	0.00	0.00	0.02	0.02
Yb ₂ O ₃	0.11	0.00	0.00	0.03	0.00	0.01	0.01	0.00	0.00	0.00	0.00	0.00	0.01
ThO ₂	0.07	0.06	0.37	0.00	0.41	0.00	0.00	0.00	0.09	0.14	0.33	0.38	0.16
CO ₂	26.50	26.50	26.50	26.50	26.50	26.50	26.50	26.50	26.50	26.50	26.50	26.50	26.50
Sum	99.86	99.20	100.00	99.10	99.26	99.22	99.63	99.19	98.76	99.86	99.91	99.49	99.46
F ≡ O	1.71	2.28	2.20	2.11	2.00	1.98	2.14	1.98	1.86	1.96	2.35	2.38	2.08
Total	98.15	96.92	97.80	96.99	97.26	97.23	97.49	97.20	96.90	97.90	97.56	97.11	97.37
Number of ions based on 7 O													
F	0.71	0.94	0.91	0.87	0.83	0.82	0.88	0.82	0.77	0.81	0.97	0.98	0.86
Ca	1.11	1.08	1.08	1.11	1.11	1.11	1.08	1.10	1.12	1.11	1.07	1.06	1.09
La	0.25	0.26	0.25	0.24	0.25	0.27	0.28	0.27	0.25	0.25	0.25	0.25	0.25
Ce	0.41	0.40	0.42	0.40	0.40	0.41	0.42	0.42	0.42	0.42	0.42	0.40	0.41
Pr	0.06	0.05	0.06	0.05	0.06	0.06	0.05	0.06	0.06	0.06	0.05	0.06	0.06
Nd	0.23	0.21	0.22	0.22	0.21	0.19	0.19	0.19	0.21	0.22	0.20	0.22	0.21
Sm	0.03	0.03	0.03	0.03	0.02	0.02	0.02	0.03	0.03	0.03	0.03	0.03	0.03
Eu	0.00	0.00	0.00	0.00	0.00	0.01	0.00	0.00	0.00	0.00	0.00	0.00	0.00
Gd	0.02	0.02	0.01	0.02	0.02	0.02	0.01	0.01	0.02	0.02	0.02	0.02	0.02
Dy	0.00	0.00	0.00	0.00	0.00	0.00	0.00	0.00	0.00	0.00	0.00	0.00	0.00
Y	0.02	0.01	0.00	0.01	0.01	0.02	0.02	0.01	0.01	0.01	0.01	0.01	0.01
Er	0.00	0.00	0.00	0.00	0.00	0.00	0.00	0.00	0.00	0.00	0.00	0.00	0.00
Yb	0.00	0.00	0.00	0.00	0.00	0.00	0.00	0.00	0.00	0.00	0.00	0.00	0.00
Th	0.00	0.00	0.00	0.00	0.01	0.00	0.00	0.00	0.00	0.00	0.00	0.00	0.00
C	2.00	1.99	1.99	1.99	2.00	2.00	1.99	2.00	2.01	1.99	1.98	1.99	1.99

ΣREE + Th: 0.99

Ca: 1.09

F: 0.86

C: 1.99

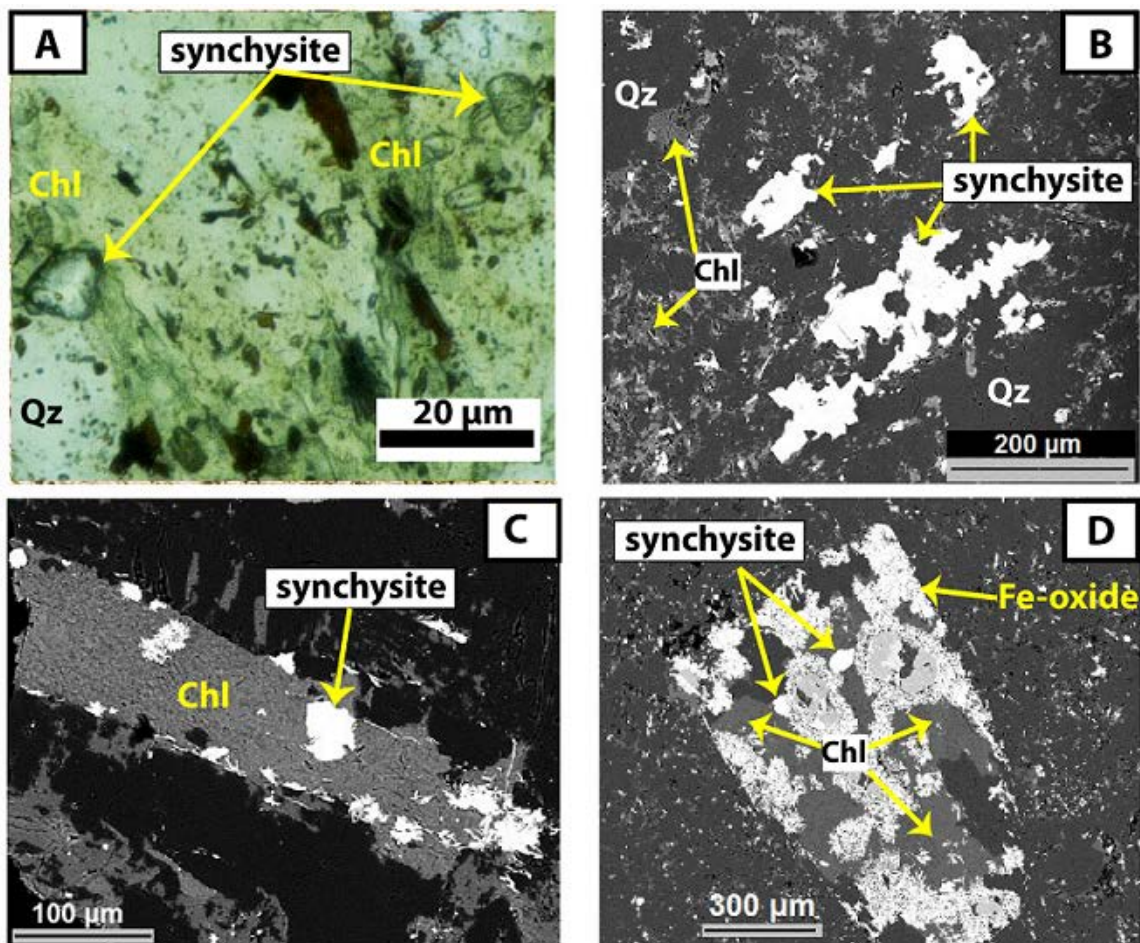


Figure 2.15 Typical synchysite occurrences in the LREE-enriched rhyolitic dyke B35. A) Photo-micrograph shows small subhedral synchysite grains (up to 20 μm) in a quartz-rich matrix. B) Backscattered electron micrograph of anhedral synchysite (up to 300 μm) associated with quartz and chlorite. C) backscattered electron micrograph of synchysite within chlorite. D) backscattered electron micrograph of synchysite associated with chlorite in an Fe-oxide grain.

2.8 Discussion

2.8.1 Sources and magma generations

The first studies of the Jbel Boho complex were reported by [Choubert \(1952\)](#), [Leblanc \(1971\)](#) and [Leblanc \(1981a\)](#). These studies were mainly restricted to petrographical observations and misinterpreted this complex as a calc-alkaline magmatic complex because the main volcanic rocks were classified as andesites. Our geochemical work identified no andesites at Jbel Boho and instead highlights the alkaline nature of these rocks (shown on both the TAS diagram ([Fig. 2.8](#)) and the alteration-resistant HFSE ratio plot ([Fig. 2.10](#)), in agreement with the few data presented as average values by [Alvaro et al. \(2006\)](#).

The similarities in incompatible trace element ratios in all Jbel Boho magmas suggest that the complex as a whole is derived from one source type. The most primitive volcanic rocks (low SiO₂) of Jbel Boho have high enrichment of the LREE relative to the depleted HREE and very high Nb/Ta and Zr/Hf ratios. This may indicate a garnet bearing mantle source from which LREE-enriched alkali basalt and alkali volcanics are derived by low degrees of partial melting as originally demonstrated by the model calculations of [Kay and Gast, \(1973\)](#). The enrichments in Nb and Ta relative to, for example, Ba ([Fig. 2.14](#)) and the high Zr/Hf and Nb/Ta values of the rocks of lower SiO₂ contents suggest that the source of these volcanics is not subduction-related and is more likely to be plume-like in nature. The geotectonic discrimination diagrams (Ti-Zr and 2Nb-

Zr/4-Y, [Fig. 2.13](#)) also point towards an intraplate setting for the Jbel Boho complex.

The oldest magmatic rocks in the Jbel Boho complex are the lavas. The data in the TAS diagram and their correlation with the stratigraphic position of the analysed samples suggest an evolution of an alkaline magmatic system from basanite and tephrite to trachyte and rhyolite during the eruption of the volcanics. The volcanics were then intruded by a syenitic pluton consisting of an olivine syenite and a quartz syenite magma body. The syenites do not continue the fractionation trend seen in the preceding volcanic sequence. In addition to the lower silica and higher Fe and Mg contents of the olivine syenite relative to the rhyolites, both syenites also have very different rare earth and trace elements patterns when compared to the volcanics. This can be seen, for example, in much more subdued Eu and Ba anomalies and occasional positive Pb anomalies in the syenites (c.f. [Fig. 2.14A - F](#)). This is strong evidence that the magma from which the syenites were formed represents a new generation of melt. Although the two types of Jbel Boho syenite in the field appear to belong to the same pluton, they are mineralogically and chemically distinct.

Both volcanics and syenite are cut by microsyenitic and rhyolitic dykes. The microsyenitic dykes display, in many cases, generally the same major element contents as the quartz syenite, (some microsyenites have higher CaO, as noted earlier) and are very similar to them in terms of HSF/E ratios. Nevertheless, the presence of plagioclase and strong negative Eu anomalies in the dykes (which

are absent in the quartz syenite pluton) and the much higher HFSE-contents of some microsyenitic dykes at similar SiO_2 contents (Fig. 2.11) suggest that they are not genetically related. The very high SiO_2 contents in the rhyolitic dykes suggest that they might represent the final stage of the magmatic evolution in Jbel Boho, as magma cooled and fractionation proceeded to solidification.

2.8.2 Element fractionation

Differences in absolute element concentrations (e.g. in the HFSE in the microsyenitic dykes, see Fig 2.11) suggests that differing degrees of partial melting or paths of fractional crystallization or crustal contamination have been followed by the various magma batches identified above once they left this source.

We see evidence at Jbel Boho for fractionation taking place under unusual conditions, leading for example to negative correlations between ratios of similarly incompatible elements such as Nb/Ta and an index of fractionation like SiO_2 (Fig. 2.12). Although the fractionation of Nb-Ta (and also Zr-Hf) could be a result of the fractional crystallization of Ti bearing phases like rutile, titanite and ilmenite together with zircon (Chen and Zheng, 2015; Claiborne et al., 2006; John et al., 2011; Linnen and Keppler, 2002; Marks et al., 2008; Pfänder et al., 2007), we see a positive correlation between TiO_2 and Nb/Ta or Zr/Hf. $D_{\text{Nb/Ta}}$ and $D_{\text{Zr/Hf}}$ in rutile and ilmenite are less than 1 (see Pfänder (2007) and references therein) and the fractionation of such minerals would increase these ratios in the melt, which is the opposite to what we see. In addition, we see a positive

correlation between fractionation indices and absolute concentrations of HFSE even in the most evolved volcanics, which argues against the fractionation of zircon or other HFSE bearing phases playing a significant role. Some authors (e.g., [Huang et al., 2011](#); [Niu, 2012](#)) propose the process of “mass-dependent fractionation during magmatism” to explain Nb-Ta and Zr-Hf fractionation in magmatic systems. They suggest that the lighter elements $^{90-96}\text{Zr}$ and ^{93}Nb would behave more incompatibly than the heavier elements $^{174-180}\text{Hf}$ and ^{181}Ta in magmatic processes. In terms of crystal fractionation, this should lead to Zr/Hf and Nb/Ta ratios increasing in the melt as fractionation proceeds, again the opposite of what we see in the evolved volcanics of Jbel Boho. This indicates that neither mineral fractionation nor mass-dependent fractionation can explain the fractionation of these HFS elemental twins in the Jbel Boho volcanics.

[Dostal and Chatterjee \(2000\)](#) and [Green \(1995\)](#) have proposed that fluid fractionation and the addition of mineralizing fluids could fractionate Ta and Nb with preference for Ta in the fluids. Fluorine (F) could play an important role in the form of F^- to facilitate the transport of the HFSE in the magma and hydrothermal fluids, forming HFSE-F complexes which could lead to high enrichment of some HFSE ([Agangi et al., 2010](#); [Demartis et al., 2014](#); [Sheard et al., 2012](#); [Timofeev et al., 2015](#)). Alkaline magmatic rocks are generally enriched in volatiles, and the evidence from fluorine-containing secondary minerals such as fluorite and synchysite at Jbel Boho suggests that fluorine may be an important volatile component there.

2.8.3 Syenite petrogenesis

The present data do not allow us to clearly determine the petrogenesis of the Jbel Boho syenites, which are particularly distinctive in the Jbel Boho context due to their virtual absence of negative Eu anomalies. [Yang et al. \(2012, 2008, 2005\)](#) discuss three main petrogenetic models for the formation of syenitic rocks in general: 1) extensive fractional crystallization of mantle derived melts, 2) magma mixing processes of mantle-derived undersaturated alkaline magma with crustal-derived silicic melts, and 3) partial melting of underplated crustal rocks. The absence of negative Eu anomalies in the Jbel Boho syenites argues against the first model, as extensive fractional crystallization would lead to the formation of evolved rocks with strong negative Eu anomalies. The second model was proposed by [Yang et al. \(2012, 2008\)](#) to explain the occurrence of syenitic intrusions without negative Eu anomalies in the eastern and northern North China Craton. However it is not fully understood why this process should lead to highly evolved rocks without negative Eu anomalies. [Markl \(2001\)](#) suggested that varying Eu anomalies could be the result of mixing of plagioclase cumulates (positive Eu-anomalies) with residual magmas with pronounced negative anomalies, although at Jbel Boho we do not see the correlation between Eu/Eu^* and indices of fractionation such as SiO_2 that this should produce. Partial melting of underplated mafic cumulate rocks appears to be the most likely model to explain the formation of the Jbel Boho syenitic pluton. The absence of distinct negative Eu anomalies in highly evolved rocks like syenites which are

presumably derived from more mafic compositions by crystal fractionation implies that the mafic precursors must have had high Eu contents. Mafic rocks with some cumulate plagioclase, representing a reservoir for Eu would produce melts that are Eu-enriched (Shellnutt and Iizuka, 2012; Shellnutt and Zhou, 2008, 2007). These authors have explained the petrogenesis of fayalite syenite in the Panxi region SW of China, which has a very similar composition and REE pattern to the Jbel Boho fayalite syenite, by this melting model. Moreover, Shellnutt and Iizuka (2012) have attributed the formation of such syenites to melting under relatively oxidizing conditions ($fO_2 > FMQ$), which will produce a preference for Eu^{3+} over Eu^{2+} that preclude fractionation of Eu over the other REE by feldspar.

2.8.4 REE enrichment

Alkaline igneous rocks form by low degree partial melting of the mantle and therefore highly enriched in incompatible elements such as alkali elements, REE, Zr, Ba and Nb. As the LREE are more incompatible than the HREE, they are in the resulting melts always highly enriched relative to the HREE. The REE contents in the melt tend therefore to increase with increasing magma differentiation, which is obviously seen as expected in the REE patterns of the Jbel Boho magmatic rocks (Fig. 2.14).

The Σ LREE contents in the dykes vary from 252 ppm to 678 ppm. Unusually strong LREE enrichment (Σ LREE = 1750 ppm) is found in one rhyolitic dyke B35 (Fig. 2.14). This very high LREE content is associated with the presence of the REE-F-Ca carbonate synchysites, which occurs as tiny subhedral crystals (up to

30 μm) and as much bigger anhedral and altered minerals (up to 300 μm) together with quartz and chlorite both in the matrix and within Fe-oxides (e.g. [Fig. 2.15 A-D](#)). Dyke B35 is, with the exception of its LREE enrichment, very similar to the other dykes chemically, falling on the same trends in both major ([Figure 2.8](#)) and trace ([Figure 2.12](#)) element diagrams. This suggests that processes of partial melting or fractional crystallization are not alone responsible for its extreme LREE enrichment. Evidence of fluid effects is reflected by tiny carbonate and quartz veins within the dyke ([Fig 2.7H](#)). In addition, strong feldspar albitization and the common association of the REE-Ca-F carbonate synchysite with chlorite and Fe-oxides (which form pseudomorphs after primary Fe-Mg minerals) argue for later hydrothermal fluid impregnation. We suggest that the rare earth mineralization originates most likely from the influence of REE-rich hydrothermal fluids.

Recent experimental studies have further shown that LREE-chloride complexes are highly mobile in hydrothermal fluids at acidic conditions and high ligand activity ([Migdisov et al., 2009](#); [Williams-Jones and Migdisov, 2014](#); [Williams-Jones et al., 2012](#)). The mineralization model we propose here consists of the transport of REE as chloride complexes at acidic hydrothermal fluid conditions in the presence of fluorine. These low pH fluids may create pathways in the host-rock by provoking acidic alteration. The REE will be precipitated from the fluids when their pH rises. In the case of Jbel Boho veins, they are ubiquitously associated with calcite and dolomite, suggesting that carbonate-rich fluids were

available for the neutralisation. These fluids probably also provided the CO_3^{2-} and Ca^{2+} needed for the formation of synchysite. Similar REE mineralization model have also been implicated in the formation of some pegmatite REE deposits (Gysi and Williams-Jones, 2013).

Quartz veins with REE mineralization (synchysite) were also found in proximity to the quartz syenite and will be described in more detail in a separate paper.

2.9 Conclusion

The Jbel Boho alkaline complex contains some the best preserved magmatic rocks produced during an event marking the transition from Neoproterozoic to Cambrian in the Anti-Atlas. It was formed after the emplacement of the Bou Azzer ophiolite under shallow marine conditions in an extensive regime south of the AAMF along the northern edge of the WAC.

The magmatic evolution of the Jbel Boho alkaline complex is characterized by three magma generations, which have experienced different petrogenetic processes. 1) The first magma generation produced a suite of volcanics evolving in time from primitive basanites/tephrites to trachytes and eventually rhyolites by fractional crystallization. 2) The second magma generation led to the formation of the syenitic pluton. The composition of the two syenite types (olivine syenite and quartz syenite) including high alkali contents, the absence of negative Eu anomalies and a new mineral assemblage with fayalite, Ca-pyroxene, hornblende and arfvedsonite suggests they were produced by partial melting of mafic cumulates at deep crustal levels. In addition, the occurrence of quartz and

a positive Pb in the quartz syenite suggests that this magma was affected by crustal contamination. 3) The magmas of the later dyke swarm (microsyenitic and rhyolitic dykes) are more plagioclase-rich than either the syenite or the most evolved volcanics. This and their strongly differing high field-strength element contents suggest they are derived from a third batch of magma .

Negative correlations between ratios such as Nb/Ta and Zr/Hf (which should not normally be affected by crystal fractionation) and SiO₂ suggest that element fractionation processes involving complexation, perhaps by fluorine, played a petrogenetic role in many of the magmas. That the magmas were fluorine-rich is attested to by the presence of fluorite both in the groundmass of a trachyte and as inclusions in the Na-amphibole of the rhyolitic lavas as well as the presence of REE-F-Ca carbonate synchysite-(Ce) in some of the late, REE-enriched rhyolite dykes.

Synchysite-(Ce) is the unique REE mineral identified by EPMA analysis in a rhyolitic dyke with strong LREE enrichment (Σ LREE = 1750ppm). This unusually high LREE content probably does not reflect a magmatic signature, but instead most likely crystallized from REE-rich hydrothermal fluid in the presence of F, Cl, Ca and CO₃. Such highly-fractionated intrusives in alkaline complexes are good prospects for REE mineralization.

The Jbel Boho alkaline magmas show clear within-plate geochemical signatures. This implies that, by the time of their emplacement, the compressive regime

which had previously characterized the margin of the West African Craton and led to the formation of the Bou Azzer ophiolite, had ended.

References

- Agangi, A., Kamenetsky, V.S., McPhie, J., 2010. The role of fluorine in the concentration and transport of lithophile trace elements in felsic magmas: Insights from the Gawler Range Volcanics, South Australia. *Chemical Geology* 273, 314–325.
- Algouti, A., Algouti, A., Chbani, B., Zaim, M., 2001. Sedimentation et volcanisme synsédimentaire de la série de base de l'adoudounien infra-cambrien à travers deux exemples de l'Anti-Atlas du Maroc. *Journal of African Earth Sciences* 32, 541–556.
- Álvaro, J.J., Ezzouhairi, H., Vennin, E., Ribeiro, M.L., Clausen, S., Charif, A., Ayad, N.A., Moreira, M.E., 2006. The Early-Cambrian Boho volcano of the El Graara massif, Morocco: Petrology, geodynamic setting and coeval sedimentation. *Journal of African Earth Sciences* 44, 396–410.
- Baker, B., 1987. Outline of the petrology of the Kenya rift alkaline province, in: Fitton, J.G., Upton, B.G.J. (Eds.), *Alkaline Igneous Rocks*. Geological Society, London, Special Publications, pp. 293–311.
- Blein, O., Baudin, T., Chèvremont, P., Soulaïmani, A., Admou, H., Gasquet, P., Cocherie, A., Egal, E., Youbi, N., Razin, P., Bouabdelli, M., Gombert, P., 2014. Geochronological constraints on the polycyclic magmatism in the Bou Azzer-El Graara inlier (Central Anti-Atlas Morocco). *Journal of African Earth Sciences* 99, 287–306. doi:10.1016/j.jafrearsci.2014.04.021
- Bouabdellah, M., Hoernle, K., Kchit, A., Duggen, S., Hauff, F., Klugel, A., Lowry, D., Beaudoin, G., 2010. Petrogenesis of the Eocene Tamazert Continental Carbonatites (Central High Atlas, Morocco): Implications for a Common Source for the Tamazert and Canary and Cape Verde Island Carbonatites. *Journal of Petrology* 51, 1655–1686.
- Bouougri, E.H., 2003. The Moroccan Anti-Atlas: the West African craton passive margin with limited Pan-African activity. Implications for the northern limit of the craton—discussion. *Precambrian Research* 120, 179–183.
- Bousquet, R., El Mamoun, R., Saddiqi, O., Goffé, B., Möller, A., Madi, A., 2008. Mélanges and ophiolites during the Pan-African orogeny: the case of the Bou-Azzer ophiolite suite (Morocco), in: Ennih, N., Liégeois, J.-P. (Eds.), *The Boundaries of the West African Craton*. Geological Society, London, Special Publications, 297, pp. 233–247.

- Chakhmouradian, A.R., Zaitsev, A.N., 2012. Rare Earth Mineralization in Igneous Rocks: Sources and Processes. *Elements* 8, 347–353.
- Chen, Y.X., Zheng, Y.F., 2015. ScienceDirect Extreme Nb/Ta fractionation in metamorphic titanite from ultrahigh-pressure metagranite. *Geochemica et Cosmochemica Acta* 150, 53–73. doi:10.1016/j.gca.2014.12.002
- Choubert, G., 1952. Geologie du Maroc: Histoire geologique du domaine de l'Anti-Atlas, in: XIX^e Congrès Géologique International, Monographies Régionales 3. Rabat, pp. 75–195.
- Claiborne, L.L., Miller, C.F., Walker, B.A., Wooden, J.L., Mazdab, F.K., Bea, F., 2006. Tracking magmatic processes through Zr/Hf ratios in rocks and Hf and Ti zoning in zircons: An example from the Spirit Mountain batholith, Nevada. *Mineralogical Magazine* 70, 517–543.
- D'Lemos, R.S., Inglis, J.D., Samson, S.D., 2006. A newly discovered orogenic event in Morocco: Neoproterozoic ages for supposed Eburnean basement of the Bou Azzer inlier, Anti-Atlas Mountains. *Precambrian Research* 147, 65–78.
- Demartis, M., Melgarejo, J.C., Colombo, F., Alfonso, P., Coniglio, J.E., Pinotti, L.P., D'Eramo, F.J., 2014. Extreme F activities in late pegmatitic events as a key factor for LILE and HFSE enrichment: The Angel pegmatite, Central Argentina. *The Canadian Mineralogist* 52, 247–269.
- Dostal, J., Chatterjee, A.K., 2000. Contrasting behaviour of Nb/Ta and Zr/Hf ratios in a peraluminous granitic pluton (Nova Scotia, Canada). *Chemical Geology* 163, 207–218. doi:10.1016/S0009-2541(99)00113-8
- Ducrot, J., Lancelot, J.R., 1977. Problème de la limite Précambrien-Cambrien: étude radiochronologique par la méthode U-Pb sur zircons du volcan du Jbel Boho (Anti-Atlas marocain). *Canadian Journal of Earth Sciences* 14, 2771–2777.
- El Hadi, H., Simancas, J.F., Martínez-Poyatos, D., Azor, A., Tahiri, A., Montero, P., Fanning, C.M., Bea, F., González-Lodeiro, F., 2010. Structural and geochronological constraints on the evolution of the Bou Azzer Neoproterozoic ophiolite (Anti-Atlas, Morocco). *Precambrian Research* 182, 1–14.
- Ennih, N., Liégeois, J.-P., 2001. The Moroccan Anti-Atlas: the West African craton passive margin with limited Pan-African activity. Implications for the northern limit of the craton. *Precambrian Research* 112, 289–302.

- Ennih, N., Liégeois, J.-P., 2003. The Moroccan Anti-Atlas: the West African craton passive margin with limited Pan-African activity. Implications for the northern limit of the craton: reply to. *Precambrian Research* 120, 185–189.
- Ennih, N., Liégeois, J.-P., 2008. The boundaries of the West African craton, with special reference to the basement of the Moroccan metacratonic Anti-Atlas belt, in: Ennih, N., Liégeois, J.-P. (Eds.), *The Boundaries of the West African Craton*. Geological Society, London, Special Publications, 297, pp. 1–17.
- Ezzouhairi, H., Ribeiro, M.L., Ait Ayad, N., Moreira, M.E., Charif, A., Ramos, J.M.F., de Oliveira, D.P.S., Coke, C., 2008. The magmatic evolution at the Moroccan outboard of the West African craton between the Late Neoproterozoic and the Early Palaeozoic, in: Ennih, N., Liégeois, J. (Eds.), *The Boundaries of the West African Craton*. Geological Society, London, Special Publications, pp. 329–343.
- Gasquet, D., Ennih, N., Liégeois, J.-P., Soulaïmani, A., Michard, A., 2008. The Pan-African Belt, in: Michard, A., Saddiqi, O., Chalouan, A., de Lamotte, D.F. (Eds.), *Continental Evolution: The Geology of Morocco*. Springer, Berlin Heidelberg, pp. 33–64.
- Gasquet, D., Levresse, G., Cheilletz, A., Azizi-Samir, M.R., Mouttaqi, A., 2005. Contribution to a geodynamic reconstruction of the Anti-Atlas (Morocco) during Pan-African times with the emphasis on inversion tectonics and metallogenic activity at the Precambrian–Cambrian transition. *Precambrian Research* 140, 157–182.
- Green, T.H., 1995. Significance of Nb/Ta as an indicator of geochemical processes in the crust-mantle system. *Chemical Geology* 120, 347–359. doi:10.1016/0009-2541(94)00145-X
- Guastoni, A., Nestola, F., Giaretta, A., 2009. Mineral chemistry and alteration of rare earth element (REE) carbonates from alkaline pegmatites of Mount Malosa, Malawi. *American Mineralogist* 94, 1216–1222.
- Gysi, A.P., Williams-Jones, A.E., 2013. Hydrothermal mobilization of pegmatite-hosted REE and Zr at Strange Lake, Canada: A reaction path model. *Geochimica et Cosmochimica Acta* 122, 324–352.
- Hawthorne, F.C., Oberti, R., 2007. Amphiboles: Crystal Chemistry. *Reviews in Mineralogy and Geochemistry* 67, 1–54.
- Hefferan, K.P., Admou, H., Hilal, R., Karson, J.A., Saquaque, A., Juteau, T., Bohn, M.M., Samson, S.D., Kornprobst, J.M., 2002. Proterozoic blueschist-

- bearing mélange in the Anti-Atlas Mountains, Morocco. *Precambrian Research* 118, 179–194.
- Hefferan, K.P., Admou, H., Karson, J.A., Saquaque, A., 2000. Anti-Atlas (Morocco) role in Neoproterozoic Western Gondwana reconstruction. *Precambrian Research* 103, 89–96.
- Huang, H., Niu, Y., Zhao, Z., Hei, H., Zhu, D., 2011. On the enigma of Nb-Ta and Zr-Hf fractionation-A critical review. *Journal of Earth Science* 22, 52–66.
- John, T., Klemd, R., Klemme, S., Pfänder, J.A., Hoffmann, J.E., Gao, J., 2011. Nb-Ta fractionation by partial melting at the titanite-rutile transition. *Contributions to Mineralogy and Petrology* 161, 35–45.
- Kay, R.W., Gast, P.W., 1973. The rare earth content and origin of alkali-rich basalts. *The Journal of Geology* 653–682.
- Le Bas, M.J., 1987. Ultra-alkaline magmatism with or without rifting. *Tectonophysics* 143, 75–84.
- Leblanc, M., 1971. Faible teneurs de Niobium dans un filon lamprophyrique du volcan Infracambrien, calco-alkalin, du Jbel Boho (Anti-Atlas central). *Service d'Etudes des Gites Minéraux (S.E.G.M) N° 913*, 5.
- Leblanc, M., 1972. Un complexe ophiolitique dans le Précambrien II de l'Anti-Atlas central (Maroc): description, interprétation et position stratigraphique. *Notes et Mémoires du Service géologique du Maroc* 236, 119–144.
- Leblanc, M., 1981a. Ophiolites précambriennes et gites arseniés de cobalt: Bou Azzer (Maroc). *Note et Mémoires du Service Géologique N280*, Maroc.
- Leblanc, M., 1981b. The late Proterozoic ophiolites of Bou Azzer (Morocco): evidence for Pan-African plate tectonics. *Developments in Precambrian Geology* 4, 435–451.
- Leblanc, M., Lancelot, J.R., 1980. Interprétation géodynamique du domaine pan-africain (Précambrien terminal) de l'Anti-Atlas (Maroc) à partir de données géologiques et géochronologiques. *Canadian Journal of Earth sciences* 17, 142–155.
- Leblanc, M., Moussine-Pouchkine, A., 1994. Sedimentary and volcanic evolution of a Neoproterozoic continental margin (Bleida, Anti-Atlas, Morocco). *Precambrian Research* 70, 25–44.

- Linnen, R.L., Keppler, H., 2002. Melt composition control of Zr/ Hf fractionation in magmatic processes. *Geochimica et Cosmochimica Acta* 66, 3293–3301.
- Markl, G., 2001. REE constraints on fractionation processes of massive-type anorthosites on the Lofoten Islands, Norway. *Mineralogy and Petrology* 72, 325–351.
- Marks, M.A., Coulson, I.M., Schilling, J., Jacob, D.E., Schmitt, A.K., Markl, G., 2008. The effect of titanite and other HFSE-rich mineral (Ti-bearing andradite, zircon, eudialyte) fractionation on the geochemical evolution of silicate melts. *Chemical Geology* 257, 153–172.
- Meschede, M., 1986. A method of discriminating between different types of mid-ocean ridge basalts and continental tholeiites with the Nb-1bZr-1bY diagram. *Chemical Geology* 56, 207–218.
- Migdisov, A.A., Williams-Jones, A.E., Wagner, T., 2009. An experimental study of the solubility and speciation of the Rare Earth Elements (III) in fluoride- and chloride-bearing aqueous solutions at temperatures up to 300°C. *Geochimica et Cosmochimica Acta* 73, 7087–7109.
- Miyashiro, A., 1978. Nature of alkalic volcanic rock series. *Contributions to Mineralogy and Petrology* 66, 91–104. doi:10.1007/BF00376089
- Mouttaqi, A., Rjimati, E.C., Michard, A., 2011. Moroccan Mines : An Introduction. *Notes et Mémoires du Service géologique du Maroc. N°564* 9, 13–22.
- Münker, C., Pfänder, J.A., Weyer, S., Büchl, A., Kleine, T., Mezger, K., 2003. Evolution of planetary cores and the Earth-Moon system from Nb/Ta systematics. *Science* 301, 84–87. doi:10.1126/science.1084662
- Naidoo, D.D., Bloomer, S.H., Saquaque, A., Hefferan, K., 1991. Geochemistry and significance of metavolcanic rocks from the Bou Azzer-El Graara ophiolite (Morocco). *Precambrian Research* 53, 79–97.
- Niu, Y., 2012. Earth processes cause Zr–Hf and Nb–Ta fractionations, but why and how? *RSC Advances* 2, 3587–3591. doi:10.1039/c2ra00384h
- ONHYM, 2013. Annual Report 2013. Office National des Hydrocarbures et des mines (ONHYM), Morocco.
- ONHYM, 2015. Les Terres Rares Au Maroc. Office National des Hydrocarbures et des mines (ONHYM), Morocco.

- Orris, G.J., Grauch, R.I., 2002. Rare earth element mines, deposits, and occurrences. USGS Open-File Report 2–189.
- Pearce, J.A., 1982. Trace element characteristics of lavas from destructive plate boundaries, in: Thorpe, R.S. (Ed.), *Andesites: Orogenic Andesites and Related Rocks*. John Wiley & Sons, Chichester, pp. 525–548.
- Pearce, J.A., 1996. A user's guide to basalt discrimination diagrams, in: Wyman, D.A. (Ed.), *Trace Element Geochemistry of Volcanic Rocks: Applications for Massive Sulphide Exploration*. Geological Association of Canada, Short Course Notes, v. 12, pp. 79–113.
- Pfänder, J.A., Münker, C., Stracke, A., Mezger, K., 2007. Nb/Ta and Zr/Hf in ocean island basalts - Implications for crust-mantle differentiation and the fate of Niobium. *Earth and Planetary Science Letters* 254, 158–172. doi:10.1016/j.epsl.2006.11.027
- Piqué, A., Bouabdelli, M., Soulaïmani, A., Youbi, N., Iliani, M., 1999. Les conglomérats du P III (Néoprotérozoïque supérieur) de l'Anti Atlas (Sud du Maroc): molasses panafricaines, ou marqueurs d'un rifting fini-protérozoïque? *Comptes Rendus de l'Académie des Sciences-Series IIA-Earth and Planetary Science* 328, 409–414.
- Qalbi, A., Mouttaqi, A., Rjimati, E.C., Zemmouri, A., Michard, A., Saddiqi, O., 2011. The Nb-Ta-U-REE Prospects of the Glibat Lafhouda Carbonatites (Awserd Province). *Notes et Mémoires du Service géologique du Maroc*. N°564 9, 183–187.
- Salvi, S., Williams-Jones, A.E., 2005. Alkaline granite-syenite deposits, in: Linnen, R.L., Samson, I.M. (Eds.), *Rare-Element Geochemistry and Mineral Deposits*. Geological Association of Canada, SCN, 17, pp. 315–342.
- Saquaque, A., Admou, H., Karson, J., Hefferan, K., Reuber, I., 1989. Precambrian accretionary tectonics in the Bou Azzer-El Graara region, Anti-Atlas, Morocco. *Geology* 17, 1107–1110.
- Sheard, E.R., Williams-Jones, A.E., Heiligmann, M., Pederson, C., Treumann, D.L., 2012. Controls on the concentration of zirconium, niobium, and the rare earth elements in the Thor Lake Rare Metal Deposit, Northwest Territories, Canada. *Economic Geology* 107, 81–104.
- Shellnutt, J.G., Iizuka, Y., 2012. Oxidation zonation within the Emeishan large igneous province: Evidence from mantle-derived syenitic plutons. *Journal of Asian Earth Sciences* 54-55, 31–40. doi:10.1016/j.jseaes.2012.03.011

- Shellnutt, J.G., Zhou, M., 2007. Permian peralkaline, peraluminous and metaluminous A-type granites in the Panxi district, SW China: Their relationship to the Emeishan mantle plume. *Chemical Geology* 243, 286–316. doi:10.1016/j.chemgeo.2007.05.022
- Shellnutt, J.G., Zhou, M., 2008. Permian, rifting related fayalite syenite in the Panxi region, SW China. *Lithos* 101, 54–73. doi:10.1016/j.lithos.2007.07.007
- Soulaimani, A., Bouabdelli, M., Piqué, A., 2003. L'extension continentale au Néoproterozoïque supérieur-Cambrien inférieur dans l'Anti-Atlas (Maroc). *Bulletin de la Société géologique Français* 174, 83–92.
- Soulaimani, A., Jaffal, M., Maacha, L., Kchikach, A., Najine, A., Saidi, A., 2006. Modélisation magnétique de la suture ophiolitique de Bou Azzer–El Graara (Anti-Atlas central, Maroc). Implications sur la reconstitution géodynamique panafricaine. *Comptes Rendus Geoscience* 338, 153–160.
- Thomas, R.J., Chevallier, L.P., Gresse, P.G., Harmer, R.E., Eglington, B.M., Armstrong, R.A., De Beer, C.H., Martini, J.E.J., De Kock, G.S., Macey, P.H., Ingram, B.A., 2002. Precambrian evolution of the Sirwa Window, Anti-Atlas Orogen, Morocco. *Precambrian Research* 118, 1–57. doi:10.1016/S0301-9268(02)00075-X
- Thomas, R.J., Fekkak, A., Ennih, N., Errami, E., Loughlin, S.C., Gresse, P.G., Chevallier, L.P., Liégeois, J.-P., 2004. A new lithostratigraphic framework for the Anti-Atlas Orogen, Morocco. *Journal of African Earth Sciences* 39, 217–226.
- Timofeev, A., Migdisov, A.A., Williams-Jones, A.E., 2015. An experimental study of the solubility and speciation of niobium in fluoride-bearing aqueous solutions at elevated temperature. *Geochimica et Cosmochimica Acta*. doi:10.1016/j.gca.2015.02.015
- Villeneuve, M., El Archi, A., Nzamba, J., 2010. Les chaînes de la marge occidentale du Craton Ouest-Africain, modèles géodynamiques. *Comptes Rendus Geoscience* 342, 1–10.
- Williams-Jones, A.E., Migdisov, A., 2014. Experimental Constraints on the Transport and Deposition of Metals in Ore-Forming Hydrothermal Systems. *Society of Economic Geologists, Inc. Special Publication* 18, 77–95.
- Williams-Jones, A.E., Migdisov, A.A., Samson, I.M., 2012. Hydrothermal Mobilisation of the Rare Earth Elements - a Tale of “Ceria” and “Yttria.” *Elements* 8, 355–360.

- Woolley, A.R., 2001. Alkaline rocks and carbonatites of the world: Africa. Geological Society of London, pp. 187–192.
- Yang, J.H., Chung, S.L., Wilde, S.A., Wu, F.Y., Chu, M.F., Lo, C.H., Fan, H.R., 2005. Petrogenesis of post-orogenic syenites in the Sulu Orogenic Belt, East China: geochronological, geochemical and Nd–Sr isotopic evidence. *Chemical Geology* 214, 99–125.
- Yang, J.H., Sun, J.F., Zhang, M., Wu, F.Y., Wilde, S.A., 2012. Petrogenesis of silica-saturated and silica-undersaturated syenites in the northern North China Craton related to post-collisional and intraplate extension. *Chemical Geology* 328, 149–167.
- Yang, J.H., Wu, F.Y., Wilde, S.A., Chen, F., Liu, X.M., Xie, L.W., 2008. Petrogenesis of an Alkali Syenite-Granite-Rhyolite Suite in the Yanshan Fold and Thrust Belt, Eastern North China Craton: Geochronological, Geochemical and Nd-Sr-Hf Isotopic Evidence for Lithospheric Thinning. *Journal of Petrology* 49, 315–351.
- Zerdane, A., Rjimati, E.C., Zemmouri, A., Mouttaqi, A., Michard, A., 2011. Aghracha Iron Mine and Uranium-REE prospect (Awserd Province). Notes et Mémoires du Service géologique du Maroc. N°564 9, 177–182.

CHAPTER 3

REE enrichment and synchysite mineralization in the late hydrothermal quartz carbonate veins in the Jbel Boho complex in the Bou Azzer inlier (Anti-Atlas/Morocco).

Abstract

High LREE-enrichment and the potential for REE ore formation occur in the late differentiation stage associated with hydrothermal veins of the Jbel Boho alkaline complex in the district of Bou Azzer in the Anti-Atlas of Morocco. The complex itself consists of a sequence of basic to silicic lavas intruded by a polyphase quartz- or olivine-syenite intrusion, all of which are cut by a later dyke swarm. Two categories of veins were distinguished: the ore bearing veins and the ore barren veins.

The ore-bearing veins consist of quartz jasper and quartz veins, which are associated with a N50°E oriented fault, cutting the quartz syenite and the adjacent volcanics together north of the pluton. The predominant host mineral for rare earth elements in the two mineralized rock types is the Ca-LREE-

fluorcarbonate synchysite ($\text{REE-Ca}(\text{CO}_3)_2(\text{F-OH})$), which is observed in thin section as crystals up to 200 μm . The predominant REE hosted in synchysite are Ce, La and Nd. A very small amount of rhabdophan-(Ce) ($\text{LREE-PO}_4(\text{H}_2\text{O})$) is also found in the REE enriched quartz vein together with synchysite.

Fluid inclusion (mainly LVS inclusions) analyses of quartz crystals in the synchysite-bearing veins suggest very high salinity corresponding to NaCl equivalent between 32 and 37 wt%. Very low eutectic temperatures (T_E) ranging between -50 and -54°C argue against a pure NaCl system and suggest more complex salinity of the fluid. Representative homogenization temperatures (from 150 to 250°C) obtained for most inclusions provide the minimum temperature conditions in which the corresponding quartz veins were formed.

LREE are very mobile as chloride complexes at low pH. We propose a model for the formation of hydrothermal REE-Ca-F carbonate deposits in the veins involving the transport of REE as chloride complexes at low pH conditions in the presence of fluorine as HF with other ligands such Ca^{2+} and CO_3^{2-} also present. The deposition of synchysite is proposed to result from neutralization of this fluid by carbonate minerals (dolomite), which buffer its acidity and allow REE precipitation as Ca-F carbonate in the vein. Both REE mineralization types appear to be formed from a similar hydrothermal source.

The ore barren veins have very low REE contents and show two types of veins: Veins with enrichment of LREE over HREE and veins with quite flat REE pattern and high carbonate and iron contents associated with jasper and carbonate

coated with Fe-oxides. The LREE/HREE fractionation in these veins seems to be controlled by an interplay of two factors: a low activity of ligands like Cl that favour LREE transport and the formation of siderite, which has a much higher partition coefficient for HREE than for LREE, due to the HREE having similar ionic radii to Fe^{2+}

3.1 Introduction

The most important rare earth elements (REE) deposits in the world are associated with alkaline intrusions, for example, Bayan Obo Fe-Nb-REE deposits in Inner Mongolia, China (the world's largest mined REE deposit) and Mountain Pass in the USA (Long et al., 2010; Wu et al., 1996). The increasing need for REE for the electronics industry and the present production from only a few localities worldwide (e.g., China with about 97% of the world REE production, Humphries (2013)) has led to an increase in prospection for alternative REE deposits. Initially (e.g., Gieré (1996, 1990)) the REE were considered to be immobile in aqueous fluids and so deposits were not sought in hydrothermal systems. The discovery of the Bayan Obo REE hydrothermal deposit provided evidence that these elements may be transported by magmatic and hydrothermal fluids and form valuable ore deposits (Smith and Henderson, 2000; Smith et al., 2015, 2000).

Morocco possesses several alkaline complexes, of which the Tamazert complex (syenite-carbonatite) in Central High Atlas is known for its association with REE minerals such as monazite, parisite and synchysite (Woolley, 2001). The Government's Office National des Hydrocarbures et des Mines (ONHYM) has additionally recently reported the occurrence of REE deposits with very high REE concentration (up to 3%) linked with carbonatite rocks in the Ouled Dlim nappes of the Moroccan Mauritanides (ONHYM, 2015, 2013; Qalbi et al., 2011; Zerdane et al., 2011) in southern Morocco (Fig. 3.1).

The alkaline magmatic complex of Jbel Boho is one of several additional alkaline complexes found in the Anti Atlas, which have not been subject to extensive prospection. It was the subject of some work ([Álvarez et al., 2006](#); [Choubert, 1952](#); [Ezzouhairi et al., 2008](#); [Leblanc, 1981a](#)), however no published study is available on the rare earth mineralization in this area. Here we present the first geochemical and petrological data on Jbel Boho REE deposits as part of an integrated study that aims to identify the most REE enriched rocks, the corresponding rare earth minerals and the origin of the ore-forming fluid responsible for the REE mineralization.

We find both the Ca-LREE-fluor-carbonate mineral synchysite ($\text{REECa}(\text{CO}_3)_2(\text{F-OH})$) and the REE-P mineral rhabdophane ($\text{REEPO}_4 \cdot n\text{H}_2\text{O}$) in late hydrothermal quartz veins. Synchysite has potential as a new source of rare earth elements, and Mount Burgess Mining (MTB) recently identified synchysite as the main REE-host mineral in Tsumkwe in NE Namibia ([MTB, 2011](#)).

3.2 Geological setting

The Jbel Boho alkaline complex is the best preserved igneous complex in the south-western part of the Bou Azzer inlier in Anti-Atlas ([Fig. 3.1](#)). The Bou Azzer inlier is a productive mining area, known in particular for its famous cobalt-arsenide deposits in the Bou Azzer mine, the copper deposit at Bleida and gold-palladium deposits at Bleida Far West related to the ophiolite of Bou Azzer ([Belkabir et al., 2008](#); [El Ghorfi et al., 2008](#); [Ennaciri et al., 1995](#); [Leblanc, 1981b, 1972](#); [Oberthür et al., 2009](#)).

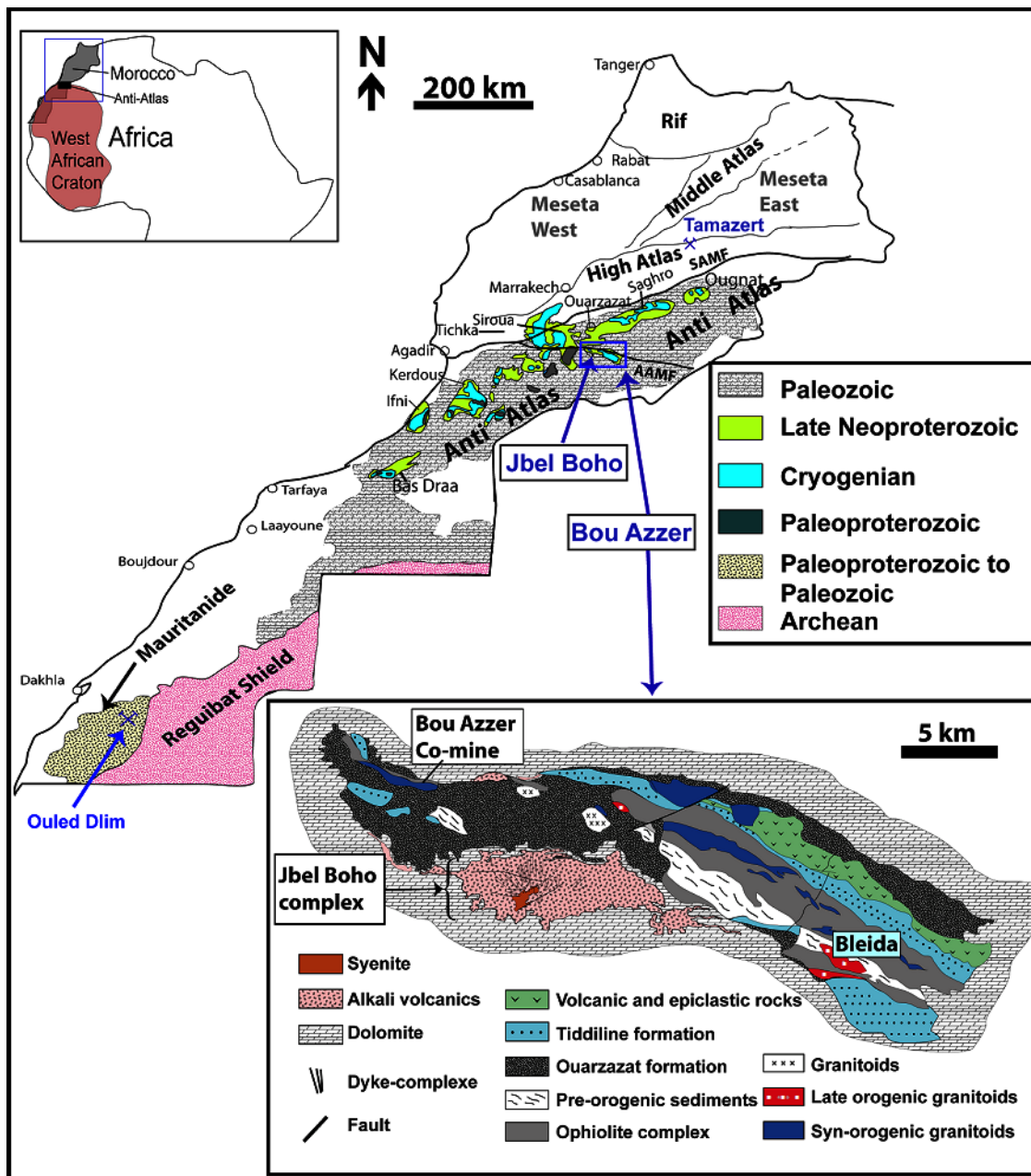


Figure 3.1 A) Simplified geological map of Anti Atlas showing the location of the Bou Azzer inlier, modified after [Guasquet et al. \(2005\)](#). B) Simplified geological map of Bou Azzer showing the location of Jbel Boho complex, modified after [Leblanc \(1975\)](#). SAMF (south Atlas major fault) and AAMF (Anti-Atlas major fault)

Zircon U-Pb geochronological studies on the syenite (534 ± 10 Ma) and trachyte of Aghbar (531 ± 5 Ma) show that the Jbel Boho complex is Early Cambrian in age (Ducrot and Lancelot, 1977; Gasquet et al., 2005). It was emplaced on the northern edge of the West African Craton (WAC). It represents a late magmatic event in the Pan-African evolution of the region, which was itself marked by two tectonic regimes: a compressive regime, which is reflected by the emplacement of the ophiolite comprising much of the core of the Bou Azzer inlier, and a later extensional regime represented by calc-alkaline magmatism of the Ouarzazate group and the alkaline magmatism of the Jbel Boho complex (Gasquet et al., 2008, 2005).

The lava flows associated with Jbel Boho magmatism are intercalated with the lower Infracambrian dolomites (from the lower Adoudounian formation) and overlapped by the upper Adoudounian dolomite and lie-de-vin series. According to several authors (Algouti et al., 2001; Álvaro et al., 2006; Piqué et al., 1999; Soulimani et al., 2003) normal faulting accompanied by an extensional tectonic regime related to rifting led to the alkaline magmatism of Jbel Boho and simultaneously to the deposition of the Adoudounian carbonate under sub-aerial to shallow water conditions.

Chapter 2 (Benaouda et al. Paper in preparation) showed, based on major- and trace element analyses, that the Jbel Boho complex consists of three magma generations. The first magmatic event generates successive alkaline lava flows from alkaline basanites to trachytes and rhyolites. The volcanics crop out in the

field with an inclination of about 30° to the South and display relative chronology from the oldest in the north to youngest towards south. The majority of the volcanic rocks show a porphyritic texture with alkali feldspar and plagioclase phenocrysts. The enrichment of the LREE relative to the HREE, the high alkaline contents in all volcanic and the strong negative Eu anomalies in the high evolved volcanics suggest that they are formed through fractional crystallization from a magma derived by small degrees of partial melting of garnet peridotite mantle.

The second magmatic event is represented by the syenitic intrusion ([Fig. 3.1](#)) which cuts the volcanics. Two types of syenite are present: olivine syenite and quartz syenite, which display different REE patterns and trace element anomalies. They are considered to be formed from a second generation of magma that probably derived from partial melting of underplated mafic rocks and crustal contamination.

The third magmatic event consists of microsyenitic and subalkaline rhyolitic dykes. Unlike the syenite pluton, the dykes contain plagioclases and have different HFSE signatures. They are interpreted to be evolved from a new magma generation by feldspar fractionation leading to a decrease of the alkali elements in the subalkaline rhyolitic dykes. Aeromagnetic studies on the Jbel Boho area ([unpublished data from Managem mining company](#)) show two strong magnetic anomalies, one related to the syenitic pluton and another further south, in an area overlain by the dolomitic cover ([Fig. 3.2](#)).

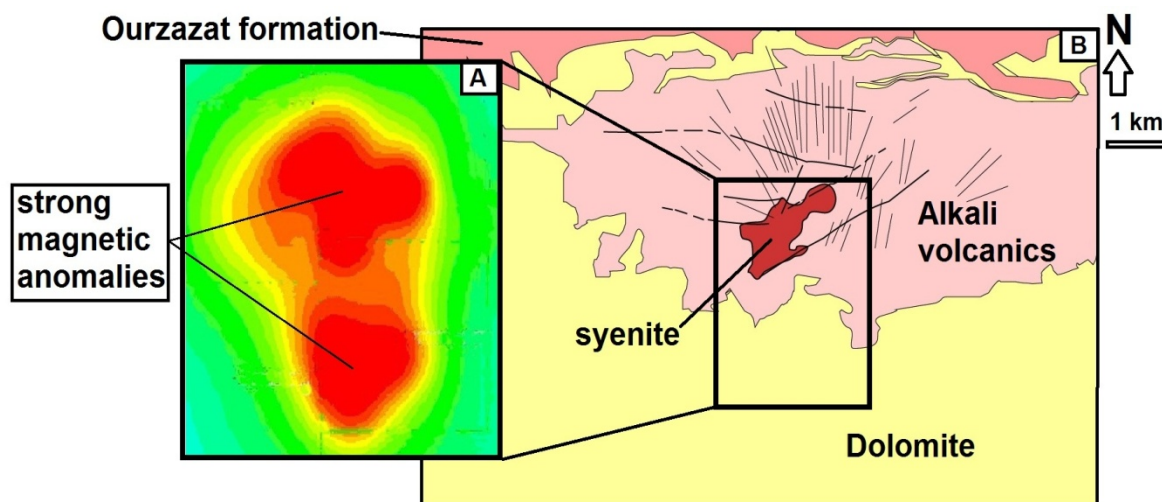


Figure 3.2 A) Magnetic anomaly map (Managem internal document) shows two strong anomalies around the syenitic intrusion and the dolomite, B) geological map of Jbel Boho modified after [Leblanc \(1975\)](#)

The cause of the southern anomaly is unknown, although it may be related to another pluton. These anomalies led to mineral exploration work in this area.

All Jbel Boho rocks are cross cut by quartz carbonate veins with different forms and mineral assemblages. The rare earth mineralization, which is associated with N50°E oriented veins and a N-S oriented rhyolitic dyke, is the focus of this study.

Both mineralized rock types crop out north of the syenite pluton.

3.3 Samples and methodology

Samples of quartz carbonate veins were collected systematically along a broad northeast-southwest transect across the complex ([Fig. 3.3](#)). After macroscopic and microscopic examination, 26 samples were selected for chemical analysis.

Whole rock analyses of major- and trace elements were performed at the ACME

Analytical Laboratories Ltd, Vancouver (Canada) using X-ray fluorescence (XRF) and laser ablation inductively coupled plasma mass spectrometer (LA-ICP-MS). Major elements detection limits range from 0.01 to 0.1 wt% and trace elements detection limits range from 0.01 to 1 ppm, except the values of gold (Au), which are given in ppb with detection limit of 0.5 ppb. The compositions of mineral and fluid inclusions were determined using a JEOL JXA 8900R electron microprobe and a Linkam THM 600, respectively, at the Institute of Geosciences, University of Kiel, Germany.

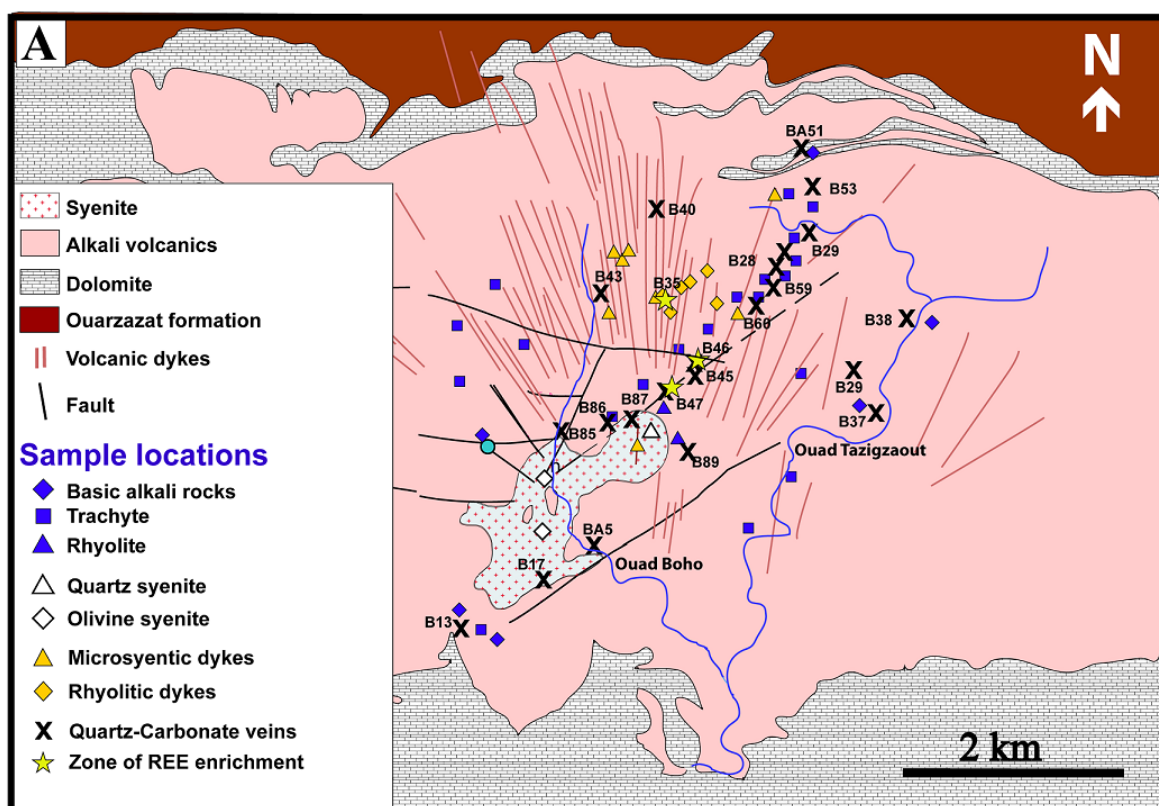


Figure 3.3 Geological map of Jbel Boho complex showing the different location of the samples, modified after [Leblanc \(1975\)](#).

3.4 Petrography and geochemistry of the late hydrothermal veins.

3.4.1 Petrography

Hydrothermal quartz carbonate veins occur in all rock types of the Jbel Boho alkaline complex (Fig. 3.4 and Fig. 3.5) and display different thicknesses (most veins vary from 20 cm to 2m in thickness) and orientations. They crop out over a distance of a few metres to several ten metres on the surface. The hydrothermal veins are mainly quartz dominated with various contents of dolomites and calcites as well as opaque variety of silica called jasper. The latter occur only around the quartz syenite.

Since the objective of this work is the study of REE ore mineralization, the veins are subdivided into two categories, namely the ore-bearing veins and ore-barren veins.

3.4.1.1 The ore bearing veins

Two types of REE mineralization can be distinguished in the Jbel Boho alkaline complex (Fig. 3.3). Type-I consists of synchysite mineralization within a discordant subalkaline rhyolitic dyke (sample B35) which strikes in a N-S direction and lies north of the quartz syenite. The dyke consists of feldspar phenocrysts (from 0.5 and 2 mm in size) in a quartz-rich matrix which also contains chlorite, opaques, and synchysite, the latter considered as being of hydrothermal origin (Chap 2). Type-II (this study) consists also of synchysite mineralization within two late hydrothermal veins, a quartz vein (sample B46-3)

and quartz-jasper vein (B47-5, B47-6 and B47-7). The REE ore bearing veins (Fig. 3.3; Table 3.1 G1) are oriented N50°E along a subvertical fault zone and show thicknesses up to ~1.5 m.

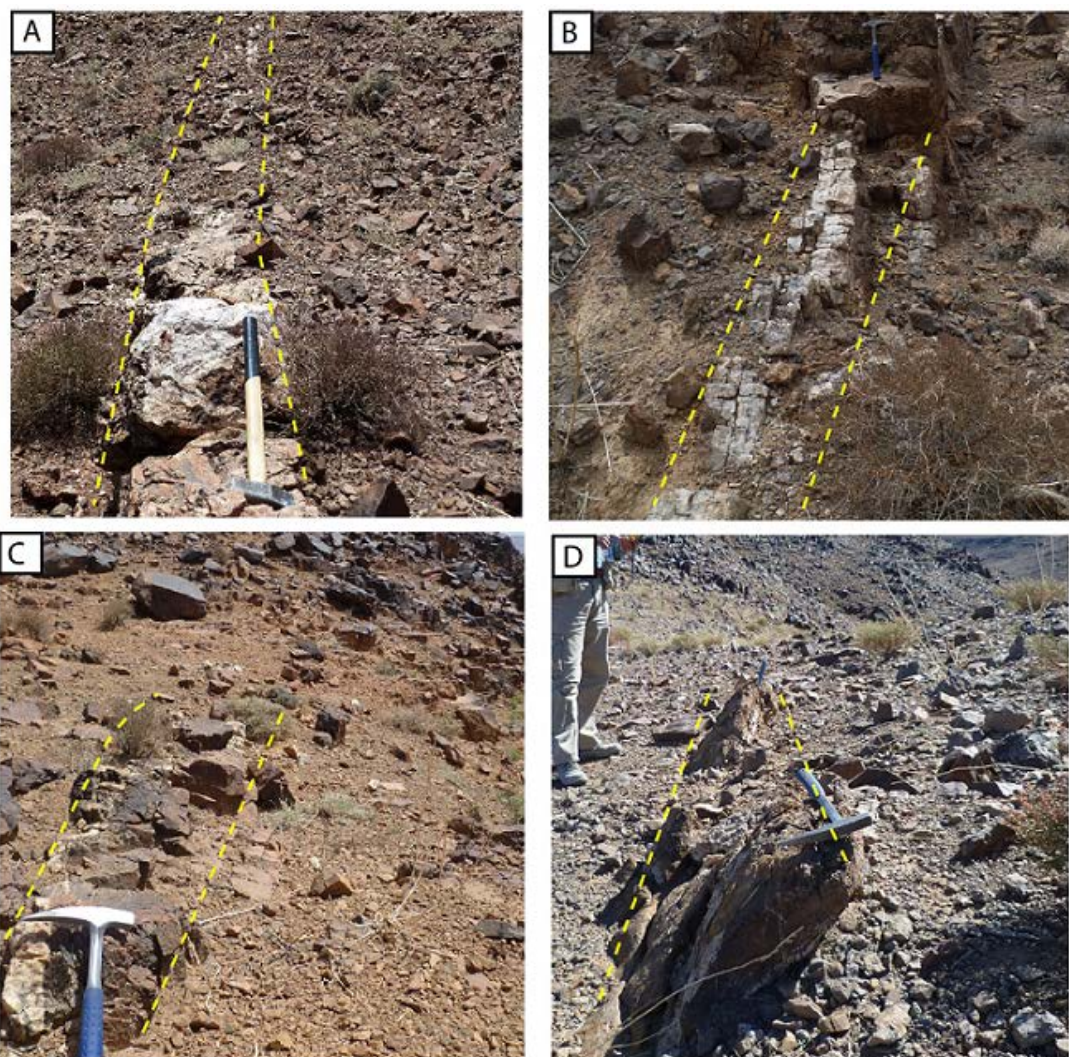


Figure 3.4 Examples of hydrothermal ore barren veins with low REE contents: A) Quartz vein cutting trachyte (view toward south) , B) quartz vein cutting phonotephrite (view toward south), C) quartz-jasper vein in trachyte near syenite (view toward east), D) carbonate dominated vein in trachyte (view toward east).

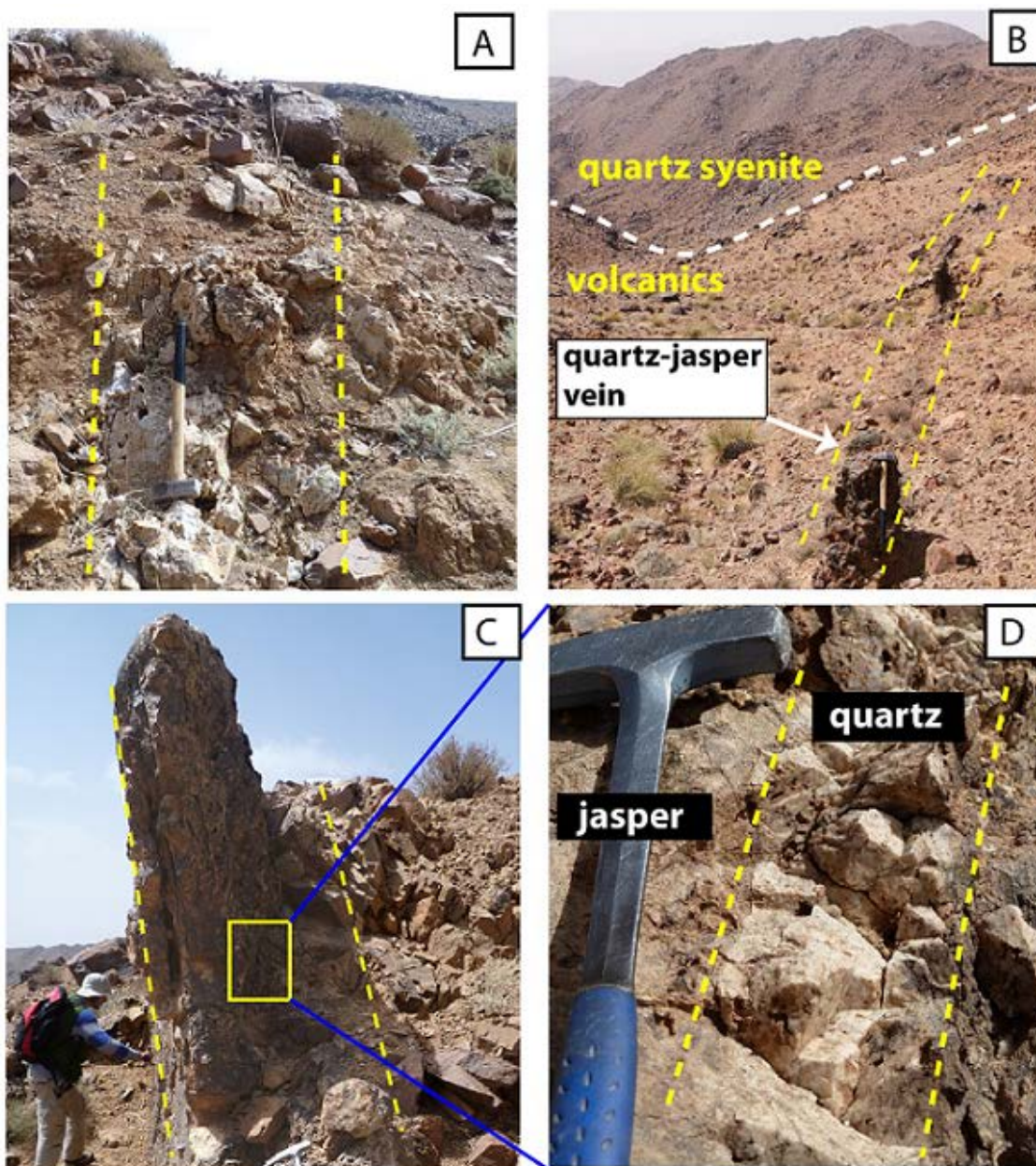


Figure 3.5 Examples of synchysite bearing veins with high REE contents: A) synchysite and rhabdophane bearing quartz vein (B46) in trachyte (view toward NE), B) large synchysite bearing quartz-jasper vein (B47) next to the quartz syenite cutting the neighbouring volcanic (view toward SW), C) and D) the same vein (B47) showing quartz veins within jasper.

The presence of *slickensides* (polished fault surfaces) on the footwall of the quartz-jasper vein indicates that the fault continued to move after the formation of the vein (Fig. 3.6). The fault plane and the direction of the slickenlines, which form slip vector of 25° to the SW relative to the fault strike (N50°E), indicates an oblique dextral strike-slip fault.

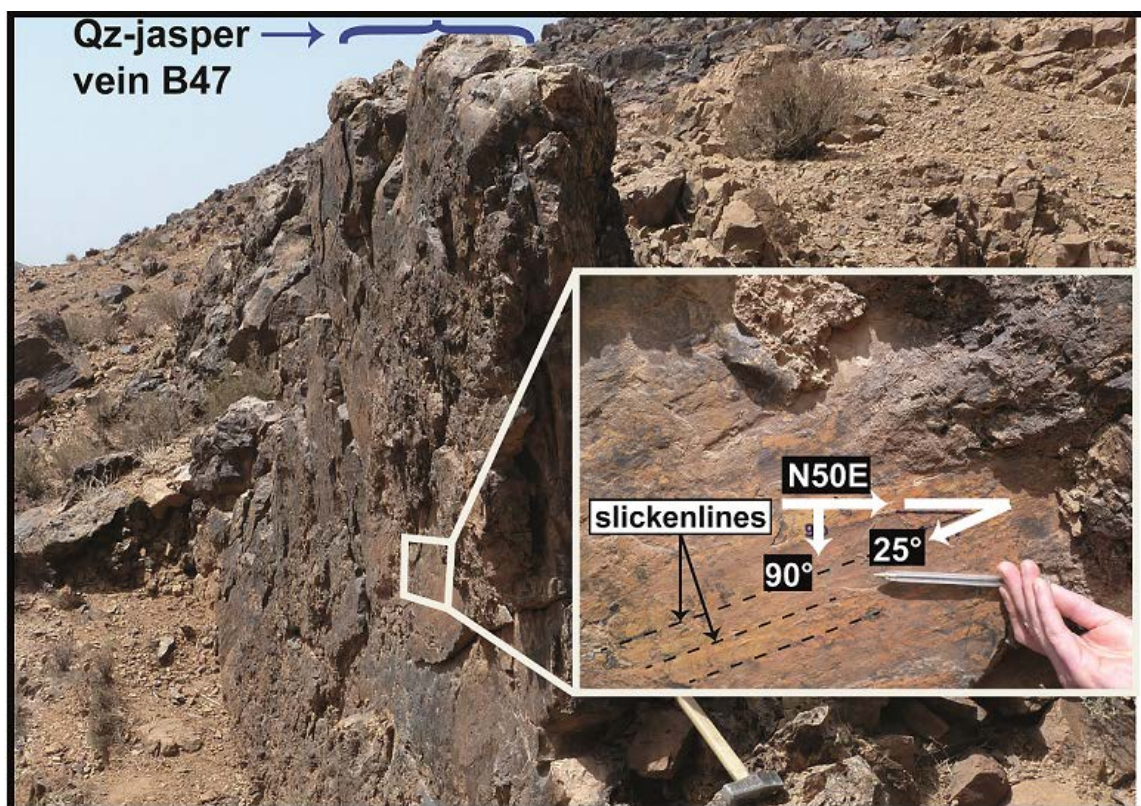


Figure 3.6 The picture displays structural characteristics of the fault hosting LREE enriched quartz-jasper vein, which occurs in the footwall of the fault. The orientation of the slickenlines indicates an oblique dextral strike-slip movement.

The quartz-jasper vein is composed of jasper (dense and opaque microcrystalline quartz that is of red-brownish colour due to Fe- and Mn-Fe oxides), which is itself cut by later quartz veins (Fig. 3.5 B, C, D) that contain small REE-F-Ca carbonate minerals synchysites (up to 100 μm). Synchysites

occur both as inclusions in quartz crystals and in equilibrium with them (Fig. 3.7A). Between the synchysite bearing quartz and the jasper occur also dolomitic rhombs (Fig. 3.7B) comparable in shape to that of the ore barren veins, although they are more strongly leached and darker. The leached zones in the rhombs correspond to replacement of carbonate with Mn- and Fe-oxides. Synchysite is the only REE-host mineral in the LREE-enriched quartz-jasper vein.

The ore bearing quartz vein (B46-3) is composed of zoned and coarse-grained quartz crystals (1 mm to 3 mm in size) cross-cut by fine grained quartzes (up to 250 µm) that contain synchysite minerals with very similar petrographic relationships to those seen in the quartz-jasper vein. The ore bearing quartz vein contains two REE-host minerals, synchysite (the main REE-host mineral) and occasionally tiny rhabdophan minerals associated with the fine-grained quartz, whereas the coarse grained zoned quartz crystals show no rare earth host minerals. Under the polarising microscope the synchysite minerals in both types of ore-bearing vein appear colourless to slightly yellow with high relief. They form subhedral to euhedral crystals (Fig. 3.7A and 3.7C), which display sometime very good idiomorphic form as illustrated in a thick section micrograph (Fig. 3.7D).

The other veins of the G1 group have feeble synchysite contents, which are optically very difficult to identify in dispersion of the other fine grained carbonates like dolomite and calcite. Similar synchysite minerals also occur in the ground masse of a rhyolitic dyke (B35; Fig. 3.7E and 3.7C), which is described with more detail in Chapter 2.

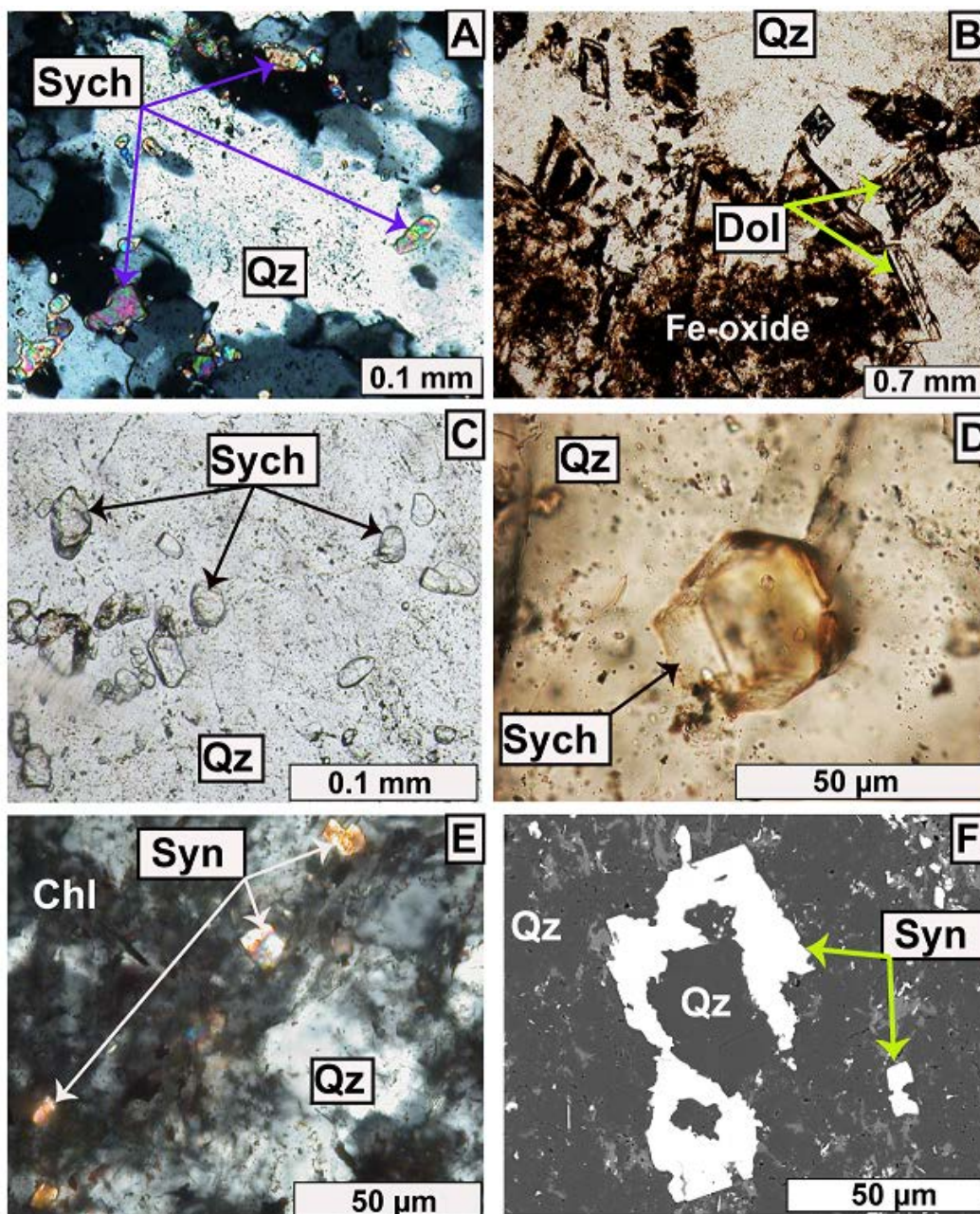


Figure 3.7 Photomicrographs showing the occurrence of synchysite and carbonate in the ore bearing veins: A) association of synchysite with quartz crystals in the quartz jasper vein (B47-5), B) altered dolomitic rhombs between quartz and jasper, C) synchysite grains within quartz in the quartz vein (B46-3), C) idiomorphic synchysite in 3D show from a thick section (B46-3), E) and F) show synchysite occurrences within a rhyolitic dyke.

3.4.1.2 The ore barren veins

The ore-barren veins (Table 3.2, 3.3 and e.g. Fig. 3.4) occur in all Jbel Boho rock types. They consist of quartz carbonate (dolomite and calcite) veins with dominance of quartz in most veins.

The lower dolomites are also intruded by small quartz veins, in which euhedral dolomite rhombs (generally from 10 to 400 μm in size), anhedral calcite and occasionally chabazite crystals occur (Fig. 3.8A). The carbonate rhombs show strong dissolution of the core and part of the rim or vice versa. The chabazite crystals are colourless and idiomorphic with high relief similar to apatite, but optically positive.

The quartz crystals in the hydrothermal veins within the magmatic rocks are anhedral to subhedral with varying grain sizes from 0.1 to 3 mm (Fig. 3.8B). The dolomite rhombohedrons occur within quartz as isolated euhedral crystals or subhedral aggregate with sizes mostly in the range from 0.1 mm to 0.7 mm. Zonation within individual dolomite crystals is reflected by either clear core or cloudy rims or vice versa. Microprobe examination shows that the dark and light zones in the dolomite rhombs correspond to Mg rich- and Ca-rich carbonate zones respectively (Fig. 3.8C). Muscovite occurs occasionally as small colourless inclusions in some quartz veins with grain sizes up to 0.15 mm (Fig. 3.8D).

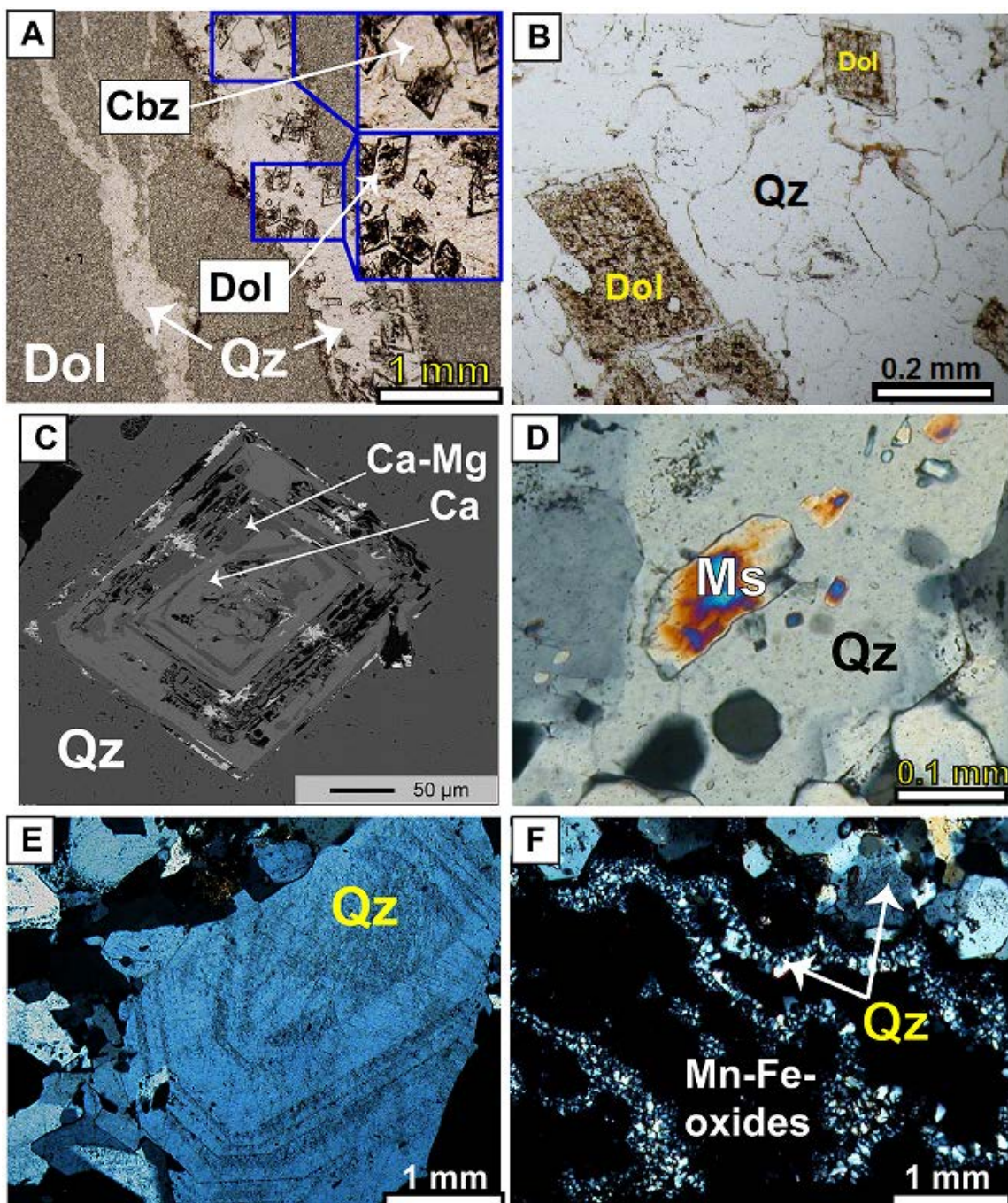


Figure 3.8 Sample micrographs: A) Dolomite and chabazite bearing quartz veins in the lower dolomite. B) Example of diomorphic carbonate crystals in the quartz veins. C) Back-scattered image of a dolomite rhombs (B) showing zones of Ca and Ca-Mg enrichments. D) Example of muscovite in a quartz vein. E) Zonations of Quartz crystals in some quartz veins (B46). F) Crystallization of quartz in the chalcedon form in jasper of quartz jasper veins (B47).

Some quartz veins near to the syenite show quartz crystals with euhedral zoning. The zonation can be easily observed under a polarisation microscope (Fig. 3.8E) especially for quartz crystals with sizes over 1 mm. With decreasing crystal sizes the growth zones become less evident and even invisible.

The jasper ore barren veins are mainly found adjacent to the quartz syenite. They are the least abundant of all veins and have a prefer orientation from N20°E to N50°E similar to the orientation of the ore bearing veins, but with thickness generally less than 30 cm. In thin section, the microcrystalline quartz in the jasper is fibrous and so is classified as chalcedony (Fig. 3.8F).

3.4.2 Geochemistry

The REE patterns of all vein samples plotted relative to C1-chondrite are shown in Figure 9. The samples have been divided into three groups (G1-G3) based on their LREE enrichment and the presence of visible REE minerals: Group G1 consists of samples from the ore-bearing veins, Group G2 veins are ore-barren but still show some LREE enrichment relative to HREE; Group G3 has no LREE enrichment..

All veins show negative Eu anomalies (Fig. 3.9 A, B and C). The sample (B51-1) from the lower carbonates, which are intercalated with basic volcanic rocks, is added to Fig. 9D for comparison. It shows also slight enrichment of the LREE relative to the HREE, but without any Eu anomaly.

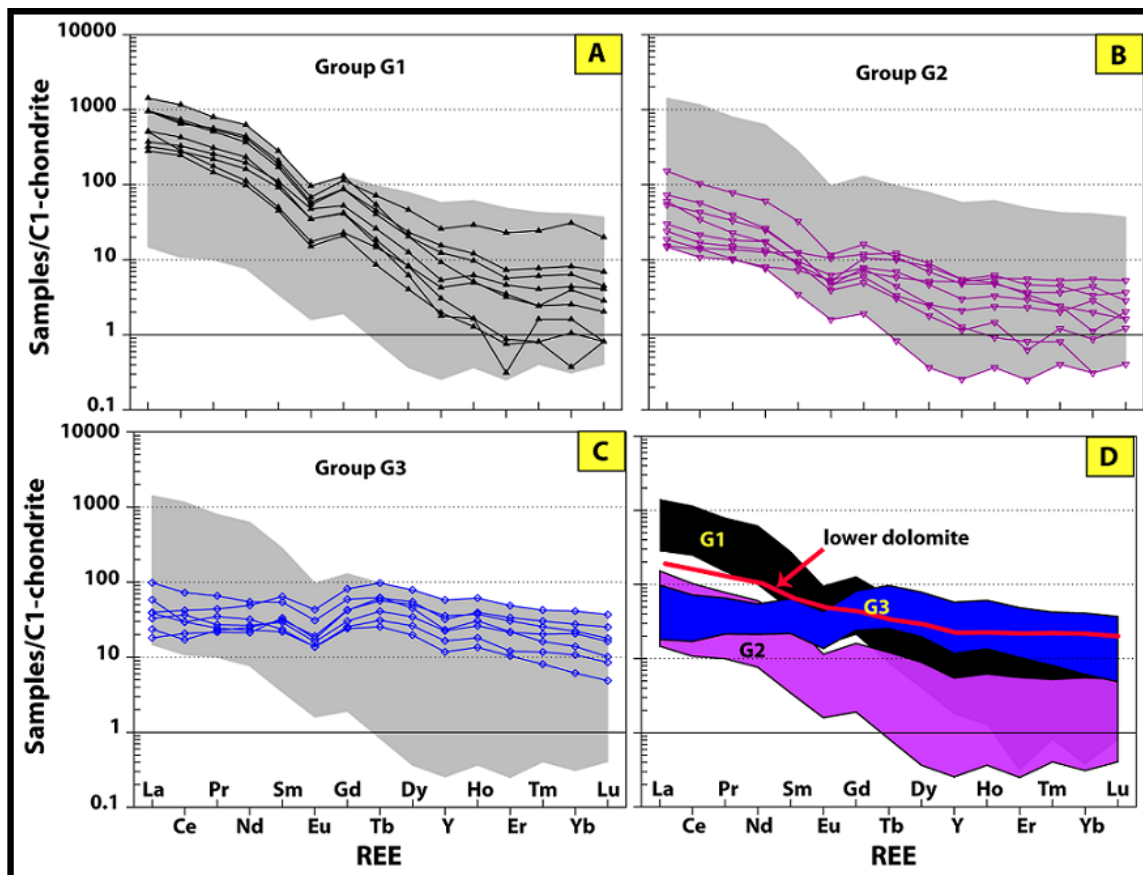


Figure 3.9 Chondrite normalized REE patterns (McDonough & Sun, 1995) of all vein samples in three groups. (A) REE plot of the LREE highly enriched veins (G1), (B) REE plot of REE poor veins (G2), (C) REE plot the veins with flat REE patterns and (D) plot of REE highlights the different veins in three groups (G1, G2 and G3). The REE pattern of the lower dolomite (B51-1) is added for comparison.

The group G1 (see also Table 3.1) shows strong LREE enrichment relative to the HREE, which is related to its different REE ore (synchysite-(Ce) and rhabdophane-(Ce)) compositions. They have all very similar LREE element patterns with somewhat more variable HREE, and Σ REE contents between 1505 and 292 ppm.

Table 3-1 Major (wt%) and trace elements (ppm) contents of Jbel Boho hydrothermal veins (G1 group) (* data from W. Schink, Pers.com)

	G1								
	B46-3	B47-5*	B47-6*	B47-7	B46-2	B17-1	B13-2	B5-1	B86
SiO2	97.30	90.60	96.50	97.80	98.40	91.50	78.70	95.60	98.40
TiO2	0.15	0.06	0.03	0.08	0.06	<0.01	<0.01	<0.01	0.01
Al2O3	1.04	0.16	0.53	0.22	0.73	0.58	0.70	0.32	0.20
Fe2O3	0.29	5.16	0.88	0.42	0.28	1.90	0.75	0.42	0.59
MnO	0.02	0.90	0.11	0.05	0.03	0.07	0.10	0.05	<0.01
MgO	0.08	0.08	0.06	<0.01	0.06	0.05	3.62	0.05	0.01
CaO	0.15	0.22	0.09	0.05	0.15	2.84	5.83	1.37	0.05
Na2O	0.03	<0.01	0.06	0.05	0.07	<0.01	0.01	<0.01	0.07
K2O	0.32	0.03	0.14	0.07	0.23	0.09	0.10	0.03	0.06
P2O5	0.06	0.02	0.01	<0.01	0.02	0.03	0.05	0.02	<0.01
Cr2O3	<0.001	<0.001	<0.001	<0.001	<0.001	<0.001	<0.001	0.00	<0.001
LOI	0.53	1.87	0.60	0.37	0.47	2.74	9.02	1.35	0.42
Total	99.97	99.10	99.01	99.11	100.50	99.80	98.88	99.21	99.81
Ba	33.00	464.00	70.00	37.00	21.00	116.00	77.00	17.00	28.00
Rb	8.20	1.10	6.00	2.80	5.50	2.70	4.10	0.90	2.60
Sr	16.90	41.50	18.00	13.00	8.70	21.30	95.70	17.20	21.30
Zr	29.80	18.80	61.80	45.70	9.50	11.20	6.90	1.50	4.90
Nb	7.30	3.00	10.70	6.40	2.20	1.10	1.00	0.80	2.70
Ni	0.50	3.00	2.00	0.80	0.30	1.40	0.20	0.80	0.50
Co	0.80	2.70	2.90	2.90	0.20	2.10	0.60	0.90	0.70
Zn	5.00	11.00	6.00	5.00	2.00	18.00	2.00	2.00	6.00
La	335.80	226.80	228.40	224.00	121.90	88.10	119.90	76.10	66.60
Ce	712.10	396.20	449.80	422.70	262.80	201.20	173.90	170.20	150.10
Pr	74.19	52.64	50.58	47.59	28.77	23.94	16.44	20.39	13.65
Nd	286.80	202.40	189.70	168.50	106.60	90.00	51.60	74.00	44.90
Sm	41.77	30.90	28.04	25.24	15.23	16.39	7.41	13.58	6.68
Eu	5.44	3.83	3.29	3.05	1.96	2.68	0.98	1.97	0.85
Gd	25.72	22.71	17.55	17.35	8.40	10.47	4.57	8.20	4.18
Tb	1.96	2.59	1.65	1.46	0.67	0.94	0.53	0.59	0.31
Dy	5.02	11.36	5.71	5.03	1.99	3.09	2.04	1.53	0.99
Y	14.60	40.50	24.40	19.50	4.80	8.40	6.70	2.80	3.10
Ho	0.28	1.59	0.66	0.53	0.09	0.34	0.27	0.09	0.07
Er	0.51	3.67	1.17	0.91	0.05	0.74	0.56	0.14	0.12
Tm	0.06	0.60	0.19	0.15	0.04	0.10	0.06	0.02	0.02
Yb	0.64	4.98	1.32	1.03	0.26	0.71	0.41	0.17	0.06
Lu	0.07	0.49	0.17	0.11	0.02	0.10	0.05	0.02	0.02
ΣREE	1504.96	1001.26	1002.63	937.15	553.58	447.20	385.42	369.80	291.65
Ta	0.40	0.30	0.70	0.50	0.20	<0.10	<0.10	0.10	<0.10
Hf	1.00	0.30	1.70	1.00	0.30	<0.10	<0.10	<0.10	0.10
As	<0.50	34.30	5.70	3.10	0.80	31.70	<0.50	1.60	<0.50
Ag	<0.10	<0.10	<0.10	<0.10	<0.10	<0.10	<0.10	<0.10	<0.10
Au	1.50	3.40	3.20	<0.50	1.80	<0.50	0.90	0.70	14.80
Ga	2.90	2.10	1.40	1.00	2.30	1.70	1.60	0.70	<0.50
Mo	1.20	38.40	4.50	2.40	0.40	7.00	0.40	1.00	0.90
Cu	30.30	51.90	9.20	9.90	23.10	66.40	11.70	40.90	604.80
Pb	1.40	2.20	2.60	2.00	0.60	4.50	0.50	1.10	2.50
Th	2.60	2.70	11.30	8.70	2.40	0.70	0.20	<0.2	0.30
U	0.50	2.50	0.90	0.50	0.10	0.10	0.10	<0.10	0.20
Cs	0.20	<0.10	0.20	0.10	0.10	0.10	0.20	<0.10	0.40
V	15.00	97.00	13.00	<8.00	12.00	<8.00	<8.00	<8.00	<8.00

Table 3-2 Major (wt%) and trace elements (ppm) contents of Jbel Boho hydrothermal veins (G2 group) (* data from W. Schink, Pers.com)

	G2								
	B40-4	B87	B46-1	B37	B53-2*	B40-1	B53-1*	B28-1	B38
SiO2	95.40	97.40	97.20	96.10	75.50	98.20	66.50	82.40	98.70
TiO2	0.06	<0.01	0.14	<0.01	0.05	<0.01	0.03	0.09	<0.01
Al2O3	1.30	0.23	1.00	0.86	1.00	0.45	0.57	6.48	0.24
Fe2O3	0.33	0.82	0.36	0.22	1.23	0.16	0.35	1.37	0.04
MnO	0.03	<0.01	0.02	0.02	0.22	0.03	0.26	0.04	<0.01
MgO	0.08	<0.01	0.08	0.22	0.27	0.02	1.95	0.27	<0.01
CaO	0.29	0.05	0.05	0.50	12.23	0.23	15.17	1.84	0.16
Na2O	0.02	0.07	0.09	<0.01	0.02	0.04	<0.01	0.05	<0.01
K2O	0.35	0.05	0.51	0.20	0.15	0.11	0.12	3.27	0.02
P2O5	0.02	<0.01	0.01	<0.01	<0.01	<0.01	<0.01	0.04	<0.01
Cr2O3	<0.001	<0.001	<0.001	<0.001	<0.001	<0.001	<0.001	0.00	<0.001
LOI	0.77	0.81	0.49	0.99	9.92	0.55	14.18	2.52	0.31
Total	98.65	99.43	99.95	99.11	100.59	99.79	99.13	98.37	99.47
Ba	159.00	27.00	52.00	50.00	241.00	56.00	34.00	2760.00	8.00
Rb	10.10	2.00	11.70	7.30	5.50	1.70	3.40	86.70	0.60
Sr	42.60	27.10	17.00	14.20	27.40	8.10	36.90	67.20	9.10
Zr	41.70	5.10	36.30	7.80	20.10	7.00	14.80	60.90	1.30
Nb	8.20	2.00	5.50	1.20	3.50	1.30	2.60	3.30	0.40
Ni	1.40	0.80	0.50	0.50	1.20	0.40	0.80	0.80	0.10
Co	0.90	1.00	0.40	0.40	0.30	0.40	4.10	0.60	0.60
Zn	3.00	8.00	7.00	3.00	1.00	2.00	30.00	2.00	<1
La	36.10	17.30	12.80	14.20	4.40	7.10	5.70	3.50	3.60
Ce	63.20	35.00	26.30	21.10	8.70	13.20	10.30	6.60	8.50
Pr	7.26	3.68	3.08	2.11	1.27	1.67	1.41	0.93	0.96
Nd	27.70	12.00	11.40	7.80	5.70	8.00	6.20	3.70	3.50
Sm	4.82	1.84	1.82	1.27	1.85	1.29	1.41	1.07	0.51
Eu	0.65	0.26	0.26	0.29	0.59	0.22	0.35	0.30	0.09
Gd	3.20	1.18	1.53	2.08	2.36	0.98	1.56	1.37	0.38
Tb	0.39	0.12	0.16	0.36	0.44	0.11	0.25	0.21	0.03
Dy	1.70	0.60	0.62	1.99	2.20	0.44	1.15	1.27	0.09
Y	7.50	2.00	3.30	8.60	8.60	1.80	4.70	8.00	0.40
Ho	0.26	0.05	0.13	0.27	0.34	0.08	0.18	0.31	0.02
Er	0.59	0.13	0.37	0.55	0.74	0.10	0.47	0.89	0.04
Tm	0.09	0.02	0.05	0.06	0.11	0.03	0.06	0.13	0.01
Yb	0.71	0.05	0.46	0.32	0.54	0.14	0.18	0.89	0.05
Lu	0.07	0.01	0.04	0.04	0.09	0.03	0.05	0.13	0.01
ΣREE	154.24	74.24	62.32	61.04	37.93	35.19	33.97	29.30	18.19
Ta	0.50	0.10	0.30	<0.10	0.30	<0.10	0.10	0.30	<0.10
Hf	1.00	0.20	0.80	0.20	0.60	0.10	0.30	1.60	<0.10
As	4.30	<0.50	1.00	0.60	3.10	1.30	6.30	<0.50	<0.50
Ag	<0.10	<0.10	<0.10	<0.10	<0.10	<0.10	<0.10	<0.10	<0.10
Au	<0.50	<0.50	<0.50	2.20	0.80	1.40	1.90	<0.50	<0.50
Ga	3.50	<0.50	2.60	1.70	1.50	3.10	1.30	6.00	2.10
Mo	0.60	<0.10	0.70	0.30	0.50	0.20	0.60	0.50	<0.10
Cu	7.50	4932.90	6.80	19.60	4.80	25.10	68.50	1.10	14.70
Pb	1.00	2.30	1.40	1.00	1.80	1.20	10.60	1.10	1.30
Th	1.50	0.20	1.10	0.20	0.70	0.20	0.40	2.70	<0.2
U	0.50	<0.10	0.40	0.10	1.40	0.10	0.80	0.60	<0.10
Cs	0.20	0.50	0.30	0.30	0.30	<0.10	0.10	1.70	0.10
V	25.00	<8.00	16.00	<8.00	14.00	<8.00	9.00	13.00	<8.00

Table 3-3 Major (wt%) and trace elements (ppm) contents of Jbel Boho hydrothermal veins (G3 group) (* data from W. Schink, Pers.com)

	G3							
	B29	B89	B59-1	B-60	B45-1*	B43	B85-4	B51-1
SiO2	4.20	88.90	89.60	17.10	89.50	14.30	94.00	51.00
TiO2	0.04	0.03	0.03	<0.01	<0.01	0.10	<0.01	0.41
Al2O3	0.28	0.39	0.40	0.11	0.22	0.88	0.22	11.87
Fe2O3	3.49	6.63	5.82	4.33	6.08	7.78	3.69	4.87
MnO	0.78	1.10	0.91	0.82	1.05	1.20	0.43	0.32
MgO	1.22	0.07	0.10	11.50	0.22	0.64	0.03	0.51
CaO	49.39	0.25	0.18	30.30	0.13	40.95	0.14	13.70
Na2O	<0.01	<0.01	<0.01	<0.01	0.02	0.03	<0.01	6.22
K2O	0.02	0.10	0.12	0.01	0.03	0.11	0.05	0.68
P2O5	0.01	0.03	0.02	<0.01	0.03	0.02	0.01	0.11
Cr2O3	0.00	<0.001	<0.001	<0.001	<0.001	0.00	<0.001	<0.001
LOI	40.34	2.42	2.35	34.59	2.74	33.99	1.65	9.55
Total	99.77	99.92	99.53	98.76	100.02	100.00	100.22	99.24
Ba	909.00	1224.00	1332.00	551.00	848.00	13.00	229.00	115.00
Rb	3.00	3.70	4.40	0.50	0.30	7.20	1.00	18.00
Sr	76.20	27.30	18.30	39.20	75.50	128.80	21.90	141.90
Zr	4.50	11.70	11.30	1.60	0.40	7.10	3.90	398.40
Nb	1.20	2.10	1.90	0.40	0.30	1.70	0.80	75.50
Ni	<0.10	3.80	3.40	2.30	4.20	<0.10	0.40	0.70
Co	1.50	4.30	4.10	2.50	4.10	4.10	0.90	2.30
Zn	3.00	32.00	47.00	2.00	6.00	4.00	3.00	18.00
La	9.40	23.30	5.60	4.30	7.80	9.20	13.80	50.60
Ce	25.80	44.40	10.50	12.70	22.50	18.10	18.00	107.40
Pr	4.09	6.11	2.12	2.00	2.52	2.27	3.25	13.26
Nd	22.40	25.00	11.40	9.70	12.10	10.50	14.60	53.50
Sm	9.53	8.02	4.63	4.94	4.33	3.23	3.47	10.90
Eu	2.43	1.74	1.08	0.99	0.90	0.78	0.77	3.13
Gd	16.25	11.74	8.51	8.39	6.03	5.07	4.80	9.85
Tb	3.51	2.26	2.04	2.22	1.48	1.12	0.92	1.39
Dy	19.38	11.07	12.38	13.48	8.48	6.45	4.86	8.20
Y	90.90	36.40	55.90	50.60	35.40	26.00	18.50	40.40
Ho	3.35	1.67	2.04	2.16	1.43	0.99	0.74	1.42
Er	7.80	3.49	4.88	5.40	3.43	1.93	1.66	4.03
Tm	1.05	0.40	0.63	0.75	0.50	0.29	0.20	0.63
Yb	6.62	2.24	3.58	4.43	3.32	1.73	0.99	4.02
Lu	0.91	0.25	0.44	0.62	0.40	0.21	0.12	0.57
ΣREE	223.42	178.09	125.73	122.68	110.62	87.87	86.68	309.30
Ta	0.10	0.20	0.20	<0.10	<0.10	0.10	<0.10	4.90
Hf	0.10	0.40	0.50	<0.10	<0.10	0.20	0.20	10.00
As	1.90	37.60	133.90	5.10	24.30	7.80	7.00	1.50
Ag	<0.10	<0.10	<0.10	<0.10	<0.10	<0.10	<0.10	<0.10
Au	0.90	1.30	2.10	0.60	1.70	2.30	1.00	<0.50
Ga	1.80	1.80	1.80	0.80	1.90	2.90	0.60	8.90
Mo	1.30	63.10	18.70	0.20	15.00	14.60	8.00	0.60
Cu	0.40	78.30	173.20	3.20	100.10	80.20	202.40	1.00
Pb	0.50	1.60	2.00	0.50	1.80	1.20	0.50	3.00
Th	<0.2	0.40	0.40	0.40	<0.2	0.30	<0.2	10.40
U	1.00	1.50	1.30	0.20	1.70	1.20	0.70	3.20
Cs	0.10	<0.10	0.10	<0.10	<0.10	0.30	<0.10	0.40
V	17.00	91.00	72.00	<8.00	44.00	38.00	<8.00	15.00

It is important to note that the veins of the groups G1 all occur directly adjacent to the syenite and show similar NE-SW directions and that some veins even cut the syenitic pluton, whereas the veins of the groups G2 and G3 occur elsewhere within the volcanic rocks.

The group G2 ([Table 3.2](#)) has similar HREE patterns to G1 but with much lower LREE concentrations. The Σ REE content ranges from 154 to 18 ppm, with no specific REE minerals identifiable.

The group G3 ([Table 3.3](#)) shows, unlike the two other groups, very flat REE patterns with a peak in the middle REE (Gd, Tb and Dy). This group consists of carbonate-dominated veins, which show generally higher iron contents than the other veins with Fe_2O_3 ranging from 3.5 to 7.8 wt%.

3.5 Composition of the observed accessory rare earth minerals.

The REE-host minerals responsible for the high LREE enrichment were subject to microprobe chemical analysis. The results of the chemical analysis for these minerals are summarized in [Table 3.4](#) and [Table 3.5](#) and described below.

3.5.1 *Synchysite-(Ce)*

Synchysite is a member of the REE-fluorcarbonate mineral group, whose principal mineral bastnäsite is the main REE ore mineral in the world. The atomic arrangement of synchysite was described by [Ni et al. \(1993\)](#) and [Wang et al. \(1994\)](#) who, based on 3D X-ray-diffraction data, suggested a layered structure, with bastnäsite (CeF) and (Ca) layers separated by layers of carbonate groups

(CO₃²⁻). Considering the ratios of (CeF): (CO₃) (CaCO₃) layers, the synchysite can be cast as 1:1:1 whereas bastnäsite is 1:1:0. Unlike the hexagonal symmetry of bastnäsite, these authors show that the true symmetry of synchysite is monoclinic, which confirms the predictions of [Donnay and Donnay \(1953\)](#).

Table 3-4 Chemical analysis of synchysite-(Ce) in the REE-rich quartz veins (B47 and B46-3). The values of BA35 (Chap 2).

	Synchysite B46						Synchysite B47						Average	B35 average
	1	2	3	4	5	6	7	8	9	10	11	12	13	
F	4.36	3.97	4.36	4.52	3.82	4.13	4.20	4.32	4.25	4.36	4.51	4.40	4.27	4.94
CaO	15.56	18.11	18.30	15.74	18.13	18.31	17.79	18.38	18.19	18.07	18.02	18.45	17.75	18.58
La ₂ O ₃	14.46	12.50	12.53	13.23	11.65	12.03	13.16	12.10	12.78	13.21	12.83	13.06	12.79	12.53
Ce ₂ O ₃	22.48	20.70	20.53	21.60	19.85	20.61	21.04	20.06	20.25	19.99	20.68	19.78	20.63	20.35
Pr ₂ O ₃	2.75	2.73	2.31	3.02	2.80	2.66	2.38	2.61	2.70	2.63	2.80	2.48	2.66	2.82
Nd ₂ O ₃	10.17	10.23	10.20	10.91	10.85	10.58	9.40	9.62	9.37	9.25	9.75	9.58	9.99	10.60
Sm ₂ O ₃	1.37	1.41	1.30	1.27	1.61	1.56	1.33	1.54	1.21	1.31	1.47	1.13	1.37	1.42
Eu ₂ O ₃	0.11	0.08	0.10	0.10	0.16	0.17	0.00	0.17	0.24	0.18	0.13	0.17	0.13	0.09
Gd ₂ O ₃	0.94	1.04	1.13	1.26	1.40	0.99	0.97	0.99	1.13	0.94	0.94	0.86	1.05	1.03
Dy ₂ O ₃	0.08	0.00	0.00	0.12	0.00	0.00	0.04	0.05	0.04	0.06	0.00	0.07	0.04	0.01
Y ₂ O ₃	0.67	0.43	0.54	0.46	0.35	0.38	0.54	0.74	0.63	0.62	0.54	0.71	0.55	0.39
Er ₂ O ₃	0.00	0.01	0.00	0.02	0.02	0.00	0.00	0.00	0.00	0.00	0.00	0.00	0.00	0.02
Yb ₂ O ₃	0.00	0.00	0.00	0.03	0.00	0.02	0.00	0.07	0.00	0.05	0.03	0.12	0.03	0.01
ThO ₂	0.04	0.01	0.01	0.02	0.00	0.00	0.04	0.00	0.00	0.00	0.06	0.02	0.01	0.16
CO ₂	26.54	26.54	26.54	26.54	26.54	26.54	26.54	26.54	26.54	26.54	26.54	26.54	26.54	26.50
SUM	99.52	97.75	97.84	98.83	97.18	97.96	97.42	97.19	97.34	97.21	98.29	97.37	97.82	99.46
O ≡ F	1.835	1.6737	1.835	1.902	1.61	1.738	1.768	1.821	1.791	1.837	1.899	1.854	1.7969	2.08
Total	97.68	96.08	96.00	96.93	95.56	96.22	95.65	95.36	95.55	95.37	96.39	95.51	96.03	97.37
Number of ions based on 7 O														
F	0.77	0.68	0.75	0.78	0.66	0.71	0.72	0.75	0.74	0.76	0.77	0.75	0.74	0.86
Ca	0.93	1.05	1.06	0.92	1.06	1.07	1.04	1.08	1.08	1.06	1.04	1.07	1.04	1.09
La	0.30	0.25	0.25	0.27	0.23	0.24	0.26	0.25	0.26	0.27	0.26	0.26	0.26	0.25
Ce	0.46	0.41	0.41	0.43	0.40	0.41	0.42	0.40	0.41	0.40	0.41	0.39	0.41	0.41
Pr	0.06	0.05	0.05	0.06	0.06	0.05	0.05	0.05	0.05	0.05	0.06	0.05	0.05	0.06
Nd	0.20	0.20	0.20	0.21	0.21	0.21	0.18	0.19	0.19	0.18	0.19	0.18	0.19	0.21
Sm	0.03	0.03	0.02	0.02	0.03	0.03	0.02	0.03	0.02	0.02	0.03	0.02	0.03	0.03
Eu	0.00	0.00	0.00	0.00	0.00	0.00	0.00	0.00	0.00	0.00	0.00	0.00	0.00	0.00
Gd	0.02	0.02	0.02	0.02	0.03	0.02	0.02	0.02	0.02	0.02	0.02	0.02	0.02	0.02
Dy	0.00	0.00	0.00	0.00	0.00	0.00	0.00	0.00	0.00	0.00	0.00	0.00	0.00	0.00
Y	0.02	0.01	0.02	0.01	0.01	0.01	0.02	0.02	0.02	0.02	0.02	0.02	0.02	0.01
Er	0.00	0.00	0.00	0.00	0.00	0.00	0.00	0.00	0.00	0.00	0.00	0.00	0.00	0.00
Yb	0.00	0.00	0.00	0.00	0.00	0.00	0.00	0.00	0.00	0.00	0.00	0.00	0.00	0.00
Th	0.00	0.00	0.00	0.00	0.00	0.00	0.00	0.00	0.00	0.00	0.00	0.00	0.00	0.00
C	2.01	1.95	1.96	1.98	1.97	1.98	1.97	1.99	2.00	1.98	1.95	1.96	1.98	1.99
ΣREE+Th: 0.98 Ca: 1.04 F: 0.74 C: 1.98														

The OH⁻ content in synchysite was, however, not reported in these works. [Guastoni et al. \(2009\)](#) reported experimentally the OH content in synchysite, which, according to these authors, should correspond to the pfu missing by F in the calculated chemical formula of [Wang et al. \(1994\)](#).

[Table 3.4](#) summarizes the synchysite compositions in the LREE enriched quartz veins (this study) and the rhyolitic dyke B35 ([Chap 2](#)). All analysed minerals in this study have Ce as the dominant cation and may therefore be termed synchysite-(Ce). All synchysites are enriched in the LREE especially La, Ce and Nd. The La₂O₃ values range from 11.65 to 14.46 wt%, Ce₂O₃ from 19.78 to 22.48 wt% and Nd₂O₃ from 9.25 to 10.85 wt%. These values are similar to the values of the synchysite minerals in the subalkaline rhyolitic dyke B35 (see [Chap 2](#) and [Table 3.4](#)). Thorium is very low in synchysite-(Ce), generally less than 0.04 wt%. The calculated formula (Σ REE + Th: 0.98, Ca: 1.04, F: 0.74 and C: 1.98) is consistent with the synchysite composition with an F pfu deficit of ~ 0.26.

3.5.2 Rhabdophane-(Ce)

The REE-P mineral rhabdophane is a hydrated phosphate of REE with mineral chemistry similar to monazite XPO₄.nH₂O [X: REE, Ca, Th, U and n: number of water molecules]. Unlike monazite, which is monoclinic, the crystal structure of rhabdophane was identified for the first time by [Mooney \(1950\)](#) as hexagonal with a postulated H₂O content (n) between 0.5 and 1.5. Thermal reactions of rhabdophane led to the water corresponding to nH₂O being considered as zeolitic water ([Hikichi et al., 1996, 1988, 1978](#)). This water is incorporated as

non-stoichiometric molecules in large channels along the c-axes in the hexagonal structure of rhabdophane (Kijkowska et al., 2003).

Rhabdophane is found only in the LREE-rich quartz vein B46-3 as small isolated grains with sizes up to 25 μm . The analysed rhabdophane minerals contain abundant LREE, notably Ce, La and Nd while the proportion of the HREE is very low.

Table 3-5 Chemical analysis of rhabdophane-(Ce) in the REE-rich quartz vein (B46-3)

Rhabdophane (B46)													
	1	2	3	4	5	6	7	8	9	10	11	12	Average
La ₂ O ₃	14.54	14.59	13.80	14.25	14.52	14.41	14.37	14.49	15.99	15.25	15.41	15.27	14.74
Ce ₂ O ₃	23.92	25.54	23.66	24.45	24.76	31.42	30.17	31.28	27.70	29.89	30.88	29.46	27.76
Pr ₂ O ₃	3.17	3.31	3.04	3.39	3.58	3.35	3.28	3.47	3.63	3.04	3.26	3.15	3.31
Nd ₂ O ₃	11.97	12.25	11.65	11.71	12.42	12.34	12.31	12.29	13.49	11.67	11.77	11.44	12.11
Sm ₂ O ₃	1.62	1.62	1.72	1.84	1.82	1.93	1.87	1.76	2.06	1.87	1.63	1.75	1.79
Eu ₂ O ₃	0.02	0.04	0.00	0.21	0.00	0.19	0.21	0.13	0.26	0.23	0.04	0.22	0.13
Gd ₂ O ₃	0.93	0.90	0.93	0.92	0.92	0.99	1.13	0.86	1.10	1.09	0.94	1.17	0.99
Y ₂ O ₃	0.18	0.20	0.18	0.16	0.11	0.14	0.22	0.14	0.34	0.31	0.19	0.34	0.21
CaO	2.59	2.22	2.71	2.99	2.62	2.46	2.61	2.28	2.76	2.94	2.92	3.71	2.73
P ₂ O ₅	29.69	30.60	28.99	30.34	28.45	27.61	27.89	27.73	28.85	27.74	27.09	27.12	28.51
ThO ₂	0.11	0.05	0.35	0.04	0.00	0.01	0.05	0.02	0.01	0.00	0.00	0.00	0.05
SiO ₂	1.15	1.70	1.33	1.03	0.20	1.18	1.46	1.70	0.35	1.11	0.31	0.31	0.99
Total	89.89	93.02	88.35	91.33	89.40	96.03	95.56	96.14	96.54	95.14	94.44	93.94	93.31
Ionic formula based on 16 O atoms													
													Average
La	0.869	0.840	0.838	0.836	0.900	0.850	0.840	0.842	0.943	0.903	0.943	0.933	0.878
Ce	1.419	1.459	1.426	1.424	1.524	1.839	1.750	1.805	1.621	1.756	1.876	1.786	1.641
Pr	0.187	0.188	0.183	0.196	0.219	0.195	0.189	0.199	0.211	0.178	0.197	0.190	0.195
Nd	0.693	0.683	0.685	0.665	0.745	0.705	0.697	0.692	0.770	0.669	0.697	0.677	0.698
Sm	0.090	0.087	0.097	0.101	0.105	0.106	0.102	0.095	0.114	0.104	0.093	0.100	0.100
Eu	0.001	0.002	0.000	0.012	0.000	0.010	0.011	0.007	0.014	0.013	0.002	0.012	0.007
Gd	0.050	0.047	0.051	0.049	0.051	0.052	0.059	0.045	0.058	0.058	0.052	0.064	0.053
Y	0.015	0.017	0.016	0.013	0.010	0.012	0.019	0.012	0.029	0.026	0.017	0.030	0.018
Ca	0.449	0.372	0.479	0.509	0.472	0.422	0.444	0.385	0.472	0.506	0.519	0.658	0.474
P	4.073	4.044	4.042	4.085	4.048	3.737	3.743	3.701	3.904	3.769	3.807	3.802	3.896
Th	0.004	0.002	0.013	0.001	0.000	0.000	0.002	0.001	0.000	0.000	0.000	0.000	0.002
Si	0.186	0.266	0.219	0.164	0.033	0.188	0.231	0.267	0.057	0.178	0.052	0.052	0.158
Total	8.038	8.006	8.049	8.055	8.108	8.116	8.087	8.051	8.194	8.160	8.256	8.304	8.119
	REE+Ca: 4.063			P+Si: 4.054									

The results are summarized in [Table 3.5](#) and show Ce_2O_3 content ranging between 23.7 and 31.3 wt%, La_2O_3 content between 14 and 16 wt% and Nd_2O_3 between 11.5 and 13.5 wt%. The Pr_2O_3 content is about 3.3 wt% and Sm_2O_3 is about 1.8 wt%. Of the HREE, only two elements were detected in minor amounts ($\text{Gd}_2\text{O}_3 \sim 1$ wt% and $\text{Y}_2\text{O}_3 \sim 0.2$ wt%). All other REE are under the detection limit for EPMA. Like synchysite-(Ce), rhabdophane shows a predominance of Ce over all other REE, classifying this REE mineral as rhabdophane-(Ce). Unlike monazite, the CaO content is significant with an average of 2.7 wt% and the ThO_2 content is very low with an average of 0.05 wt%.

3.6 REE distribution patterns

The REE_{nc} patterns (nc: chondrite normalized) of the synchysite-(Ce) minerals from the rhyolitic dyke B35 and the two quartz veins B47 and B46-3 as well as the rhabdophane-(Ce) from the B46-3 are presented in [Figure 3.10](#).

The REE minerals are strongly enriched in LREE. The grey field represents the REE distribution patterns of both analysed REE minerals (synchysite and rhabdophane). The synchysite-(Ce) REE patterns are almost identical and similar to those of rhabdophane-(Ce). Their REE patterns decline from La to Gd with slight to strong negative Eu anomalies. The HREE contents of rhabdophane are, with the exception of Y, below the detection limits. The highest LREE content (especially Ce content) is found in some rhabdophane grains (see samples 6 to 12, [Table. 3.5](#))

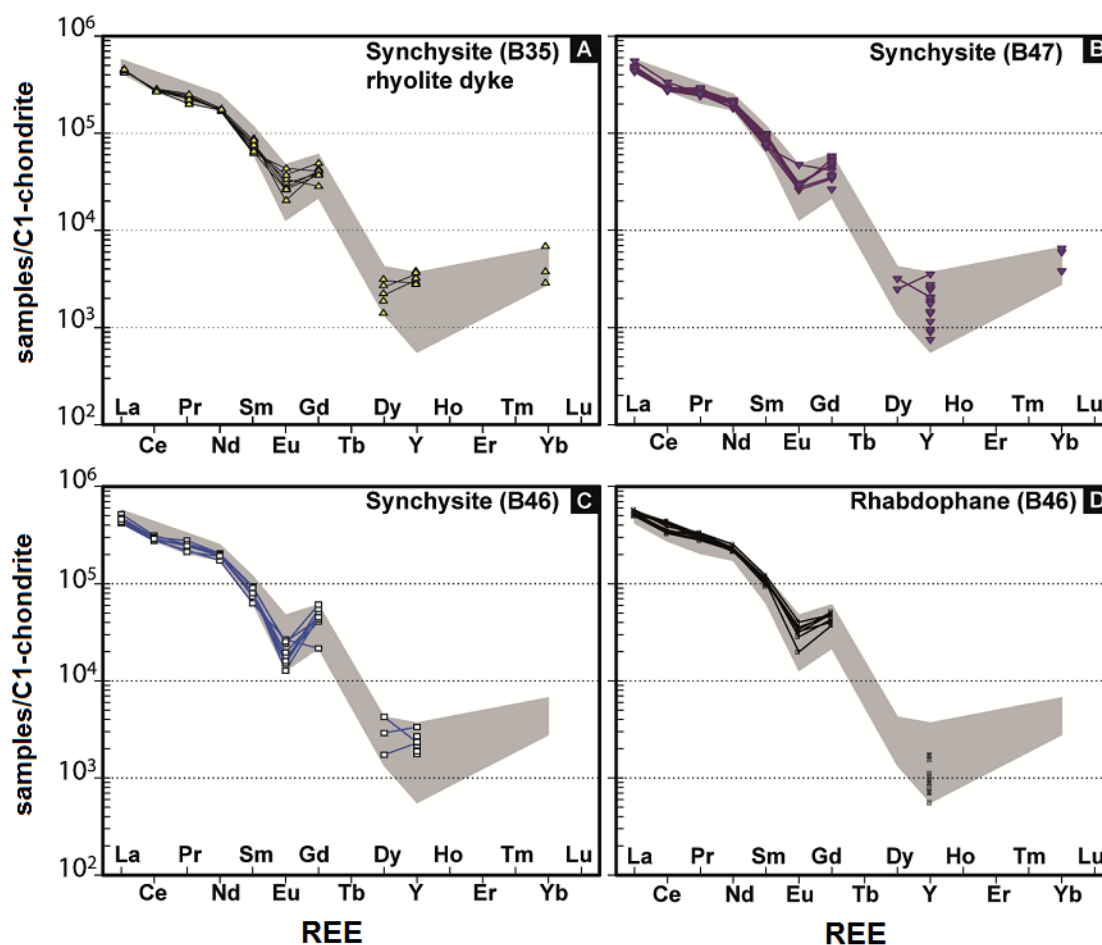


Figure 3.10 REE pattern of synchysite and rhabdophane from the late late rhyolitic dyke (B35) and quartz carbonate veins near the quartz syenite.

3.7 Fluid inclusions

3.7.1 Petrography

Fluid inclusion analyses were restricted to the two veins in which the rare earth bearing minerals occur. In the quartz-jasper vein (samples labelled B47-) the fluid inclusions occur in quartz together with synchysite, whereas in the quartz vein

(B46-3) they occur mainly in the coarse grained zoned quartz and occasionally in the fine grained synchysite-bearing quartz. It is important to note that the associated rare-earth minerals themselves contain no fluid inclusions.

Thick sections from the quartz samples were prepared at the Institute of Mineralogy in Kiel (Germany) with a thickness about 150 μm .

Two types of fluid inclusions can be distinguished in the quartz veins based on the number of the included phases at room temperature: two phases, liquid-vapor (LV phases) inclusions and three phases liquid-vapor-solid (LVS phases) inclusions. The LVS inclusions may even contain two solids and can be considered as complex salt solutions.

The fluid inclusions in both samples show similar characteristics. They are relatively small (generally in the range of 3 to 10 μm , although some can reach 30 μm). The volumes of the liquid phase present in the inclusions were estimated visually. All fluid inclusions are fluid-rich with a liquid phase of about 80 vol%. Tiny inclusions (< 3 μm) are also present but they are too small to be studied.

In the quartz-jasper sample (B47) most fluid inclusions occur spatially isolated or in small clusters within the core of the host quartz grains (Fig. 3.11 A, B), without obvious evidence for simultaneous trapping. The inclusions in the centre have irregular shapes. Fluid inclusions up to 10 μm in size are often subhedral (Fig. 3.11C), but euhedral morphologies might also be present (Fig. 3.11D). Elongated and rounded inclusions are larger than euhedral and anhedral inclusions and can have sizes up to 30 μm (Fig. 3.11E).

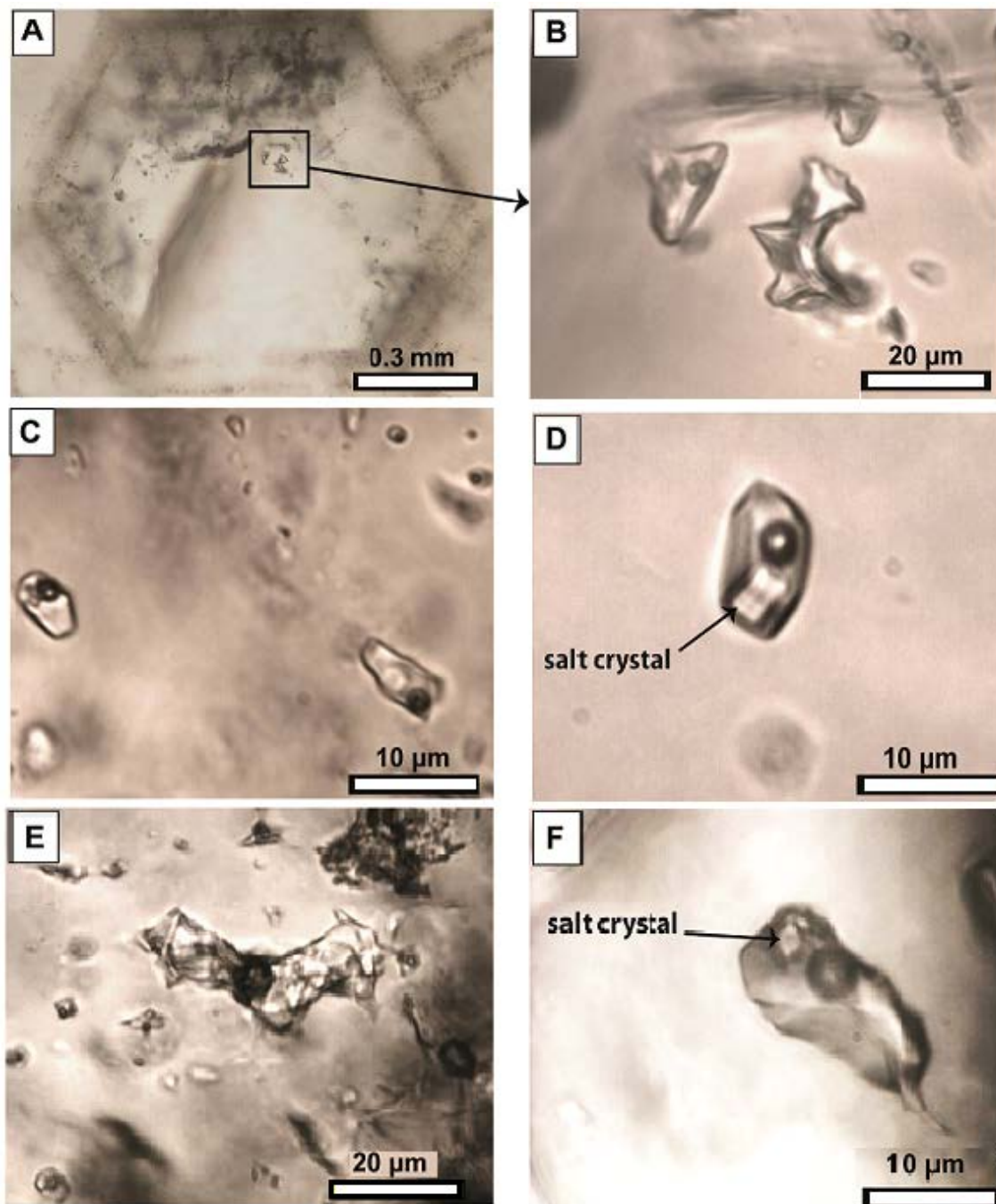


Figure 3.11 Photomicrographs (room temperature) of fluid inclusions present in the synchysite bearing quartz veins. A,B) Fluid inclusions as cluster within a zoned host quartz (B46). C,D) Subhedral to euhedral fluid inclusions (B47). E) Large fluid inclusion surrounded by tiny inclusions (B47). F) Example of partially decrepitated fluid inclusions showing tail form at its end.

Some fluid inclusions show tail-like emanations while still containing fluids and a gas bubble (Fig. 3.11F) suggesting partial decrepitation. The growth zone of quartz shows rarely fluid inclusions.

3.7.2 Microthermometry

First the fluid inclusions in thick sections were examined in detail microscopically to characterize the texture. Then the double polished wafers were examined microthermometrically with a heating and freezing stage (Linkam THM 600) attached to an Olympus microscope. This allows microthermometry to be performed on the fluid inclusions over the temperature range from 600 to -196°C. The calibration of a temperature was carried out using a set of synthetic inclusions distributed by Fluid Inc., USA, in the temperature range of -56.6°C to 0.0°C. The precision of the temperature measurements was about $\pm 0.2^\circ\text{C}$ in a temperature range of -60 to +100°C, within $\pm 0.5\text{--}2^\circ\text{C}$ in the range of -60 to -120°C, within $\pm 3^\circ\text{C}$ from -120 to -140°C and about $\pm 2^\circ\text{C}$ for temperatures above 100°C.

In the REE bearing quartz jasper vein most liquid-vapor inclusions homogenize during heating to the liquid phase at temperatures (T_h) between 119 and 256°C (Fig. 3.12) with single exceptions of high homogenization temperatures over 380°C. In the REE bearing quartz vein the temperatures of homogenization to liquid phase are between 94 and 260°C with some exceptions of T_h over 300°C (Fig 3.12).

The homogenization temperatures over 300°C were measured after the measurement of the dissolution temperatures (T_{dis}) for the solid phases.

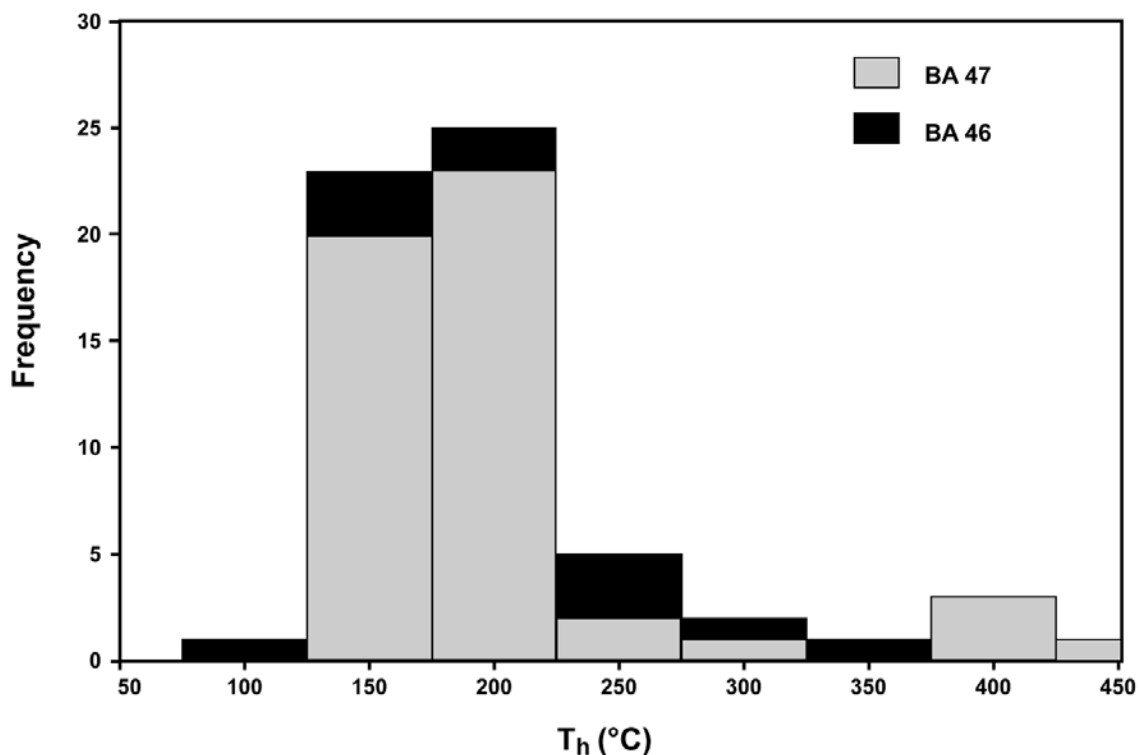


Figure 3.12 Histogram of homogenisation temperatures (to the liquid phase) for the studied fluid inclusions in the synchysite bearing quartz veins (BA 46 and BA 47).

The solid phases in the LVS inclusion types in both REE bearing veins dissolve between 212 and 276°C, which indicates that the solids within the fluid inclusions should be salt crystals. From these dissolution temperatures salinities of 32-37% NaCl equivalents can be deduced if a pure NaCl system is assumed (Bodnar and Vityk, 1994; Bodnar, 2003). These dissolution temperatures would be sufficient to cause decrepitation of fluid inclusions and thus increase the T_h values. That is

why all T_h values obtained after the heating up to 276°C during the measurement of T_{dis} are considered to be unrepresentative homogenization temperatures.

The eutectic temperatures (T_e) are generally between -50 and -54°C. However during the heating from -190 to room temperatures obvious changes in appearance of some fluid inclusions were detected twice at very low temperatures (about -71°C). This phenomenon could be the result of some re-crystallization or real phase transitions at very low temperatures, thus indicating complex aqueous solutions. Solid state transitions are documented for glass in aqueous system (Angell, 2002). Furthermore final melting temperatures (T_m) of ice in the fluid inclusions of these veins range from 19 to 23°C.

3.8 Discussion

Since the discovery of giant REE deposits of hydrothermal origin in China (Bayan Obo), the study of the REE mobilisation in hydrothermal system has been aimed at understanding why REE are highly mobile in some geological environments. The presence of quartz-carbonate veins in igneous rocks is an indicator for fluids circulation through fractures. They are typically found in low grade metamorphic rocks, formed at about 2-3 kbar and 250-350 C° (Bons, 2001). To have a good knowledge about the hydrothermal formation of REE ore deposits, it is important to understand the speciation of the REE in hydrothermal fluids.

3.8.1 Speciation of REE in hydrothermal fluids

The REE mineralization in late stage quartz-carbonate veins and the late subalkaline rhyolitic dykes in Jbel Boho provide evidence for REE mobilization through hydrothermal process to form rare earth ore minerals. In order to explain the variable REE distributions in the late hydrothermal veins in Jbel Boho shown in [Figure 3.9](#), it is necessary to understand the REE behaviour in hydrothermal system. As indicated above, the quartz-carbonate veins occur in all rock types and show some variations in mineralogy (although they consist predominantly of quartz and carbonate) and REE compositions. This diversity suggests that they are formed under a range of hydrothermal conditions with variations possible in: REE concentration in the fluids; temperature; pH; and the availability of the necessary ligands (e.g. Cl^- , F^- , CO_3^{2-} , OH^- , PO_4^{3-} , SO_4^{2-}). To mobilize and transport REE in the hydrothermal fluids, F and Cl are the most favoured ligands, because they form significant complexes with the REE ([Haas et al., 1995](#); [Linnen et al., 2014](#); [Lottermoser, 1990](#); [Migdisov et al., 2009](#); [Wood, 2004, 1990a](#)). The hard-soft acid-base principles gained from Pearson's rules ([Pearson, 1963](#)) help to understand the stability and the aqueous complexation of the REE in hydrothermal processes. According to this concept, hard acids tend to bind preferentially with hard bases and soft acids tend to bind preferentially with soft bases. Because of the +3 valence and the sizes of the REE ions, they are considered to be hard acids. Thus, they tend to form strong complexes with hard bases (ligands) like F^- and OH^- . Theoretical estimations and extrapolations of

thermodynamic data using Pearson's rules (Haas et al., 1995; Wood, 1990a, 1990b) predicted that the strongest REE complexes would form with F^- and OH^- , moderately weaker complexes with the other ligands such as CO_3^{2-} , SO_4^{2-} , PO_4^{2-} and HCO_3^- , and that REE complexes with Cl^- should be the weakest. Moreover, they concluded that the REE complex stability constants would increase with increasing temperature (from 25 to 300 °C) at a greater rate for fluoride and carbonate than for other ligands. As a result, the REE-fluoride complexes were considered to be the most favourable candidates for transporting significant REE concentrations in solution and so having the highest ore-forming potential. Based on these theoretical studies and the fact that the REE-F carbonate bastnäsité is the main source of the REE in the world, the hydrothermal REE deposits have generally been considered to have been formed by the transport of REE as fluoride complexes (Ruberti et al., 2008; Salvi and Williams-Jones, 1990; Smith and Henderson, 2000; Williams-Jones et al., 2000; Wood and Ricketts, 2000) and high concentration of fluorine in late-stage magmatic fluid were thought to allow REE to be transported in solution and to behave much more fluid-compatibly than expected (Agangi et al., 2010).

Recently experimental studies (Migdisov and Williams-Jones, 2008, 2007; Migdisov et al., 2009, 2008, 2006) have shown that the theoretical extrapolations cited above significantly overestimate the stability of REE-fluoride complexes and underestimate the stability of REE-chloride complexes. The cause of these contrasting results is the decrease in the dielectric constant of water with

temperature, which cause softening of ions by reducing their resistance to electron transfer, which affects the relative stability of the corresponding REE complexes (Williams-Jones et al., 2012). The experimental data suggest that at elevated temperatures the LREE-fluoride species are more stable than the HREE-fluoride species and that the same is true for REE-chloride species. Moreover Migdisov and Williams-Jones (2007) experimentally demonstrated that chloride species have a similar potential for REE transport as fluoride species at elevated temperatures up to 250 °C, although they did not consider the solubility of the REE-bearing phases. REE-fluorides are extremely insoluble over a wide range of pH. Their solubility only increases at relatively low temperature in fluids of intermediate pH, implying that REE-fluoride species are insignificant for REE transport in hydrothermal system (Migdisov and Williams-Jones, 2014; Williams-Jones et al., 2012) as <1ppm of REE can be transported as fluoride at all conditions considered. Instead, REE chloride species dominate in solutions at low pH and are able to transport appreciable concentrations of REE under acidic conditions. The presence of fluoride ions in REE chloride-bearing fluids acts as a binding ligand that promotes REE mineral deposition, which then occurs as a response to an increase in pH and a decrease of temperature (Migdisov and Williams-Jones, 2014; Williams-Jones and Migdisov, 2014).

3.8.2 REE in the ore bearing veins

The outcropping of highly LREE-enriched veins adjacent to the syenite with similar orientations (NE-SW) and very similar REE patterns (Fig. 3.9) argue for a

cogenetic origin of their hydrothermal fluids. Synchysite mineralization occurs only in the thick hydrothermal veins along a N50°E faulting zone. The fault plane presumably acted as a major fluid pathway, leading to high fluid/rock ratio in comparison to the other veins. This is an important parameter that affects the wall-rock alteration and leads to either significant or negligible mineral deposits.

In the synchysite-bearing quartz-jasper vein (B47), jasper is well consolidated and forms the main volume of the vein. The brown-reddish colour is attributed to Mn-Fe oxide impregnation. The formation of siliceous hydrothermal veins (Jasper, chalcedony) was most likely driven by hydrothermal activity that caused alteration of the host rock. The jasper was also fractured and percolated by REE ore mineralizing fluids, resulting in the formation of REE bearing quartz phases within jasper. The synchysite bearing quartz is therefore younger than jasper.

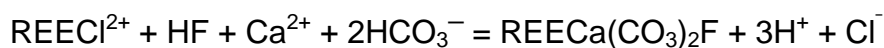
The coarse-grained quartz in the synchysite and rhabdophane bearing quartz vein (B46-3) shows subhedral to euhedral crystal shapes and concentric zoning, formed likely during crystal growth within the cracks permitting upward fluid flow, which compensates the crystal settling during deposition ([Okamoto and Tsuchiya, 2009](#)). The coarse-grained quartz is intruded itself by fine grained quartz veins, which are associated with synchysite and occasionally rhabdophane. Both ore-bearing veins (B46 and B47) seem therefore to be formed by successive episodes of hydrothermal fluids. The restricted occurrence of rhabdophane-(Ce) in the quartz vein (46-3) indicates limited presence of P in the REE bearing fluid. The high content of Ca and the absence of radioactive

elements such as Th in rhabdophane suggests that apatite from the host rock possibly contributed the P to rhabdophane in the vein. As both synchysite and rhabdophane have very similar REE composition and co-exist in the same vein, they may originate from the same hydrothermal fluid.

The dominant salt component in hydrothermal ore fluids is generally the strong electrolyte NaCl, which is most likely the main source of Cl^- . Our fluid inclusion work suggests that the hydrothermal fluids at Jbel Boho were highly saline (32.4 - 36.7 wt% NaCl equivalents in a pure halite system). However, the very low T_e ranging between -50 and -54°C suggests that NaCl ($T_e = 21.2^\circ\text{C}$) was not the only salt component of the hydrothermal fluid. [Bodnar et al. \(2014\)](#) and [Steele-MacInnis et al. \(2011\)](#) show experimentally that fluid inclusions from active seafloor hydrothermal systems which show first melting in the vicinity of 50 °C contain Ca^{2+} in addition to NaCl. Additional components in the aqueous fluids will influence the salinity determination, something which has to be considered when interpreting the salinity values.

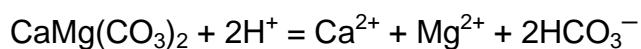
Based on the mineralogical, geochemical and fluid inclusion data, we suggest the model proposed by [Williams-Jones et al., \(2012\)](#) and [Migdisov and Williams-Jones \(2014\)](#) as the best possible explanation for the petrogenesis of the synchysite mineralization in the hydrothermal quartz veins of the Jbel Boho complex. According to this model, we propose that the transport of REE in the ore bearing veins was dominated by chloride complexes at acidic conditions with the presence of fluorine in the form of HF. When this acidic hydrothermal fluid

enters the vein it will precipitate REE minerals if the pH is raised. The REE-Ca fluorcarbonate synchysites will deposit in response to an increase in pH in the presence of excess HCO_3^{2-} according to the reaction:



The generation of H^+ by this reaction will again decrease the pH, eventually inhibiting synchysite precipitation. Thus the deposition of synchysite will only occur when continuous neutralization of the fluid acidity is possible.

In view of the petrographic evidence for carbonate minerals in all the veins studied, the best candidate for a pH-raising reaction is carbonates because of the reaction:



It is not possible to deduce directly the temperature of the synchysite formation because no fluid inclusions were detected in the synchysite minerals. The obtained temperatures of homogenization (from 150 to 250°C) for most inclusions provide the minimum temperature conditions in which the corresponding quartz veins were formed.

The very high REE contents in the synchysite of Jbel Boho (ca. 50% by mass of the synchysite consists of REE) make it a very concentrated source of REE. Additionally, unlike monazite and allanite, synchysite and rhabdophane are very low in both Th and U, thereby reducing complications related to radioactivity during metallurgical processes through concentration and separation. They are

consequently more favourable for REE exploitation as ecologically friendly minerals.

As in the ore-bearing veins, synchysite occur also in the late intrusive dykes especially the rhyolitic dyke B35 with the highest REE enrichment ($\Sigma\text{REE} \sim 1795$ ppm) among all magmatic rocks of Jbel Boho (Chap 2). The very similar sizes (up to 100 μm) and chemistry of synchysite in both mineralized dyke and veins and their location in the REE mineralized zone north of the quartz syenite indicate that their hydrothermal fluids might have a similar source. The crystallization of REE-F-Ca synchysite rather than the most abundant REE-F carbonate bastnäsite indicates very high activity of Ca^{2+} in the medium. Moreover the geographic location and orientation of both REE deposits (Fig. 3.3) indicate that they might be connected at depth. The REE mineralizations in the late stage of the magmatic evolution of the Jbel Boho complex were likely associated with mineralizing hydrothermal processes.

3.8.3 REE in the ore-barren veins

The ore-barren veins (G2 and G3 Table 3.2, 3.3) occur elsewhere in the Jbel Boho magmatic rocks with different orientations and generally smaller thicknesses (up to 30 cm). In comparison to the ore bearing veins (G1), the G2 veins have similar REE patterns with more pronounced LREE enrichment, although they have much lower REE contents, whereas the G3 veins show a totally different REE signature with quite flat REE patterns and slight enrichment of the HREE (Fig. 3.9). The low REE contents of the ore-barren veins suggest

depletion of REE and complexing ligands (Cl and F) in the hydrothermal fluid from which they were formed. No REE-minerals were observed in these veins and the REEs are probably hosted in the carbonate fraction of the veins.

The enrichment of LREE relative to HREE in the G2 veins is possibly related to sorption process such as ion exchange, which control fluid-rock interaction in situations where complexing ligands are rare and lead, under mildly acidic conditions, to low mineral REE contents with enrichment of LREE over the HREE (Bau and Möller, 1992; Bau, 1991). Another, more efficient means of LREE enrichment over HREE with low total REE contents in these veins would also be the presence of low concentrations of NaCl in the mineralising geothermal fluid, as this has the capacity to enhance LREE solubility by forming chloride complexes (Allen and Seyfried, 2005; Tropper et al., 2013, 2011; Tsay et al., 2014).

The G3 veins have generally high carbonate and iron contents, which is reflected by the presence of jasper and carbonate minerals that are commonly coated with Fe-oxides, which suggests that sideritization processes happened. HREE³⁺ have ionic radii which are smaller than LREE³⁺ but similar to Fe²⁺ and Mg²⁺. Thus the flat REE patterns in these veins can be explained by a change of the REE signature through the preferential incorporation of HREE over LREE in siderite. This behaviour was previously described and termed “mineralogical control” (Bau and Möller, 1992; Morgan and Wandless, 1980), consisting of ionic substitution based on ionic size and charge of trace elements.

The lower dolomites, which are intercalated with the volcanic rocks, contain more REE than G2 and G3 veins ($\Sigma\text{REE} \sim 309$ ppm) and display slight enrichment of LREE over HREE (Fig. 9D). This signature is unlikely to be a primary sedimentary feature of the dolomite - REE abundance in natural waters like sea water range from 10^{-6} to 10^{-4} ppm (Qing and Mountjoy, 1994) and carbonate rocks precipitated from such waters should have very low REE concentrations. The Jbel Boho lower dolomite contain tiny quartz carbonate veins (Fig. 3.8A), which commonly contain dolomitic rhombs and chabazite. The occurrence of zeolite minerals like chabazite in hydrothermal veins is considered to result from basaltic and volcanic glass alteration (Mees et al., 2005; Montagna et al., 2010; Weisenberger and Spuergin, 2009). The hydrothermal impregnation of the lower dolomite can therefore explain their anomalous REE signature. This suggests that significant quantities of REE were transported into the dolomite by means of saline hydrothermal fluids which can induce substitution of Ca^{2+} in the carbonate lattice, by adsorption due to remnant ionic charges and by occupation of lattice positions which are free due to structural defects (Qing and Mountjoy, 1994).

3.9 Conclusion

The Jbel Boho alkaline igneous complex shares some interesting aspects of hydrothermal REE mineralization in the late differentiation stage. Hydrothermal veins occur in Jbel Boho in all rock types with distinct texture and morphology (usually quartz, carbonate and jasper in variable proportion within the veins).

Two categories of veins were distinguished: 1) REE ore bearing veins (~ 2m thick) exposed along a N50E vertical fault zone cutting both quartz syenite and adjacent rocks and composed mainly of quartz, quartz-jasper and some carbonate including REE-F-Ca minerals synchysite and occasionally REE-P rhabdophane. Both REE minerals occur only in association with quartz. These veins (termed G1 veins) are characterized by very high LREE enrichment. Microprobe analysis indicate synchysite-(Ce) and rhabdophane-(Ce) with very high Ce, La and Nd contents. 2) REE ore barren veins (up to 30 cm thick) occur elsewhere in the magmatic rocks and show two types of veins (termed G2 and G3 veins). G2 veins have lower REE contents than G1 but show similar with enrichment of LREE over HREE, whereas G3 veins show low REE contents with quite flat REE pattern. Unlike the other veins, G3 have high carbonate and iron contents associated with jasper and carbonate coated with Fe-oxides. This suggests they were formed from relatively REE-depleted fluids and that the LREE/HREE fractionation was controlled both by very low activity of Cl^- ligands (limited transport of LREE) and sideritization (preferential incorporation of HREE owing to their similar ionic sizes to Fe^{2+}).

Our fluid inclusion study on quartz of the ore bearing veins indicates high salinities (between 32 and 37 wt% NaCl equivalent in a pure system), with the very low T_e (ranging between -50 and -54°C) arguing for more complex composition of the aqueous solutions than just NaCl. Representative

homogenization temperatures that range from 150 to 250°C suggest the minimum temperature conditions for the veins formation.

Based on recent experimental data, the REE mineralization model proposed here is the transport of REE as chloride complex by low pH and REE-rich hydrothermal fluids with the presence of fluorine as HF and high Ca^{2+} activity. The precipitation of synchysite-(Ce) happens as the result of the neutralization of the acidic fluids by interaction with carbonates, which also provide the CO_3^- necessary for synchysite formation.

Another synchysite mineralization type occurs within a late N-S rhyolitic dyke north of the synchysite bearing veins. The very strong similarity of synchysite characteristics (in size and REE composition) in both REE ore bearing veins and REE ore bearing dyke suggest its crystallization from similar REE-rich hydrothermal fluids.

Synchysite is a very important REE mineral that can provide new potential sources of rare earth elements in addition to bastnäsite. The late hydrothermal veins associated with high differentiated alkaline rocks are good candidates for REE mineralization.

References

- Agangi, A., Kamenetsky, V.S., McPhie, J., 2010. The role of fluorine in the concentration and transport of lithophile trace elements in felsic magmas: Insights from the Gawler Range Volcanics, South Australia. *Chemical Geology* 273, 314–325.
- Algouti, A., Algouti, A., Chbani, B., Zaim, M., 2001. Sedimentation et volcanisme synsédimentaire de la série de base de l'adoudounien infra-cambrien à travers deux exemples de l'Anti-Atlas du Maroc. *Journal of African Earth Sciences* 32, 541–556.
- Allen, D.E., Seyfried, W.E., 2005. REE controls in ultramafic hosted MOR hydrothermal systems: An experimental study at elevated temperature and pressure. *Geochimica et Cosmochimica Acta* 69, 675–683.
doi:10.1016/j.gca.2004.07.016
- Álvaro, J.J., Ezzouhairi, H., Vennin, E., Ribeiro, M.L., Clausen, S., Charif, A., Ayad, N.A., Moreira, M.E., 2006. The Early-Cambrian Boho volcano of the El Graara massif, Morocco: Petrology, geodynamic setting and coeval sedimentation. *Journal of African Earth Sciences* 44, 396–410.
- Angell, C.A., 2002. Liquid fragility and the glass transition in water and aqueous solutions. *Chemical reviews* 102, 2627–2650.
- Bau, M., 1991. Rare-earth element mobility during hydrothermal and metamorphic fluid-rock interaction and the significance of the oxidation state of europium. *Chemical Geology* 93, 219–230.
- Bau, M., Möller, P., 1992. Rare earth element fractionation in metamorphogenic hydrothermal calcite, magnesite and siderite. *Mineralogy and Petrology* 45, 231–246. doi:10.1007/BF01163114
- Belkabir, A., Jébrak, M., Maacha, L., Samir, M.R.A., Madi, A., 2008. Gold mineralization in the Proterozoic Bleida ophiolite, Anti-Atlas, Morocco, in: Ennih, N., Liegeois, J.-P. (Eds.), *The Boundaries of the West African Craton*. Geological Society, London, Special Publications, 297, pp. 249–264.
- Benaouda, R., Holzheid, A., Schenk, V., Badra, L., Ennaciri, A., n.d. Magmatic evolution and REE Mineralization in the Early Cambrian Jbel Boho Complex In The Bou Azzer Inlier (Anti-Atlas/Morocco). Paper in preparation.

- Bodnar, R.J., 2003. Introduction to aqueous-electrolyte fluid inclusions, in: Samson, I., Anderson, A., Marshall, D. (Eds.), *Fluid Inclusions: Analysis and Interpretation*. Mineral. Assoc. Canada, Short Course 32, Canada, pp. 81–99.
- Bodnar, R.J., Lecumberri-Sanchez, P., Moncada, D., Steele-MacInnis, M., 2014. Fluid Inclusions in Hydrothermal Ore Deposits, in: Holland, H.D., Turekian, K.K. (Eds.), *Treatise on Geochemistry: Second Edition*. Elsevier Ltd., Oxford, pp. 119–142. doi:10.1016/B978-0-08-095975-7.01105-0
- Bodnar, R.J., Vityk, M., 1994. Interpretation of Microthermometric Data for H₂O-NaCl Fluid Inclusions, in: De Vivo, B., Frezzotti, M.L. (Eds.), *Fluid Inclusions in Minerals: Methods and Applications*. Short Course IMA. Virginia Tech, Blacksburg, pp. 117–130.
- Bons, P.D., 2001. The formation of large quartz veins by rapid ascent of fluids in mobile hydrofractures. *Tectonophysics* 336, 1–17.
- Choubert, G., 1952. Geologie du Maroc: Histoire géologique du domaine de l'Anti-Atlas, in: XIX^e Congrès Géologique International, Monographies Régionales 3. Rabat, pp. 75–195.
- Donnay, G., Donnay, J.D.H., 1953. The crystallography of bastnaesite, parisite, roentgenite, and synchisite. *American Mineralogist* 38, 932–963.
- Ducrot, J., Lancelot, J.R., 1977. Problème de la limite Précambrien-Cambrien: étude radiochronologique par la méthode U-Pb sur zircons du volcan du Jbel Boho (Anti-Atlas marocain). *Canadian Journal of Earth Sciences* 14, 2771–2777.
- El Ghorfi, M., Melcher, F., Oberthür, T., Boukhari, A.E., Maacha, L., Maddi, A., Mhaili, M., 2008. Platinum group minerals in podiform chromitites of the Bou Azzer ophiolite, Anti Atlas, Central Morocco. *Mineralogy and Petrology* 92, 59–80.
- Ennaciri, A., Barbanson, L., Touray, J.C., 1995. Mineralized hydrothermal solution cavities in the Co-As Aït Ahmane mine (Bou Azzer, Morocco). *Mineralium Deposita* 30, 75–77.
- Ezzouhairi, H., Ribeiro, M.L., Ait Ayad, N., Moreira, M.E., Charif, A., Ramos, J.M.F., de Oliveira, D.P.S., Coke, C., 2008. The magmatic evolution at the Moroccan outboard of the West African craton between the Late Neoproterozoic and the Early Palaeozoic, in: Ennih, N., Liégeois, J. (Eds.),

- The Boundaries of the West African Craton. Geological Society, London, Special Publications, pp. 329–343.
- Gasquet, D., Ennih, N., Liégeois, J.-P., Soulaïmani, A., Michard, A., 2008. The Pan-African Belt, in: Michard, A., Saddiqi, O., Chalouan, A., de Lamotte, D.F. (Eds.), *Continental Evolution: The Geology of Morocco*. Springer, Berlin Heidelberg, pp. 33–64.
- Gasquet, D., Levresse, G., Cheilletz, A., Azizi-Samir, M.R., Mouttaqi, A., 2005. Contribution to a geodynamic reconstruction of the Anti-Atlas (Morocco) during Pan-African times with the emphasis on inversion tectonics and metallogenic activity at the Precambrian–Cambrian transition. *Precambrian Research* 140, 157–182.
- Gieré, R., 1990. Hydrothermal mobility of Ti, Zr and REE: examples from the Bergell and Adamello contact aureoles (Italy). *Terra Nova* 2, 60–70.
- Gieré, R., 1996. Formation of rare earth minerals in hydrothermal systems, in: A.P. Jones, F. Wall, C.T.W. (Ed.), *Rare Earth Minerals: Chemistry, Origin and Ore Deposits*. Chapman and Hall, pp. 105–150.
- Guastoni, A., Nestola, F., Giaretta, A., 2009. Mineral chemistry and alteration of rare earth element (REE) carbonates from alkaline pegmatites of Mount Malosa, Malawi. *American Mineralogist* 94, 1216–1222.
- Haas, J.R., Shock, E.L., Sassani, D.C., 1995. Rare earth elements in hydrothermal systems: Estimates of standard partial molal thermodynamic properties of aqueous complexes of the rare earth elements at high pressures and temperatures. *Geochimica et Cosmochimica Acta* 59, 4329–4350.
- Hikichi, Y., Hukuo, K., Shiokawa, J., 1978. Syntheses of rare earth orthophosphates. *Bulletin of the Chemical Society of Japan* 51, 3645–3646.
- Hikichi, Y., Ota, T., Hattori, T., Imaeda, T., 1996. Synthesis and thermal reactions of rhabdophane-(Y). *Mineralogical Journal* 18, 87–96.
- Hikichi, Y., Sasaki, T., Suzuki, S., Murayama, Y., 1988. Thermal reactions of hydrated hexagonal $RPO_4 \cdot nH_2O$ (R= Tb or Dy, n= 0.5 to 1). *Journal of the American Ceramic Society* 71, 354–355.
- Humphries, M., 2013. Rare earth elements: the global supply chain. CRS Report for Congress 31.

- Kijkowska, R., Cholewka, E., Duszak, B., 2003. X-ray diffraction and Ir-absorption characteristics of lanthanide orthophosphates obtained by crystallisation from phosphoric acid solution. *Journal of materials science* 38, 223–228.
- Leblanc, M., 1972. Un complexe ophiolitique dans le Précambrien II de l'Anti-Atlas central (Maroc): description, interprétation et position stratigraphique. *Notes et Mémoires du Service géologique du Maroc* 236, 119–144.
- Leblanc, M., 1981a. Ophiolites précambriennes et gites arseniés de cobalt: Bou Azzer (Maroc). *Note et Mémoires du Service Géologique N280, Maroc*.
- Leblanc, M., 1981b. The late Proterozoic ophiolites of Bou Azzer (Morocco): evidence for Pan-African plate tectonics. *Developments in Precambrian Geology* 4, 435–451.
- Linnen, R.L., Samson, I.M., Williams-Jones, A.E., Chakhmouradian, A.R., 2014. Geochemistry of the Rare-Earth Element, Nb, Ta, Hf, and Zr Deposits, in: Holland, H.D., Turekian, K.K. (Eds.), *Treatise on Geochemistry: Second Edition*. Elsevier Ltd., Oxford, pp. 543–568. doi:10.1016/B978-0-08-095975-7.01124-4
- Long, K.R., Van Gosen, B.S., Foley, N.K., Cordier, D., 2010. The principal rare earth elements deposits of the United States: a summary of domestic deposits and a global perspective. *USGS: Scientific Investigations Report* 1–14.
- Lottermoser, B.G., 1990. Rare-earth element mineralisation within the Mt. Weld carbonatite laterite, Western Australia. *Lithos* 24, 151–167.
- Mees, F., Stoops, G., Van Ranst, E., Paepe, R., Van Overloop, E., 2005. The nature of zeolite occurrences in deposits of the Olduvai Basin, northern Tanzania. *Clays and Clay Minerals* 53, 659–673.
- Migdisov, A.A., Reukov, V.V., Williams-Jones, A.E., 2006. A spectrophotometric study of neodymium(III) complexation in sulfate solutions at elevated temperatures. *Geochimica et Cosmochimica Acta* 70, 983–992. doi:10.1016/j.gca.2005.11.001
- Migdisov, A.A., Williams-Jones, A.E., 2007. An experimental study of the solubility and speciation of neodymium (III) fluoride in F-bearing aqueous solutions. *Geochimica et Cosmochimica Acta* 71, 3056–3069. doi:10.1016/j.gca.2007.04.004

- Migdisov, A.A., Williams-Jones, A.E., 2008. A spectrophotometric study of Nd(III), Sm(III) and Er(III) complexation in sulfate-bearing solutions at elevated temperatures. *Geochimica et Cosmochimica Acta* 72, 5291–5303.
- Migdisov, A.A., Williams-Jones, A.E., 2014. Hydrothermal transport and deposition of the rare earth elements by fluorine-bearing aqueous liquids. *Mineralium Deposita* 1–11. doi:10.1007/s00126-014-0554-z
- Migdisov, A.A., Williams-Jones, A.E., Normand, C., Wood, S.A., 2008. A spectrophotometric study of samarium (III) speciation in chloride solutions at elevated temperatures. *Geochimica et Cosmochimica Acta* 72, 1611–1625.
- Migdisov, A.A., Williams-Jones, A.E., Wagner, T., 2009. An experimental study of the solubility and speciation of the Rare Earth Elements (III) in fluoride- and chloride-bearing aqueous solutions at temperatures up to 300°C. *Geochimica et Cosmochimica Acta* 73, 7087–7109.
- Montagna, G., Bigi, S., Konya, P., Szakall, S., Vezzalini, G., 2010. Chabazite-Mg: a new natural zeolite of the chabazite series. *American Mineralogist* 95, 939–945.
- Mooney, R.C.L., 1950. X-ray diffraction study of cerous phosphate and related crystals. I. Hexagonal modification. *Acta Crystallographica* 3, 337–340.
- Morgan, J.W., Wandless, G.A., 1980. Rare earth element distribution in some hydrothermal minerals: evidence for crystallographic control. *Geochimica et Cosmochimica Acta* 44, 973–980.
- MTB, 2011. Tsumkwe rare earth elements (REE) Project, Namibia.
- Ni, Y., Hughes, J.M., Mariano, A.N., 1993. The atomic arrangement of bastnasite-(Ce), Ce (C03) F, and structural elements of synchysite-(Ce), rontgenite-(Ce), and parisite-(Ce). *American Mineralogist* 78, 415–418.
- Oberthür, T., Melcher, F., Henjes-Kunst, F., Gerdes, A., Stein, H., Zimmerman, A., El Ghorfi, M., 2009. Hercynian age of the cobalt-nickel-arsenide-(gold) ores, Bou Azzer, Anti-Atlas, Morocco: Re-Os, Sm-Nd, and U-Pb age determinations. *Economic Geology* 104, 1065–1079.
- Okamoto, a., Tsuchiya, N., 2009. Velocity of vertical fluid ascent within vein-forming fractures. *Geology* 37, 563–566.
- ONHYM, 2013. Annual Report 2013. Office National des Hydrocarbures et des mines (ONHYM), Morocco.

- ONHYM, 2015. Les Terres Rares Au Maroc. Office National des Hydrocarbures et des mines (ONHYM), Morocco.
- Pearson, R.G., 1963. Hard and soft acids and bases. *Journal of the American Chemical Society* 85, 3533–3539.
- Piqué, A., Bouabdelli, M., Soulaïmani, A., Youbi, N., Iliani, M., 1999. Les conglomérats du P III (Néoprotérozoïque supérieur) de l'Anti Atlas (Sud du Maroc): molasses panafricaines, ou marqueurs d'un rifting fini-protérozoïque? *Comptes Rendus de l'Académie des Sciences-Series IIA-Earth and Planetary Science* 328, 409–414.
- Qalbi, A., Mouttaqi, A., Rjimati, E.C., Zemmouri, A., Michard, A., Saddiqi, O., 2011. The Nb-Ta-U-REE Prospects of the Glibat Lafhouda Carbonatites (Awserd Province). *Notes et Mémoires du Service géologique du Maroc*. N°564 9, 183–187.
- Qing, H., Mountjoy, E.W., 1994. Rare earth element geochemistry of dolomites in the Middle Devonian Presqu'île barrier, Western Canada Sedimentary Basin: implications for fluid-rock ratios during dolomitization. *Sedimentology* 41, 787–804.
- Ruberti, E., Enrich, G.E.R., Gomes, C.B., 2008. Hydrothermal REE fluorocarbonate mineralization at Barra do Itapirapua, a multiple stockwork carbonatite, Southern Brazil. *The Canadian Mineralogist* 46, 901–914.
- Salvi, S., Williams-Jones, A.E., 1990. The role of hydrothermal processes in the granite-hosted Zr, Y, REE deposit at Strange Lake, Quebec/Labrador: Evidence from fluid inclusions. *Geochimica et Cosmochimica Acta* 54, 2403–2418. doi:10.1016/0016-7037(90)90228-D
- Smith, M.P., Campbell, L.S., Kynicky, J., 2015. A review of the genesis of the world class Bayan Obo Fe–REE–Nb deposits, Inner Mongolia, China: Multistage processes and outstanding questions. *Ore Geology Reviews* 64, 459–476.
- Smith, M.P., Henderson, P., 2000. Preliminary fluid inclusion constraints on fluid evolution in the Bayan Obo Fe-REE-Nb deposit, Inner Mongolia, China. *Economic Geology* 95, 1371–1388.
- Smith, M.P., Henderson, P., Campbell, L.S., 2000. Fractionation of the REE during hydrothermal processes: constraints from the Bayan Obo Fe-REE-Nb deposit, Inner Mongolia, China. *Geochimica et Cosmochimica Acta* 64, 3141–3160.

- Soulaimani, A., Bouabdelli, M., Piqué, A., 2003. L'extension continentale au Néoproterozoïque supérieur-Cambrien inférieur dans l'Anti-Atlas (Maroc). *Bulletin de la Société géologique Française* 174, 83–92.
- Steele-MacInnis, M., Bodnar, R.J., Naden, J., 2011. Numerical model to determine the composition of H₂O-NaCl-CaCl₂ fluid inclusions based on microthermometric and microanalytical data. *Geochimica et Cosmochimica Acta* 75, 21–40. doi:10.1016/j.gca.2010.10.002
- Tropper, P., Manning, C.E., Harlov, D.E., 2011. Solubility of CePO₄ monazite and YPO₄ xenotime in H₂O and H₂O-NaCl at 800 °C and 1GPa: Implications for REE and Y transport during high-grade metamorphism. *Chemical Geology* 282, 58–66. doi:10.1016/j.chemgeo.2011.01.009
- Tropper, P., Manning, C.E., Harlov, D.E., 2013. Experimental determination of CePO₄ and YPO₄ solubilities in H₂O-NaF at 800°C and 1 GPa: implications for rare earth element transport in high-grade metamorphic fluids. *Geofluids* 13, 372–380. doi:10.1111/gfl.12031
- Tsay, A., Zajacz, Z., Sanchez-Valle, C., 2014. Efficient mobilization and fractionation of rare-earth elements by aqueous fluids upon slab dehydration. *Earth and Planetary Science Letters* 398, 101–112.
- Wang, L., Ni, Y., Hughes, J.M., Bayliss, P., Drexler, J.W., 1994. The atomic arrangement of synchysite-(Ce), CeCaF(CO₃)₂. *The Canadian Mineralogist* 32, 865–871.
- Weisenberger, T., Spuergin, S., 2009. Zeolites in alkaline rocks of the Kaiserstuhl Volcanic Complex, SW Germany—new microprobe investigation and the relationship of zeolite mineralogy to the host rock. *Geologica Belgica* 12, 75–91.
- Williams-Jones, A.E., Migdisov, A., 2014. Experimental Constraints on the Transport and Deposition of Metals in Ore-Forming Hydrothermal Systems. *Society of Economic Geologists, Inc. Special Publication* 18, 77–95.
- Williams-Jones, A.E., Migdisov, A.A., Samson, I.M., 2012. Hydrothermal Mobilisation of the Rare Earth Elements - a Tale of “Ceria” and “Yttria.” *Elements* 8, 355–360.
- Williams-Jones, A.E., Samson, I.M., Olivo, G.R., 2000. The genesis of hydrothermal fluorite-REE deposits in the Gallinas Mountains, New Mexico. *Economic ...* 95, 327–342.

- Wood, S.A., 1990a. The aqueous geochemistry of the rare-earth elements and yttrium: 2. Theoretical predictions of speciation in hydrothermal solutions to 350 C at saturation water vapor. *Chemical Geology* 88, 99–125.
- Wood, S.A., 1990b. The aqueous geochemistry of the rare-earth elements and yttrium: 1. Review of available low-temperature data for inorganic complexes and the inorganic REE speciation of natural waters. *Chemical Geology* 82, 159–186.
- Wood, S.A., 2004. The hydrothermal geochemistry of the Rare Earth Elements. *The Gangue* 16.
- Wood, S.A., Ricketts, A., 2000. Allanite-(Ce) from the Eocene Casto granite, Idaho: response to hydrothermal alteration. *The Canadian Mineralogist* 38, 81–100. doi:10.2113/gscanmin.38.1.81
- Woolley, A.R., 2001. Alkaline rocks and carbonatites of the world: Africa. Geological Society of London, pp. 187–192.
- Wu, C., Yuan, Z., Bai, G., 1996. Rare earth deposits in China, in: A.P. Jones, F. Wall, C.T.W. (Ed.), *Rare Earth Minerals: Chemistry, Origin and Ore Deposits*. Chapman and Hall, pp. 281–310.
- Zerdane, A., Rjimati, E.C., Zemmouri, A., Mouttaqi, A., Michard, A., 2011. Aghracha Iron Mine and Uranium-REE prospect (Awserd Province). *Notes et Mémoires du Service géologique du Maroc*. N°564 9, 177–182.

General conclusion

The aim of this work was to use mineralogical and geochemical methods combined with field observations to investigate both the formation of the Jbel Boho alkaline complex and its potential to develop REE mineralization. The field, textural, mineralogical and geochemical data allow us to determine its magmatic evolution in time more clearly and consistently than before. This has enabled us to distinguish three different generations of magma, starting with the emplacement of various volcanic rocks, then the intrusion of a syenite pluton, which shows two types of syenite (quartz syenite and olivine syenite) and finally a dyke swarm consisting of microsyenitic and rhyolitic dykes that cross-cut the preceding igneous rocks. Based on major- and trace element data we also tested hypotheses about the origins and evolution of the Jbel Boho magmas, and discuss the fundamental problems of its petrogenesis. The high LREE enrichment of all Jbel Boho magmatic rocks, the HFSE contents and the high Zr/Hf and Nb/Ta ratios of its primitive rocks suggest a mantle source which produced alkali rocks, such as a hotspot or plume, in an extensional system. The increasing alkali- and rare-earth-element contents with rising silica contents and negative anomalies of europium and other trace elements (e.g. Sr, P, Pb, Ti) indicate a magma evolution by fractional crystallization for the lavas. Although the syenites, which follow the lavas, have very high alkali element contents like

trachyte and tephriphonolite, they display REE element patterns like the basic alkali volcanics without negative Eu anomalies, which argue against fractional crystallization from mantle magmas. Therefore they are considered, by analogy with syenites from other parts of the world, to be formed from the remelting of mafic cumulate at a deep crustal level.

This study also reveals the occurrence of strong LREE enrichments associated with REE mineralization in the late magmatic stage, which is represented by microsyenitic and subalkaline rhyolitic dykes as well as different hydrothermal quartz carbonate veins. We focussed in this study on the geochemistry of the different ore bearing rocks and described by microprobe analysis the main LREE-host mineral synchysite-(Ce) ($\text{CaREE}(\text{CO}_3)_2(\text{F},\text{OH})$). The mineralized zone is localised north of the syenite pluton next to the quartz syenite and represented by synchysite mineralizations within a N-E trending rhyolitic dyke and NE-SW trending hydrothermal veins. Based on geochemical, mineralogical, fluid inclusions and previous experimental data, we propose a genetic model in which REE are transported as chloride complexes in acidic fluid conditions with the presence of fluorine as HF. The precipitation of synchysite occur when these fluids come into contact of rocks that contain neutralizing minerals (e.g. dolomite and calcite), which significantly raise the pH of the fluids. This study highlights the REE potential of late intrusive dykes and hydrothermal veins in alkaline complexes and presents an overview of the rock types and structures favoured for REE prospection and exploration.

Published and unpublished geophysical work shows that additional parts of the Jbel Boho complex are buried beneath later-formed dolomites to the south of the area studied here. These buried rocks could be very important sources for heavy mineral deposits or other ores.

We hope that the present work encourages more careful studies on REE-enriched rocks and the source of REE-rich hydrothermal fluids in this area. Such investigations are very important to better understand the formation of REE ore deposits in hydrothermal system or perhaps to discover new potential source for REE hidden in this alkaline complex.

Erklärung

Hiermit erkläre ich, Rachid Benaouda, dass die vorgelegte Abhandlung, abgesehen von der Beratung durch meinen Betreuer, nach Inhalt und Form meine eigene Arbeit ist und ausschließlich unter Verwendung der angegebenen Hilfsmittel entstanden ist. Diese Arbeit ist unter Einhaltung der Regeln guter wissenschaftlicher Praxis der Deutschen Forschungsgemeinschaft entstanden. Ferner erkläre ich, dass ich weder diese noch eine ähnliche Arbeit an anderer Stelle im Rahmen eines Prüfungsverfahrens vorgelegt habe.

Kiel, Juli 2015

Lebenslauf

Name	Rachid Benaouda
Geburtsdatum	20.02.1977 in Meknes/Marokko
Anschrift	Eutiner Str. 16, 24143 Kiel.
Telephone	+49-4318802856
Email	benouda@min.uni-kiel.de
Staatsangehörigkeit	Deutsch/Marokkanisch
Akademischer Werdegang	
WS 2010 - WS 2015	Promotion zu Dr. rer. nat. im Institut für Geowissenschaften der CAU Kiel Thema: Magma Evolution und Seltenerd Mineralisation in der magmatischen Alkali Komplex von Jbel Boho in Bou Azzer Disrikt (Anti-Atlas/Marokko)
WS 2006 - SS 2010	Master Geowissenschaften an WWU Münster Thema: Geochemisch/Petrologische Untersuchungen von Plagiograniten aus dem Omanophiolith
2004 - 2006	Deutsch: Zertifikat Deutsch (B1), Zentral Mittelstuf Prüfung (B2), DSH (C1,2)
1997 – 2003	Licence in Geowissenschaften an My Ismail Universität Meknes
Fremdsprachen	Arabisch, Deutsch, Französisch, Englisch

